THERMALLY ACTIVATED DYNAMICS: STOCHASTIC MODELS AND THEIR APPLICATIONS

CHENG XINGZHI

(Bachelor of Science, Peking University)

A THESIS SUBMITTED

FOR THE DEGREE OF DOCTOR OF PHILOSOPHY

DEPARTMENT OF ELECTRICAL & COMPUTER ENGINEERING

NATIONAL UNIVERSITY OF SINGAPORE

2007

Acknowledgements

I would like to thank my supervisor Associate Professor Mansoor B. A. Jalil. He has been very encouraging, helpful and knowledgable in my research activities. In addition, I have been given absolute freedom in choosing projects and topics during my PhD study, which broadened my horizon and gained me precious experiences for my future independent research.

My thanks also goes out to my co-supervisor Dr. Hwee Kuan Lee. Guided me into the wonderful world of Monte Carlo, he had taught me not only the academics, but also the attitude of life. I am very appreciated for his always-standby for my last-minute requests.

I have been very happy to work in Dr. Mansoor's group with many intelligent and aggressive colleagues: Guo Jie, Wang Xiaoqiang, Pooja, Saurabh, Tan Seng Ghee, Bala, Takashi, Chen Wei, Wan Fang and Ma Minjie. Thanks for the sharing and inspiration of ideas.

I wish to thank the following: Ren Chi (for the pressure he gave); Guo Jie (for allies); Goolaup (for sitting next to me for four years); Sreen (for suffering the VSM together); Debashish (for heavy bumps); Chen Wenqian (for listening to my complaints).

Thanks to my dear girl friend, Deng Leiting, for her love, her support in my career and her efforts in changing my life. Thanks to my family for their many years of support.

<div align="right">

Cheng Xingzhi

Aug 2007

</div>

Contents

Summary

Rapid development of nano-fabrication technologies has enabled manipulations and applications at the scaling regime between nano-meters to micro-meters. For these many applications, such as ultra high density magnetic recording and Brownian motors, the effect from thermal fluctuations thus becomes significant and therefore requires better understanding of its stochastic behaviors. In many complex systems under considerations however, neither analytical nor numerical solutions to the stochastic differential equations (Langevin equations) are both obvious and efficient.

In this thesis, a systematic approach using the random walk Monte Carlo method is proposed to solve the Langevin dynamics and the corresponding Fokker-Planck equations. The theoretical basis for the Monte Carlo approach is first established by examining the equivalence between the Monte Carlo method and the Langevin equations. This equivalence can be verified via either comparing the coefficients for the corresponding Fokker-Planck equations, or using the Central Limit theorem.

By applying the Monte Carlo analysis, non-equilibrium transport in Brownian

ratchets can be simplified into random walks within a site chain with two absorbing boundaries. Analytical expressions for the probability current is obtained by applying the evolutionary techniques in the Gambler's ruin problem. A faster numerical solver for the ratchets current is also proposed.

Extensions of the Monte Carlo model to multi-dimensional systems, especially the micromagnetic model, are also discussed. A proper algorithm is implemented in the Monte Carlo model to represent the precessional motion and damping motion respectively. The Monte Carlo algorithm has comparable improvement In addition, it has a distinct advantage to identify the role of the precessional motion in the micromagentic models.

List of Tables

List of Figures

Chapter **1**

Introduction

Thermally activated dynamics pertains to the dynamical behavior of a system in a finite temperature environment. These thermally activated dynamics, which generally involve randomness, have intrigued researchers in diverse fields, including physics [1], chemistry [2], economics and finance research [3, 4]. This is typically due to the fact that the thermal associated stochastic processes, especially the Brownian particle model, emerge naturally in these many fields. This thesis will focus on the stochastic theories for modeling thermally activated dynamics, establishing links between the different theoretical models and exploring their applications in actual physical systems.

1.1   Overview of Brownian Motion

The classic thermally activated dynamics is the Brownian motion, named after the Scottish botanist R. Brown, who in 1827 first discovered and described the Brownian motion related to the irregular movements of pollen particles suspended in a solvent. We refer to Gouy [5], who systematically analyzed the characteristics of the Brownian motion. Gouy's result can be summarized as follows [1, 5]:

- The motion is very irregular, composed of translations and rotations, and the trajectory appears to have no tangent;

- Two particles appear to move independently, even when they approach one another to within a distance less than their diameter.

- The smaller the particles, the more active the motion.

- The composition and density of the particles have no effect.

- The less viscous the fluid, the more active the motion.

- The higher the temperature, the more active the motion.

- The motion never ceases.

Many real physical phenomena can be recast to the Brownian motion model, i.e. a "particle" moving randomly in an external potential. One of the most important examples is the Kramers escape problem [6]. Kramers in 1940 proposed an analogy between the chemical reaction process and the Brownian motion in a potential well [7]. Like many other physical systems, the chemical reaction can be characterized by the relaxation of the system in the presence of many local minima separated by energy barriers – an often-used analogy for such complex state spaces is that of a mountainous landscape, where the heights of the mountains represent the energy with the two horizontal axis representing two of the many dimensions of the state space. A typical example of Kramers' analogy is shown in Fig. (1.1). Thermally induced perturbations of the particle result in a finite probability of the particle's escape from a potential well. The transition rate, or the inverse of the switching time, for the Brownian particle to transit from one energy minima to another via overcoming the energy barrier, is thus a critical quantity. In chemical reactions, the Kramers escape rate therefore describes the chemical reaction rate [7].

This escape problem is generic in many other natural phenomena as well. For example, it can characterize the inter-state transitions which are critical in data storage applications. In these applications, the binary data bits "0" and "1" are
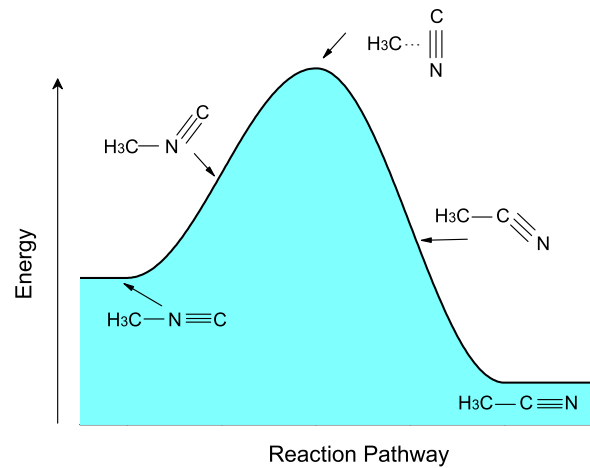
Figure 1.1: Typical example of the chemical potential for reaction.

represented by two stable magnetization states of the magnetic grains. Ideally, the inter-state transitions should occur only when the intervening energy barrier is removed in the presence of an applied field ('writing field'). However, in the presence of thermal fluctuations, there is a finite probability of escape over the energy barrier. This results in unwanted thermally induced magnetization switching and destroys the stored information. This problem becomes particularly acute in current data storage applications when small magnetic particles of a few nanometers in dimensions are used [8] in order to maximize storage density. Thus, in this specific case, a better understanding of the thermally activated micromagnetic dynamics will help us to make better predictions of the information degradation and the lifetime of the stored data.

1.1.1 Mathematical Explanations

The archetypical Brownian motion was first theoretically explained by Einstein in 1905 [9]. Einstein based his explanation on the theory of kinetic thermodynamics, which governs the collisions between the particle and neighboring molecules

in the solvent. By the early 1900s, the theory of thermodynamics had been well-established, elucidating the relationships between work, heat, energy, entropy, temperature and other physical parameters. According to the equipartition law, the state probability distribution of a classical system in thermodynamic equilibrium obeys the Maxwell-Boltzmann distribution, with an energy fluctuation of $\frac{1}{2}k_B T$ associated with each degree of freedom of the system [10].

We will give detailed discussions of Einstein's treatment of Brownian motion later in this section as well as in the next chapter. Although Einstein did the pioneering theoretical investigations into Brownian motion, a "truly dynamical theory of the Brownian motion" [5] is attributed to Langevin for his simpler and more fundamental model. Extending Newton's second law of dynamics and assuming a systematic force (viscous drag) and a rapidly fluctuating white force $\xi(t)$, Langevin proposed a class of stochastic equations which bear his name to model the stochastic dynamics of Brownian particles. For a simple one dimensional problem of mass m at a position x, the Langevin dynamical equation reads:

$$m\ddot{x} = f(x) - m\gamma\dot{x} + \xi(t) \tag{1.1}$$

where the force $f(x) = -V'(x)$ is the gradient of the potential $V(x)$, γ is the friction constant and $\xi(t)$ is a mean zero Gaussian white noise term representing the effects of thermal fluctuations, and has a δ-function self-correlation: $\langle \xi(t)\xi(s) \rangle = 2D \cdot \delta(t-s)$. This assumption is reasonable since collisions between different molecules can to a good approximation be considered as independent of each other.

Many approaches can be used to calculate the prefactor D by considering the statistical equilibrium constraints, e.g. the equipartition law. Here, we adopt the simple approach by Einstein and Smoluchowski. They noted that statistical equilibrium will yield a vanishing probability current, and hence the drift current and diffusion current should be balanced. Based on this assumption, they derived the Einstein-Smoluchowski equation that describes the time evolution behavior of

the probability distribution function $W(x, t)$:

$$\frac{d}{dt}W(x, t) = \nabla \cdot \left(-\frac{F}{\gamma}W + D\nabla W \right),$$ (1.2)

where F is the external force. With the equilibrium condition that $dW/dt = 0$ and the Maxwell-Boltzmann distribution $W(x, t)|_{t \to \infty} = W_0 \exp(-V(x)/k_B T)$, Einstein obtained the well-known formula for the diffusion constant: $D = \gamma k_B T/m$. Here k_B is Boltzmann's constant and T is the temperature in degrees Kelvin. This Einstein-Smoluchowski equation was later justified by several important experiments [5, 11].

1.2   Motivation and Objective

The one dimensional Langevin dynamical equation [Eq. (1.1)] and the associated Einstein-Smoluc-howski equation [Eq. (1.2)] are specialized forms of the general Langevin dynamical equation and the general Fokker-Planck equation [1, 12] respectively. The Fokker-Planck equation is a powerful instrument in analyzing thermally activated dynamics. It considers the time evolution behavior of the probability distribution function of the macroscopic variables. Ideally, the average value of any microscopic variables, such as the mean velocity and mean displacement, can be obtained once the Fokker-Planck equation is solved and the distribution functions are obtained.

The Langevin dynamical equation, together with the Fokker-Planck equation, constitutes the standard technique for analyzing the thermally activated dynamics. For some simple cases, e.g. linear problems, stationary problems with only one variable, analytical solutions exist. However, modern research frequently deals with complex physical systems, which may include interactions, correlations and high dimensional characteristics. The complexity increases further for driven systems which are far from equilibrium. For these complex systems, it is often not

possible to arrive at an analytical solution. Instead, many numerical and computational methods have been employed, e.g. eigenfunction expansion, numerical integration, the variational method and the matrix continued-fraction method [See Ref. [12] for a review]. However, most of these numerical methods have their own limitations. For example, the numerical simulation with Eq. (1.1) is generally applicable for most complex systems, but needs a large computing resource and suffers from inefficiency.

Therefore, the main effort in this thesis concentrates on developing new solving techniques that could lead to both analytical and numerical solutions to the Langevin equations as well as the Fokker-Planck equations. Specifically, we aim to solve these equations via a Master equation scheme.

The Master equation is another branch of theoretical modeling that is frequently used to model stochastic dynamics. In this thesis, we are particularly interested in solving the Master equation numerically via a Monte-Carlo scheme. The Monte Carlo model is concerned about the transition probability between the states, and its formalism can be described by a general Master equation [12, 13]:

$$\frac{\partial P(x,t)}{\partial t} = \dot{P}(x,t) = \int [w(x' \to x)P(x',t) - w(x \to x')P(x,t)]dx', \qquad (1.3)$$

where $P(x,t)$ is the system's probability distribution function at a microscopic state x, $w(x \to x')$ is the transition rate from x to x', and t is the time variable, usually in discrete units of Monte Carlo steps.

The Monte Carlo scheme serves as a probabilistic description of the Brownian motion, as compared to the dynamical description of the Langevin equation. It is thus interesting to gain an insight into the linkage between the two stochastic models.

1.2.1   Langevin dynamics and Monte Carlo method

The two stochastic dynamical models, the Langevin dynamical equation and the Monte Carlo method, are based on two different physical bases.

The Langevin dynamical equation, originated from Newton's second law of dynamics, is generally regarded as "the real basis of the theory of the Brownian motion" [5]. Comparing to the Einstein-Smoluchowski (Fokker-Planck type of) explanation of the Brownian motion, the Langevin equation provides a clear causality of the Brownian particle's movement. This enables the Langevin dynamical equation to model both equilibrium and non-equilibrium systems.

The Langevin dynamical equation has been extensively applied to model dynamics in different areas of research, such as chaos [14], chemical reaction [7] and micromagentism [1, 15]. Simulation on a thermal activated system by using the Langevin equation, however, relies on the integration of the stochastic differential equation of each particle via either Ito's calculus or Stratonovich's calculus [1]. To model the continuous effect of thermal fluctuations, the time interval in the simulation has to be small, thus significantly reducing the simulation efficiency. Hence, the utilization of the Langevin equation is limited to the simulation of a small number of particles over a short period of time, e.g. a few nanoseconds in practical micromagnetic media simulations [16].

Unlike the force-driven model such as Langevin dynamics, the Monte Carlo model is more concerned about the transition probability of the Brownian particle between the states of the system. Thus, the Monte Carlo method is a powerful and efficient technique in sampling the properties of a system at equilibrium [13]. The efficiency of the Monte Carlo method is particularly advantageous compared to the Langevin method for complex systems involving many stochastic variables.

The Monte Carlo dynamical model is, however, limited by the lack of a real physical

meaning for its time unit - Monte Carlo steps. This limitation has prevented Monte Carlo techniques from being used in most dynamics studies. It also leads to the belief that time does not play as significant a role in Monte Carlo methods, and that Monte Carlo methods are primarily useful for studying systems at steady-state equilibrium [17].

Although both Langevin and Monte Carlo models can be applied to model the same physical system, the mathematical expressions of the two methods appear at first glance to be very different, so that any theoretical link between the two is far from apparent. Limoge and Bocquet [18] noticed that Monte Carlo could be utilized to simulate the Poisson process, in which the relation between Monte Carlo steps and the real time could be established. Kikuchi *et al.* [19] also indicated that a random walk Monte Carlo model can be matched to a hydrodynamical Fokker-Planck equation. The first attempt to quantify the Monte Carlo steps for a random walk Monte Carlo method, as far as we know, was made by Nowak *et al.* [20]. In their study, the time quantification factor was obtained via a comparison between the derived mean square deviations of the magnetization component for both the Monte Carlo method and the Langevin dynamics (known as Landau-Liftshitz-Gilbert (LLG) equation in micromagnetic scheme). Other attempts to link the Monte Carlo with time step with physical time were done by Ph. Martin [21] and Park et al. [22] who examined the Monte Carlo dynamics in an Ising spin system.

1.2.2 Problem definition

Although the work done by Nowak *et al.* in deriving the time quantification factors appears to be specific to the micromagnetic system being considered, it does suggest that the Monte Carlo dynamical model can be linked to the Langevin dynamical equation. The equivalence between the Monte Carlo model and the Langevin dynamics, if established, could benefit researchers on both sides in reaching a fuller

understanding of stochastic dynamics. Furthermore, the Monte Carlo method is generally more efficient. For instance, it has been reported that simulation with the time-quantified Monte Carlo method is considerably more efficient than the conventional method of modeling magnetization dynamics based on time-step integration of the stochastic LLG equation [16], which is the corresponding Langevin equation for magnetization dynamics.

Another major motivation for time quantifying the Monte Carlo method is to establish an analytical connection between the two stochastic simulation schemes, the Monte Carlo and Langevin dynamics. Such an analytical connection provides alternative techniques to both stochastic models. For example, solving stochastic differential equations using advanced Monte Carlo techniques allows us to calculate the long-time reversal and stability [23, 24], which is not possible with the Langevin method. A well-designed hybrid algorithm, which combines the Langevin equation with a Monte Carlo scheme, would have advantages of both dynamical models such as having a firm physical basis (Langevin) and high simulation performance (Monte Carlo).

Motivated by the prospect of the high-performance hybrid simulation algorithm, the present research aims to:

- Uncover the hidden analytical links and prove the equivalence between the two stochastic models;

- Develop systematic approaches to map the Monte Carlo models into Langevin dynamics and analytically derive the time quantification factor of one Monte Carlo step in the Monte Carlo scheme;

- Devise and verify time quantifiable Monte Carlo algorithms;

- Discuss several applications of time-quantified Monte Carlo methods.

Theoretically, the use of the time-quantified Monte Carlo model could be advantageous in most research fields where the Langevin equation is originally used. In this thesis, we will discuss in detail the use of the time-quantified Monte Carlo method in two particular physical models, the micromagnetism and the Brownian ratchets problem. These two areas are chosen because of high academic and practical interest in utilizing them in nanotechnology applications.

1.3 Organization of Thesis

In the second chapter we give a brief review of stochastic theories of Brownian motion. The Langevin dynamical model, the Fokker-Planck equation and the Monte Carlo methods will be discussed. In chapter three, we provide the theoretical justification of using a Monte Carlo method instead of the Langevin dynamical equation to study thermally activated dynamics. In chapter four, we apply the time-quantified random walk Monte Carlo method to model the transport in Brownian ratchets. Chapter five discusses another application of the random walk Monte Carlo method, i.e. in studying thermally induced reversal of magnetic nanoparticles.

Review of Stochastic Descriptions

In this chapter we briefly review some stochastic models for the Brownian motion. These are basic ideas and conceptions that provide the foundations for the other chapters.

2.1 Brownian Motion and Langevin dynamics

2.1.1 Langevin dynamics for Brownian Motion

We first consider the Brownian motion of particles in its simplest form. Given a small particle of mass m immersed in a fluid with a friction force acting on the particle, the basic equation of motion of the particle under the influence of a frictional force is given by the Stokes' law:

$$\dot{v} = -\gamma v \qquad (2.1)$$

where γ is the friction constant. Thus the solution of $v(t)$ can be simply obtained:

$$v(t) = v(0)e^{-\gamma t}. \qquad (2.2)$$

The deterministic equation Eq. (2.1) is valid if the particle is large so that its

velocity due to thermal fluctuations is negligible. It must be modified to account for the collision effects of the environment if the particle mass is small. Inserting a fluctuating (Langevin) force $\xi(t)$ into Eq. (2.1), one obtains the equation of motion:

$$\dot{v} + \gamma v = \xi(t). \tag{2.3}$$

The properties of the Langevin force are expressed mathematically as:

$$\langle \xi(t) \rangle = 0 \tag{2.4}$$

$$\langle \xi(t)\xi(t') \rangle = 2D\delta(t - t'). \tag{2.5}$$

The first moment requires the average of Langevin force should be zero, which assumes that the Langevin force does not bias the particle to move in any particular direction. The second moment implies that any two Langevin forces at different times should be independent. The latter assumption is valid since the duration time τ_0 of a collision is much smaller than the relaxation time $\tau = 1/\gamma$ of the velocity of the small particle. The value of D which determines the magnitude of the Langevin force has been given by the Einstein relation in Chap. 1, i.e.

$$D = \gamma k_B T/m. \tag{2.6}$$

2.1.2 Langevin Equation with Many Variables

The above basic form can be generalized to N variables $\{x\} = x_1, x_2, \ldots, x_N$ and M stochastic forces as:

$$\dot{x}_i = f_i(\{x\}, t) + \sum_j^M g_{ij}(\{x\}, t) \cdot \xi_j(t). \tag{2.7}$$

Here $\xi_j(t)$ are again Gaussian random variables with zero mean and with correlation functions proportional to the δ function. When $g_{ij}(\{x\}, t)$ depend on $\{x\}$ and t, the equations are known as nonlinear Langevin equations [1, 12].

2.1.3   Applications

We will now briefly present a few important applications of the Langevin dynamical model to model real phenomena.

The Kramers Escape Problem

Kramers proposed an analogy between the chemical reaction and the transition of Brownian particles in local chemical potential minima [6, 7]. This model differs from the previous simple Brownian model in that a chemical potential is included:

$$m\ddot{x} + m\gamma\dot{x} + V'(x) = m\xi(t). \tag{2.8}$$

where $V(x)$ is the chemical potential for reaction and $\xi(t)$ is the Gaussian white noise defined as in Eq. (2.5).

Equation (2.8) is also known as the low friction Kramers equation. For large friction constants we may neglect the second order time derivative in Eq. (2.8). We thus obtain the overdamped Kramers Equation:

$$\gamma\dot{x} + V'(x)/m = \xi(t). \tag{2.9}$$

Dynamical Motion of Magnetic Moment

In micromagnetic theory, the magnetic moment of a nano-particle is represented by a unit spin vector $\mathbf{m}$ that lies on the surface of a sphere. The motion of the spin vector is driven by the torque due to an effective external magnetic force. The dynamical equation describing the magnetic moment is usually given in the Landau-Lifshitz-Gilbert form [1, 15]:

$$\frac{d\mathbf{m}}{dt} = -\frac{\gamma_0 H_k}{1 + \alpha^2}\mathbf{m} \times [(\mathbf{h}_{\text{eff}} + \mathbf{h}_{\text{th}}) + \alpha\mathbf{m} \times (\mathbf{h}_{\text{eff}} + \mathbf{h}_{\text{th}})] \tag{2.10}$$

where H_k, γ_0 and α are anisotropy field magnitude constant, gyromagnetic constant and damping constant respectively. $\mathbf{h}_{\text{eff}}$ is the effective external force and $\mathbf{h}_{\text{th}}$ is
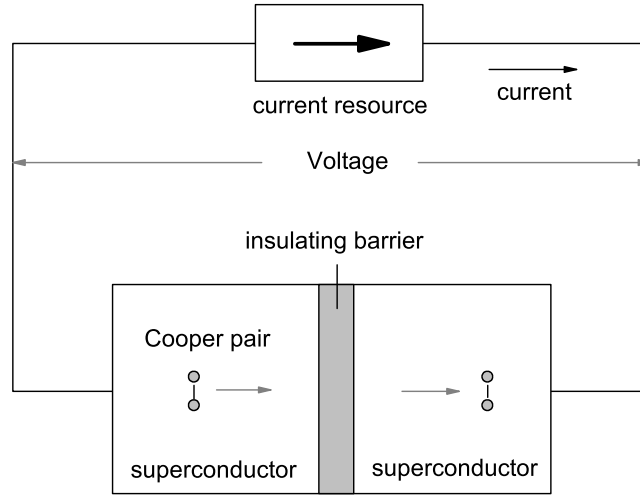
Figure 2.1: Diagram of Josephson tunneling junction.

a Gaussian white noise in three dimensional space that represents the thermal fluctuations on the magnetic moment.

Josephson Tunneling Junction

A Josephson tunneling junction, as shown in Fig. (2.1), consists of two superconductors which are separated by a thin oxide layer [25]. The phase difference between the wave functions of the Cooper pairs in the two superconductors is denoted by φ.

Without going into the details of the derivation, the equation of motion for φ is given by:

$$\left(\frac{\hbar}{2e}\right)^2 C\ddot{\varphi} + \left(\frac{\hbar}{2e}\right)^2 \frac{1}{R}\dot{\varphi} + \frac{\hbar}{2e}I_{\max}\sin(\varphi) = \frac{\hbar}{2e}I + \frac{\hbar}{2e}L(t) \qquad (2.11)$$

where $L(t)$ models a noise current, the correlation function of which is given by $\langle L(t)L(t')\rangle = (2/Rk_BT)\delta(t-t')$.

Equation (2.11) indicates that the Josephson tunneling current can be analogous to a Brownian particle moving in a periodic potential. We will discuss details of

this model in Chap. 4.

Stock Price in Financial Markets

Five years prior to Einstein's famous 1905 paper on Brownian Motion, in which Einstein derived the equation governing Brownian motion and made an estimate for the size of molecules, Louis Bachelier had worked out, in his Thesis, "*Theorie de la Speculation*", the distribution function for what is now known as the Wiener stochastic process (random walks without bias [1]).

Bachelier's work laid the foundation of modern mathematical finance, in which the motion of stock price S (or other financial derivatives such as options) can be described by a geometric Brownian motion model:

$$\frac{dS_t}{S_t} = \mu dt + \sigma dW_t \tag{2.12}$$

where S_t is the spot price of the stock; μ is the expected return; σ is the volatility (also known as the instability) of the stock; and W_t is a Wiener's stochastic process. In 1973, F. Black and M. Scholes [26] and, independently, Robert Merton [27] used geometric Brownian motion to construct a theory for determining the price of stock options. The resulting valuation formulas (a set of partial differential equations) have become indispensable tools in today's daily capital market practices.

2.2 Fokker-Planck Equation

The Langevin equations are very successfully adopted in describing thermally induced stochastic dynamics. Their solutions however require advanced techniques, i.e. the Fokker-Planck equations. The Fokker-Planck equation is an equation of motion for the distribution function of fluctuating macroscopic variables. The purpose of the Fokker-Planck equation is to convert the stochastic dynamical

(Langevin) equation into partial differential equations which are in principle solvable. The Fokker-Planck equation was first introduced by Fokker and Planck to describe the Brownian motion of particles. To become familiar with this equation, we again start with the discussion of simple one dimensional Brownian motion.

2.2.1 Fokker-Planck Equation for One Variable

Kramers-Moyal Forward Expansion

We define the transition probability $\phi(x, t + \tau | x', t)$ to link the probability density $W(x, t + \tau)$ at time $t + \tau$ ($\tau \geq 0$) and the probability $W(x, t)$ at time t:

$$W(x, t + \tau) = \int_{-\infty}^{\infty} \phi(x, t + \tau | x', t) W(x', t) dx'. \tag{2.13}$$

Introducing $\Delta = x - x'$ such that $x = x' + \Delta$, the integrand in Eq. (2.13) may be expanded in a Taylor series around x according to

$$\begin{aligned}
\phi(x, t + \tau | x', t) W(x', t) &= \phi(x + \Delta - \Delta, t + \tau | x - \Delta, t) W(x - \Delta, t) \\
&= \sum_{n=0}^{\infty} \frac{(-1)^n}{n!} \Delta^n \left(\frac{\partial}{\partial x} \right)^n \phi(x + \Delta, t + \tau | x, t) W(x, t)
\end{aligned}$$

$$\tag{2.14}$$

We remark $\int_{-\infty}^{\infty} \phi(x + \Delta, t + \tau | x, t) d\Delta = 1$. Defining

$$D^{(n)} = \lim_{\tau \to 0} \frac{\int_{-\infty}^{\infty} \Delta^n \phi(x + \Delta, t + \tau | x, t) d\Delta}{\tau} = \lim_{\tau \to 0} \frac{\langle \Delta^n \rangle}{\tau}, \tag{2.15}$$

we can thus rewrite Eq. (2.13) into

$$\frac{\partial W(x, t)}{\partial t} = \sum_{n=1}^{\infty} \left(-\frac{\partial}{\partial x} \right)^n D^{(n)}(x, t) W(x, t) \tag{2.16}$$

where we have made Taylor expansion of $W(x, t + \tau)$ on t on the left side of Eq. (2.13). Equation (2.16) is known as the Kramers-Moyal expansion.

One-dimensional Fokker-Planck Equation

The theorem of Pawula [12, 28] guarantees that for a positive transition probability ϕ, the expansion of Eq. (2.16) may stop either after the first term or after the second term. Truncating at $O(n^3)$ we obtain the Fokker-Plank equation:

$$\frac{\partial W(x,t)}{\partial t} = \left[-\frac{\partial}{\partial x} D^{(1)}(x,t) + \frac{1}{2} \frac{\partial^2}{\partial x^2} D^{(2)}(x,t) \right] W(x,t) \qquad (2.17)$$

where the drift coefficient $D^{(1)}$ and the diffusion coefficient $D^{(2)}$ follow the definition of Eq. (2.15).

2.2.2 Fokker-Planck Equation for N Variables

We consider a system consists of N variables: $\{x\} = x_1, x_2, \ldots, x_N$. Applying the similar derivation techniques presented above, we obtain the Kramers-Moyal expansion of $W(\{x\}, t)$. Letting the expansion stop at $n = 2$, we obtain the expression of the N dimensional Fokker-Planck Equation:

$$\frac{\partial W(\{x\},t)}{\partial t} = \left[-\frac{\partial}{\partial x_i} D_i(x,t) + \frac{1}{2} \frac{\partial^2}{\partial x_i x_j} D_{ij}(x,t) \right] W(\{x\},t) \qquad (2.18)$$

where the drift vector D_i and diffusion matrix D_{ij} are defined as:

$$D_i(\{x\},t) = \lim_{\tau \to 0} \frac{1}{\tau} \langle x_i(t+\tau) - x_i(t) \rangle \qquad (2.19)$$

$$D_{ij}(\{x\},t) = D_{ij}(\{x\},t)$$
$$= \lim_{\tau \to 0} \frac{1}{\tau} \langle [x_i(t+\tau) - x_i(t)][x_j(t+\tau) - x_j(t)] \rangle . \qquad (2.20)$$

2.2.3 Fokker-Planck Equations for Langevin dynamics

In this section we give some well discussed example of Fokker-Planck equations corresponding to some simple Langevin dynamical models.

Fokker-Planck Equation for Equation (2.3)

Equation (2.3) is also known as the Ornstein-Uhlenbeck process [29]. By considering the boundary condition that the system relaxes to the Maxwell distribution $W(v) \propto \exp(-mv^2/2k_BT)$ at equilibrium ($\partial W/\partial t = 0$), a simple derivation will give the drift and diffusion coefficients of the Fokker-Planck equation:

$$\frac{\partial W(v,t)}{\partial t} = \left[\frac{\partial}{\partial v}(\gamma v) + \frac{1}{2}\frac{\partial^2}{\partial v^2}\gamma k_BT/m \right] W(v,t). \tag{2.21}$$

Fokker-Planck Equation for Equations (2.8) and (2.9)

We rewrite Eq. (2.8) into a system of two first-order equations:

$$\dot{x} = v \tag{2.22}$$

$$\dot{v} = -\gamma v - V'(x)/m + \xi(t). \tag{2.23}$$

Using Eq. (2.18), the Fokker-Planck equation for Eq. (2.8) reads

$$\frac{\partial W(x,v,t)}{\partial t} = \left[-\frac{\partial}{\partial x}v + \frac{\partial}{\partial v}[\gamma v + V'(x)/m] + \frac{\partial^2}{\partial v^2}\gamma k_BT/m \right] W(x,v,t). \tag{2.24}$$

For the overdamped Langevin equation as Eq. (2.9), the Fokker-Planck equation for the distribution function $W(x,t)$ reads

$$\frac{\partial W(x,t)}{\partial t} = \left[\frac{1}{\gamma m}\frac{\partial}{\partial x}V'(x) + \frac{k_BT}{\gamma m}\frac{\partial^2}{\partial x^2} \right] W(x,t). \tag{2.25}$$

Fokker-Planck Equation for Nonlinear Langevin Equations

For one stochastic variable x, the general Langevin equation has the form:

$$\dot{x} = f(x,t) + g(x,t) \cdot \xi(t) \tag{2.26}$$

$\xi(t)$ is assumed to be a Gaussian stochastic process with zero mean and normalized δ correlation.

Without giving the full derivation, we show that the Fokker-Planck equation corresponding to the general one-dimensional Langevin equation as Eq. (2.26) [12]:

$$\frac{\partial W(x,t)}{\partial t} = \left[\frac{\partial}{\partial x} \left(f(x,t) + \frac{\partial g(x,t)}{\partial x} g(x,t) \right) + \frac{\partial^2}{\partial x^2} g^2(x,t) \right] W(x,t) \qquad (2.27)$$

Note in addition to the deterministic drift $f(x,t)$, $D^{(1)}$ contains additional noise induced drift:

$$D^{(1)}_{\text{noise-ind}} = \frac{\partial g(x,t)}{\partial x} g(x,t) = \frac{1}{2} \frac{\partial}{\partial x} D^{(2)}(x,t). \qquad (2.28)$$

2.3 Monte Carlo scheme

The Fokker-Planck equation is not the only equation of motion for the distribution function. In this section we introduce the Monte Carlo method, which in fact serves as the numerical solution to the general Master equation. In particular, we restrict our interest to Master equations for Markov processes.

2.3.1 Master equation

The Master equation and Monte Carlo methods concern about the probability distribution function at each state and the transition rates between the states. The general Master equation for a continuous variable reads

$$\frac{dW(x,t)}{dt} = \int_{-\infty}^{\infty} [\mu(x' \to x) W(x',t) - \mu(x \to x') W(x,t)] dx' \qquad (2.29)$$

where $W(x,t)$ is the probability distribution function and $\mu(x \to x')$ is the transition from x to x' which must satisfy $\mu(x \to x') \geq 0$ and $\int_{x'} \mu(x \to x') = 1$.

For a discrete variable, the Master equation is similar

$$\frac{dW(x,t)}{dt} = \sum_{x'} \mu(x' \to x) W(x',t) - \mu(x \to x') W(x,t). \qquad (2.30)$$

Reorganizing Eq. (2.30) by adopting the matrix formula, we are able to rewrite the Master equation into a simple form:

$$\frac{d\vec{P}(t)}{dt} = T \cdot \vec{P}(t) \tag{2.31}$$

where vector $\vec{P}(t) = \{W(x,t)\}$ is the state probability density vector and $T = \{\mu(x' \rightarrow x) - \delta_{x,x'}\}$ is the transition matrix.

Many physical problems in classical mechanics, quantum mechanics and problems in other sciences, can be reduced to the form of a master equation, thereby performing a great simplification of the problem.

Generalizing the Master equation, i.e. applying the Kramers-Moyal expansion, and truncating the higher order terms will lead to the Fokker-Planck equation.

2.3.2   Random walk Monte Carlo

Random walk Monte Carlo methods, sometimes also known as the Markov chain Monte Carlo methods, are a class of algorithms for sampling from probability distributions based on constructing a Markov chain that has the desired distribution as its *stationary* distribution.

Some typical examples of random walk Monte Carlo methods include, the Metropolis algorithm [13, 30], Gibbs sampling [31] and Slice sampling [32]. In this thesis, we shall focus on the Metropolis algorithm which is utilized by generating a random walk using a proposal density and a method for rejecting proposed moves. the Metropolis algorithm has been widely used in computational physics for thermally activated dynamics [13].

The principle of detailed balance (to be discussed in the next subsection) allows almost infinite formalisms when implementing the Monte Carlo methods. We will give detailed formalisms in the following chapters where applicable.

2.3.3   The Principle of Detailed Balance

The principle of *detailed balance* is important in describing the properties of the equilibrium state. A Markov process whose stationary distribution $W_{eq}(x)$ obeys

$$\mu(x' \to x)W_{eq}(x') = \mu(x \to x')W_{eq}(x) \qquad (2.32)$$

for all pairs of states x and x' is said to obey detailed balance; the stationary distribution is then often also called the equilibrium distribution.

Equation (2.32) provides a quick way to directly obtain the stationary distribution from the transition rates $\{\mu(x' \to x)\}$. For a random walk Monte Carlo algorithm with a heat-bath accepting rate $1/(1 + \exp(\beta \Delta \mathcal{H}))$, its resulting probability distribution at equilibrium (from Eq. (2.32)) gives:

$$W_{eq}(x) = W_0 \exp(-\beta \mathcal{H}),$$

which converges to the Boltzmann form of the distribution function with any time-independent appropriate Hamiltonian $\mathcal{H}$.

For a system driven out of equilibrium, however, the principle of detailed balance no longer holds. Neither does there exist a universal principle that could apply for all non-equilibrium systems, such as the open atomic system. This definitely raises concerns that whether the Markov chain Monte Carlo methods have a solid basis in describing the non-equilibrium system. We shall come back to this point in Chap. 4 in which we show that the Monte Carlo algorithm is at least applicable in systems that are driven by Markov noises.

Mapping the Monte Carlo Scheme to Langevin Dynamics

In this chapter we present the *equivalence* between a heat-bath random walk Monte Carlo model and the traditional overdamped Langevin dynamical equation. This equivalence establishes the theoretical basis of using the Monte Carlo model to analyze the time evolution of Brownian motion, such as the thermally induced stochastic dynamics in real physical problems. Typical applications of Monte Carlo models will be discussed in the following chapters for both one dimensional and multi-dimensional problems.

3.1   Introduction

We aim to prove the "equivalence" between the two stochastic descriptions: Langevin dynamics and Monte Carlo. One question may arise in a straightforward manner: how do we define the equivalence?

To simplify our description of the problem, we consider the simplest case: an over-damped Brownian "particle" moving randomly in a one-dimensional steady potential environment $V(x)$, where x is the position of the particle. The dynamics of the particle can be described by the following two dynamical models ($\mathcal{LD}1$ and $\mathcal{MC}1$):

i) **1D Langevin Dynamical Equation**, ($\mathcal{LD}1$):

$$\frac{d}{dt}x = f(x) + \xi(t), \tag{3.1}$$

where $f(x) \equiv -V'(x)$ is the external force, and $\xi(t)$ is a mean zero white noise with:

$$\langle \xi(t) \rangle = 0; \quad \langle \xi(t)\xi(s) \rangle = 2D \cdot \delta(t). \tag{3.2}$$

Here $D \equiv k_B T$ represents the magnitude of the white noise.

and

ii) **1D Random Walk Monte Carlo**, ($\mathcal{MC}1$):

The random walk on x takes a trial move of step size r: $\Delta x = r \in [-R, R]$ ($R \ll 1$) with uniform trial probability. The trial move is however subject to the heat-bath acceptance rate of $A(\Delta V) = 1/(1 + \exp(\beta \Delta V))$. Here ΔV is the energy difference in the proposed transition and $\beta \equiv 1/k_B T = D^{-1}$.

Applying the standard analysis on both stochastic models, i.e. the Maxwell-Boltzmann treatment on the Langevin dynamical model and the detailed balance analysis on the random walk Monte Carlo, we find that both models lead to an identical probability distribution function at equilibrium (the Maxwell-Boltzmann distribution). We naturally ask, are the two stochastic models still equivalent to each other during the process of approaching the equilibrium?

Strictly speaking, one may only agree that the equivalence is established when the two stochastic dynamics mimic all possible trajectories during the relaxation process. The accomplishment of this mission is very difficult and in fact of minor interest, for two reasons: 1) such a comparison requires information for all possible trajectories - which is far more fundamental and unsolvable than the problem that is currently under consideration; and 2) in many applications, we are more interested in the mean effect than being concerned with specific trajectories. Although the latter may be more fundamental, in many problems we are actually dealing with macroscopic systems.

Alternatively, the time evolution probability distribution function $W(x, t)$ can also be considered as the direct criteria to identify the equivalence between the two dynamical models. However, this criteria is also difficult to be utilized in practice as well. In most stochastic processes, except for some simple cases such as Wiener's process or Ornstein-Uhlenbeck process [12], it is not possible to analytically solve for the time evolution of the probability distribution, which provides all information during the process.

Therefore, we have to look for other indirect approaches instead of the direct criteria that have been discussed above. In fact, although the explicit expression of $W(x, t)$ is not achievable, we are still able to analyze its evolutionary behavior $dW(x, t)$. In the following chapters, we will present the proof of equivalence via this method.

3.2 The Fokker-Planck Approach

Our first approach is a systematic way of using the Fokker-Planck equation to map the Monte Carlo methods to the Langevin dynamical equation.

The Fokker-Planck equation is an equation of motion for the distribution function

of fluctuating macroscopic variables, i.e. the position of a particle under thermal fluctuation. By solving the Fokker-Planck equation one obtains distribution functions from which the mean value of any macroscopic variables can be obtained by integration. As discussed however, analytic solutions of the Fokker-Planck equation can be obtained for very few simple cases, e.g. a linear drift vector and constant diffusion tensor.

To link the Monte Carlo methods with the Langevin dynamics, we do not require the explicit solution of the Fokker-Planck equation. In fact, the equation itself could serve as the bridge to establish the link. Our approach to map Monte Carlo methods to Langevin dynamics is as follows (as shown schematically in Figure 3.1):

> STEP 1: derive the Fokker-Planck equation corresponding to the Langevin dynamical equation;
>
> STEP 2: derive the Fokker-Planck equation for the heat-bath random walk Monte Carlo method;
>
> STEP 3: perform termwise comparison between the two sets of Fokker-Planck coefficients.

For illustration, we demonstrate a mapping between a 1D heat-bath random walk Monte Carlo algorithm ($\mathcal{MC}1$) to the 1D Langevin dynamical equation ($\mathcal{LD}1$). Both models have been discussed in Sect. 3.1.

The one dimensional Fokker-Planck equation has the form:

$$\frac{\partial W(x,t)}{\partial t} = -\frac{\partial}{\partial x}(A(x)W) + \frac{1}{2}\frac{\partial^2}{\partial x^2}(B(x)W) \tag{3.3}$$

where A and B are so-called drift and diffusion coefficients, and are defined as

$$\begin{aligned}
A &\equiv \lim_{\Delta t \to 0} \frac{\langle \Delta x \rangle}{\Delta t} \\
B &\equiv \lim_{\Delta t \to 0} \frac{\langle \Delta x^2 \rangle}{\Delta t}.
\end{aligned} \tag{3.4}$$
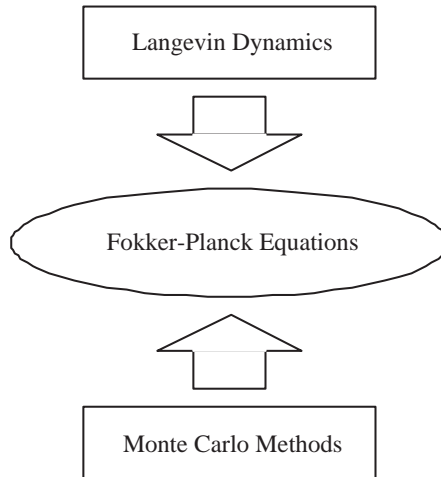
Figure 3.1: Schematics of the Fokker-Planck approach.

There are extensive studies [12] of the Langevin dynamical equation of Eq. (3.1). Its corresponding Fokker-Planck coefficients can be derived via the standard way easily:

$$
\begin{aligned}
A^{\mathrm{LD}} &= f(x) \\
B^{\mathrm{LD}} &= 2D.
\end{aligned}
\tag{3.5}
$$

We next derive the Fokker-Planck equation for the heat-bath random walk Monte Carlo algorithm ($\mathcal{MC}1$). To calculate the Fokker-Planck coefficients A^{MC} for the Monte Carlo method, we require the ensemble mean of a small change of x in *one Monte Carlo step*, i.e. $A^{\mathrm{MC}} \equiv \left\langle \Delta x^{\mathrm{MC}} \right\rangle$.

Since the random walk on x takes a trial move of step size $r \in [-R, R]$, we have the probability of the displacement to be of size r:

$$
p(r) = 1/2R.
$$

Based on the heat-bath Metropolis Monte Carlo scheme, the acceptance rate for

this trial move is given by:

$$
\begin{aligned}
A(\Delta V) &= 1/[1 + \exp(\beta \Delta V)] \approx \frac{1}{2}\left[1 - \frac{1}{2}\beta\left(\frac{\partial V}{\partial x}\Delta x\right)\right] \\
&= \frac{1}{2}\left[1 + \frac{1}{2}\beta f(x)r\right]
\end{aligned} \tag{3.6}
$$

where ΔV is the energy change in the proposed trial move and $f(x) = -V'(x)$. We hence obtain the $\langle \Delta x \rangle$:

$$
\begin{aligned}
A^{\mathrm{MC}} = \langle \Delta x \rangle &= \int_{-R}^{R} r\,dr \cdot p(r)A(\Delta V) \\
&= \frac{1}{12}\beta f(x) \cdot R^2.
\end{aligned} \tag{3.7}
$$

Similarly, one can calculate the diffusion coefficient B^{MC} in a same manner:

$$
\begin{aligned}
B^{\mathrm{MC}} = \langle \Delta x^2 \rangle &= \int_{-R}^{R} r^2\,dr \cdot p(r)A(\Delta V) \\
&= \frac{1}{6}R^2.
\end{aligned} \tag{3.8}
$$

From Eqs. (3.5), (3.7) and (3.8), we obtain two sets of Fokker-Planck equations that corresponding to Langevin ($\mathcal{LD}1$) and Monte Carlo ($\mathcal{MC}1$) models respectively:

$$
\text{Langevin:} \quad \frac{\partial W(x,t)}{\partial t} = -\frac{\partial}{\partial x}(f(x)W) + \frac{1}{2}\frac{\partial^2}{\partial x^2}(2DW) \tag{3.9}
$$

$$
\text{Monte Carlo:} \quad \frac{\partial W(x,t)}{\partial \tau} = -\frac{\partial}{\partial x}(\frac{1}{12}\beta R^2 f(x)W) + \frac{1}{2}\frac{\partial^2}{\partial x^2}(\frac{1}{6}R^2 W). \tag{3.10}
$$

Variable τ in Eq. (3.10) is the time quantity that is calibrated in Monte Carlo steps. We can now compare the Fokker-Planck factors corresponding to the Langevin equation in Eq. (3.9) with those of the heat-bath Metropolis Monte Carlo method in Eq. (3.10). Performing a termwise comparison and omitting $O(R^4)$ and higher order terms, we found that there is a one-to-one mapping between all terms in the Fokker Planck coefficients of both the Monte Carlo method and the Langevin equation if:

$$
\frac{1}{12}\beta R^2 \cdot \Delta\tau_{\mathrm{MC}} = \Delta t_{\mathrm{LD}} \tag{3.11}
$$

where $D \equiv \beta^{-1}$ is noted during the comparison.

Equation (3.11) is the requirement for the equivalence between the two stochastic models. One subsequent result from Eq. (3.11) is that we can obtain the time quantification factor for the heat-bath random walk Monte Carlo method:

$$1 \ \ \text{MCS} = \frac{\Delta t_{\text{LD}}}{\Delta \tau_{\text{MC}}} = \frac{1}{12} \beta R^2. \tag{3.12}$$

To summarize, our above discussion leads to two non-trivial findings: 1) there is an equivalence between the 1D overdamped Langevin dynamical equation and the 1D random walk Monte Carlo method at the small $R \to 0$ limit; and 2) the time quantity of one Monte Carlo step for the random walk Monte Carlo method can be obtained from the established equivalence. We should emphasize that such a time quantification factor is not fixed, but depends on the trial move distribution and the acceptance rate we choose in the Monte Carlo algorithm. We shall extend the discussion in the following sections.

We remark that the idea of using the Fokker-Planck equation to link the Monte Carlo with the Langevin dynamics is general. One can apply the same procedure to acquire the equivalence between some other stochastic models, i.e. more complex multi-dimensional system or non-equilibrium systems. Some examples and their applications will be discussed in the following chapters.

3.3 Proof From the Central Limit Theorem

In the last section we showed that by using the Fokker-Planck equation as the bridge, we could establish the equivalence between the random walk Monte Carlo algorithm and the overdamped Langevin dynamics. Naturally, we will ask why the two models yield the same dynamical process even though they have distinctly different theoretical basis. In addition, while it is not hard to write down the

corresponding Fokker-Planck equations for Langevin dynamical equations and/or Monte Carlo methods, it is certainly non-trivial to construct a Monte Carlo model for an existing Fokker-Planck equation. This difficulty poses a serious obstacle in applying Monte Carlo analysis for more complex systems, e.g. micromagnetic studies and/or biophysics. From this point of view, a microscopic understanding of the equivalence between the two stochastic models is of practical interest.

We consider an overdamped Brownian particle in a potential $V(x)$, whose dynamical behavior can be described by the two stochastic models as given in Sect. 3.1. We consider the probability distribution of the displacement Δx after a time interval of Δt from the initial point.

For the random walk Monte Carlo method, the mean μ and variance σ^2 in one Monte Carlo step can be obtained easily, i.e.,

$$
\begin{aligned}
\mu &= \int_{-R}^{R} r dr \cdot p(r) A(\Delta V) = \frac{1}{12} \beta f(x_0) R^2 \\
\sigma^2 &= \int_{-R}^{R} (r - \mu)^2 dr \cdot p(r) A(\Delta V) = -\mu^2 + \frac{1}{6} R^2 \\
&= \frac{1}{6} R^2 + O(R^4).
\end{aligned}
\tag{3.13}
$$

We note that in the limit of infinitesimal R ($R \ll 1$), the change of $f(x)$ within a few Monte Carlo steps is negligible. Hence, according to the Central Limit theorem, after a large number n Monte Carlo steps, the spread of the displacement from x_0 approximates the normal distribution:

$$
P(\Delta x_{\mathrm{MC}}) = N(n\mu, n\sigma^2) = f(x_0) \cdot n \frac{1}{12} \beta R^2 + \eta \sqrt{2n \frac{1}{12} R^2},
\tag{3.14}
$$

where $\eta \sim N(0, 1)$ follows the standard Gaussian distribution. We note that the integration form (Ito's interpretation [33]) of the overdamped Langevin equation of Eq. (3.1) also results in a normal distribution of the displacement Δx after a

time interval Δt:

$$
\begin{aligned}
P(\Delta x_{\mathrm{LD}}) &= f(x_0)\Delta t + \int_0^{\Delta t} \xi(t)dt \\
&= f(x_0)\Delta t + \eta\sqrt{2D\Delta t}.
\end{aligned}
\tag{3.15}
$$

Comparing Eq. (3.14) and Eq. (3.15), we obtain a term-by-term equivalence between Δx_{MC} and Δx_{LD} if

$$
1 \text{ MCS} = \Delta t/n = \frac{1}{12}\beta R^2.
\tag{3.16}
$$

We find not surprisingly that the time quantification factor in Eq. (3.16) is identical to the one in Eq. (3.12) which we obtained from the Fokker-Planck approach.

The proof from the Central Limit Theorem explains the nature of the Monte Carlo dynamics. In the small R limit, several random walk steps reproduce a normally distributed displacement, which can be mapped to the displacement from a small time interval in the Langevin dynamics. In other words, both models are applicable to describe the low frequency dynamics (which is of the general interest) due to the central limit effect.

It will be beneficial for us to review some properties of the Central Limit Theorem now for some implications of our proof. The Central Limit Theorem can be presented as follows [34]: Let X_1, X_2, X_3, ... be a sequence of random variables which are identical and independently distributed. Assume that both the expected value μ and the standard deviation σ exist and are finite. Consider the sum $S_n = X_1 + ... + X_n$. The expected value of S_n is $n\mu$ and its standard error is $\sigma\sqrt{n}$. Furthermore, the distribution of S_n approaches the normal distribution $N(n\mu, n\sigma^2)$ as $n \to \infty$.

We notice that the Central Limit Theorem does not require a particular probability distribution for the random variables. We are therefore justified to choose an *arbitrary trial move step* and an *arbitrary acceptance rate* for the Monte Carlo
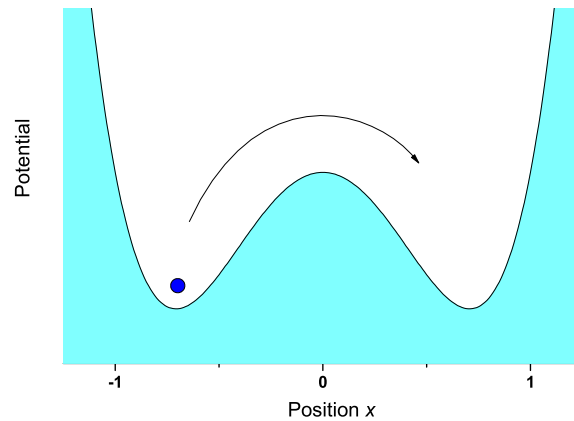
Figure 3.2: Schematics of the double potential profile.

method, as long as the mean and the standard deviation for the chosen parameters exist and are finite. This implies freedom to make improvements to the Monte Carlo model according to our needs for analysis, while preserving the equivalence to the physical Langevin model. We shall come back to this point later in this chapter.

3.4   Example: Double Well System

We now want to discuss some numerical verifications of the equivalence between the two stochastic models.

One of the simplest problems is the thermally activated dynamics in a bi-valley (double well) potential with infinite high walls on both sides, Fig. 3.2. We assume a potential profile as:

$$V(x) = -x^2(1 - x^2). \tag{3.17}$$
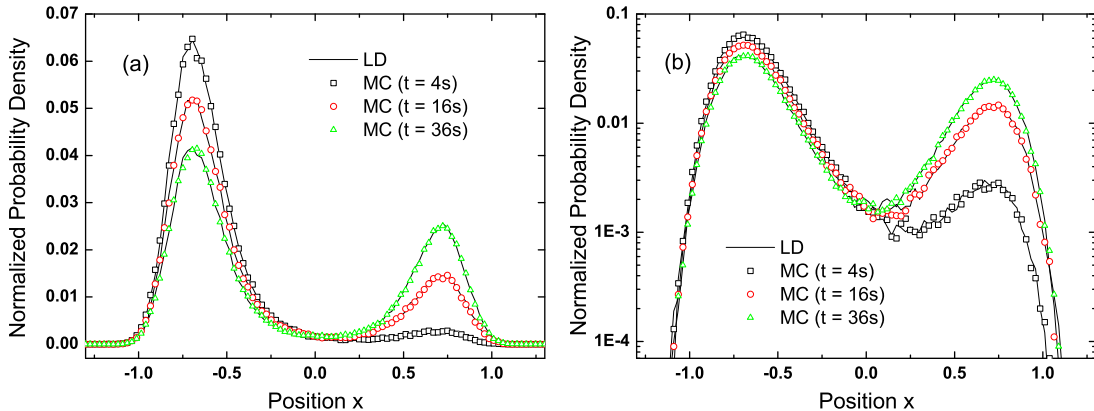
Figure 3.3: Time evolution behavior of the normalized probability distribution function in (a) linear scale and (b) logarithmic scale. Simulation parameters are: $V(x) = -x^2(1-x^2)$, $\Delta t_{\text{LD}} = 0.0001s$ in Langevin simulation and $R = 0.01$ in Monte Carlo simulation. Thermal condition $\beta = 12$ is used in both simulations. All results are averaged from a few thousand simulation runs. Error bars are smaller than the symbol size.

3.4.1 Time Dependent Probability Distribution

To verify the equivalence established in Eq. (3.11), we simulate the time dependent behaviors, e.g. the probability distribution function $W(x, t)$, of both Langevin dynamics and random walk Monte Carlo. Letting the time interval $\Delta t_{\text{LD}} = 0.0001$ (second) we ensure the accuracy of our Langevin simulations based on Eq. (3.1). In the heat-bath random walk Monte Carlo simulations, we choose a sufficiently small walk size of $R = 0.01$.

We assume that the Brownian particle starts at position $x_0 = -0.8$ and moves randomly. In Fig. 3.3 we plot the simulated normalized probability distribution with respect to position x after time $t = 4$s, 16s and 36s in both linear scale and logarithmic scale. We found that the Monte Carlo results converge with those from Langevin simulations to a very high accuracy. The convergence numerically
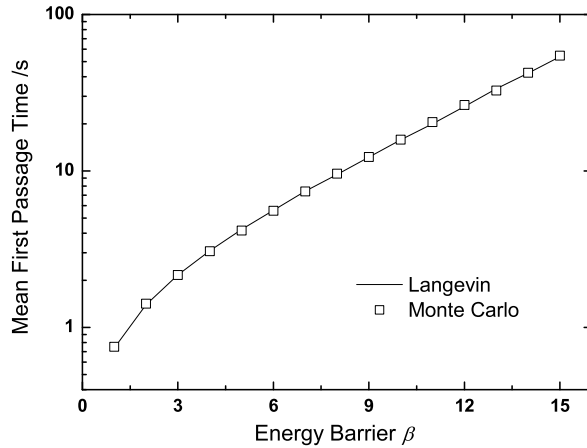
Figure 3.4: The mean first passage time with respect to the thermal condition $\beta = (k_B T)^{-1}$. Error bars are smaller than the symbol size.

verifies the equivalence between the Langevin dynamics and Monte Carlo method. We emphasize that the observed equivalence occurs during the whole relaxation process.

3.4.2 The Mean First Passage Time

In another test, we consider the mean first passage time for escape from an energy valley. The determination of mean first passage time, the inverse of which results in the Kramer's escape rate from the energy valley, has essential practical significance, e.g. in predicting the thermal stability of stored data in data storage devices [15]. In the present example, the mean first passage time is defined as the mean time elapsed for the particle to reach the peak point of the energy barrier ($x = 0$ for the potential profile as Eq. (3.17)).

Again, in Fig. (3.4) we observe a close match among results from Langevin simulation and the Monte Carlo simulation.

3.5   Comments and Remarks

In this Section, we discuss the various extensions and applications to the equivalence established in Eq. (3.11) between the Langevin dynamical equation and the Monte Carlo method.

3.5.1   Monte Carlo Method with Metropolis Rate

The Monte Carlo algorithm which adopts the Metropolis acceptance rate $A(\Delta V) = \min[1, \exp(\beta \Delta V)]$ can also reproduce the Maxwell-Boltzmann distribution at equilibrium by noting the detailed balance condition. We confirm that the Metropolis Monte Carlo can be mapped to the Langevin dynamics as Eq. (3.1) as well. Using the derivation techniques in Ref. [35], we can calculate the mean μ and variance σ^2:

$$
\begin{aligned}
\mu &= \frac{1}{6}\beta f(x_0) R^2 \\
\sigma^2 &= \frac{1}{3}R^2 + \frac{1}{8}\beta f(x_0) R^3 + O(R^4).
\end{aligned}
\tag{3.18}
$$

Truncating the μ and σ^2 to the order of $O(R^3)$ and following the same derivation process in Sec. 3.3, we achieve the equivalence formula for Metropolis Monte Carlo and Langevin dynamics:

$$
1 \text{ MCS}_{\text{Metropolis}} = \frac{1}{6}\beta R^2.
\tag{3.19}
$$

Previous studies [13] have proved that both Glauber(heat-bath) and Metropolis dynamics obey ergodicity and detailed balance. However, numerical simulations have revealed different dynamical process for these two Monte Carlo dynamics [36]. Our above derivation shows that both Glauber and Metropolis dynamics can converge to the Langevin dynamics under the assumption of infinitesimal $R \to 0$. Monte Carlo simulation with Metropolis rate is also able to reproduce the time-evolution distribution as in Fig. (3.3). However, a quick examination on statistical
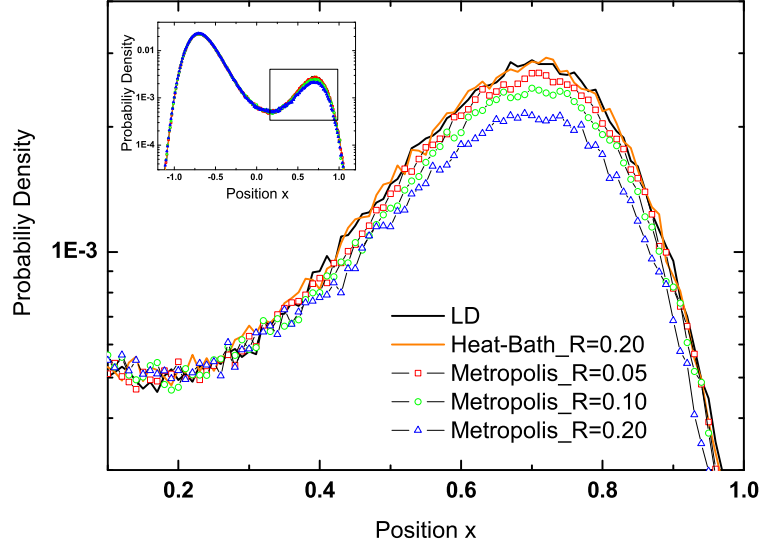
Figure 3.5: Comparison of the normalized probability density (partly) between Monte Carlo simulation and Langevin results. $V(x) = x^2(x^2 - 1)$, $x_0 = -0.8$, $t = 4$ s. Inset: the whole distribution density graph.

error shows that Metropolis Monte Carlo is less favored than the heat-bath Monte Carlo. To truncate the mean μ and variance σ^2 (Eq. (3.18)) to the order of R^2, we require:

$$\frac{1}{8}\beta f(x_0)R^3 / \frac{1}{3}R^2 = \frac{3}{8}\beta f(x_0)R \ll 1 \qquad (3.20)$$

which leads to

$$R \ll \left(\frac{3}{4}\beta f(x_0)\right)^{-1}. \qquad (3.21)$$

Comparing to the high order requirement for the heat-bath rate [c.f. Eq. (3.13)]:

$$\mu^2 / \frac{1}{6}R^2 \ll 1$$
$$\Rightarrow \quad R^2 \ll \left(\frac{1}{2}\beta f(x_0)\right)^{-2}, \qquad (3.22)$$

the use of Metropolis acceptance rate in the time quantified Monte Carlo method requires the step size R being about *an order smaller* than the step size used in the

heat-bath rate. This is thus generally undesirable. This can be seen in Fig. (3.5) where we observe large discrepancy for the random walk Monte Carlo algorithm using the Metropolis rate with $R = 0.05, 0.10, 0.20$, while very good convergence can be found for MC algorithm using heat-bath rate with $R = 0.20$.

3.5.2 Random Walk for High Frequency Dynamics

According to the Central Limit Theorem, the trial move in the Monte Carlo model is not limited to be uniformly distributed, but can adopt any type of distribution, subject to the requirement of finite mean and variance. This provides flexibility in choosing the appropriate trial move distribution in order to improve the simulation efficiency. At low frequency, the Central Limit Theorem guarantees that the random walk Monte Carlo converges to Langevin dynamics with Gaussian white noise.

The Monte Carlo model however, from this point of view, is particularly useful in some high-frequency analysis, e.g. high-frequency finance [4], in which the distribution of change in a small period of time is not Gaussian distributed (c.f. Gaussian type of white noise in Langevin dynamics). Such discussion is however beyond our exploration but still worthy to be remarked.

3.5.3 Interacting Systems

We confirm that the time quantification also works under inter-variable coupling condition. A rigorous proof can be obtained by comparing the Fokker-Planck coefficients for both Monte Carlo and Langevin dynamics, see Ref. [37] for examples on interacting spin array dynamics, as well as the Brownian dynamics with hydrodynamic interaction [19].

3.5.4   Monte Carlo Algorithm for Nonequilibrium Dynamics

The Monte Carlo algorithm is also applicable in reproducing some non-standard stochastic differential equations as Eq. (3.1). Consider an Langevin equation of more general form:

$$\dot{x} = -V'(x, z(t)) + \xi(t)$$

where $z(t)$ is a time dependent function with characteristic time τ_c, hence forcing the system in a non-equilibrium condition. We are however always able to have a sufficiently small random walk size $R \rightarrow 0$ so that 1 MCS $\ll \tau_c$. In this limit the Central Limit Theorem proves the validity of the time quantification of the Monte Carlo.

3.5.5   Time Quantification of the Master Equation

The Monte Carlo method with fixed (discrete) trial move step size R provides a numerical solution to the Master equation

$$\frac{dP(\sigma, t)}{dt} = \sum_{\sigma'} [w(\sigma' \rightarrow \sigma)P(\sigma', t) - w(\sigma \rightarrow \sigma')P(\sigma, t)] \tag{3.23}$$

under the assumption that only transitions between adjacent (nearest neighbor) states are allowed. σ and σ' in Eq. (3.23) are adjacent states of the configuration, $P(\sigma, t)$ is the probability density the system is in state σ at time t, and $w(\sigma' \rightarrow \sigma)$ is the heat-bath transition rate from state σ' to σ. Without much effort one may find the time quantification factor for Eq. (3.23) [38] by comparing with the Langevin model $\mathcal{LD}1$:

$$1 \text{ MCS} = \frac{1}{2}\beta R^2. \tag{3.24}$$

It is worthy to remark that Kampen [39] made an similar observation by deriving the diffusion equation for a master equation, which is used to describe jumps

between adjacent energy minima in a periodical potential.

3.5.6   Special Comments for Low Damping Dynamics

The random-walk Monte Carlo algorithm is well-suited to represent energy dissipative dynamical motion, but not energy conservative dynamics. For a dynamical equation under low friction condition: e.g.

$$m\ddot{x} + m\gamma\dot{x} + V'(x) = m\Gamma(t) \tag{3.25}$$

where $\Gamma(t)$ represents the stochastic thermal fluctuation, a hybrid algorithm which combines Monte Carlo random move with a deterministic move is required to describe the whole dynamics in Eq. (3.25):

(i) a Monte Carlo random move for $\dot{v} = -\gamma v + \Gamma(t)$, $(v \equiv \dot{x})$; and

(ii) a deterministic move for $\Delta x = v\Delta t; \Delta v = -V'(x)\Delta t$.

Combination of the two types of moves could give the desired Fokker-Planck equation that is equivalent to the one corresponding to Eq. (3.25). A typical example will be presented in Chap. 5 where we develop a hybrid algorithm for low damping Langevin equation in stochastic micromagnetics.

3.5.7   Simulation Efficiency

Though Monte Carlo methods are usually considered to be more efficient than the direct Langevin integration, in our simulation we do not observe significant difference in efficiency between the Monte Carlo simulation and the Langevin simulation. This can be understood that the Monte Carlo simulation shall mimic all trajectories that provided by the Langevin dynamics, due to the microscopic equivalence. According to our experience in micromagnetic studies, the Monte Carlo simulations are usually 3–5 times faster than the Langevin simulations, probably because the

fact that Monte Carlo simulations significantly reduce the computational efforts in cross products.

The microscopic equivalence between the Langevin model and the Monte Carlo method however sheds light on applying advanced Monte Carlo techniques to speed up the simulation. This topic is not covered in the present thesis but deserved certainly further research efforts.

Chapter 4

Brownian Motion in One-Dimensional Random Potentials

In Chap. 3 we have shown the equivalence between a heat-bath random walk Monte Carlo model and the overdamped Langevin dynamical equation. This enables us to use the Monte Carlo model to analyze the stochastic processes, such as the thermally induced stochastic dynamics in real physical problems.

In this and the next Chapters, we shall devote to two applications of the random walk Monte Carlo method. Our main focus in this chapter is the transport problem for an overdamped Brownian particle in a one dimensional periodical potential. Many practical problems can be mapped to this model. Hence characterizing the Brownian particle's transport in such a system is of practical interest.

4.1 Introduction to Brownian Ratchets

4.1.1 Overview

The problem of Brownian motion in a periodical potential arises from several fields of science. Restricting ourselves to the one-dimensional case, we deal with particles which are impacted about by Langevin forces (thermal fluctuations) and move in a one-dimensional periodic potential. Typical examples of Brownian motion in aperiodical potential may include but not be limited to the Josephson tunneling junction (two superconductors separated by a thin oxide layer) [25, 40, 41], superionic conductors [42, 43], a pendulum in a viscous fluid, and rotation of dipoles in a constant field [44, 45]. Additionally, the periodic potentials can also be classified into symmetric profiles (Fig. 4.1a) and asymmetric profiles (Fig. 4.1b). Symmetric periodic potentials, especially the sinusoidal potential model, are widely adopted in real physical problems such as a Josephson tunneling junction and pendulum problems.

Our research interests, however, focus on the transport phenomena of Brownian particles in asymmetric periodic potentials (usually termed as ratchet potentials). Affected by the thermal fluctuations, the Brownian particle in the valley spreads according to its probability distribution on both directions. According to the second law of thermodynamics, we should observe *no directed transport* (or no net probability current) of Brownian particles in unbiased periodic potentials in thermal equilibrium, regardless of the profile of the periodic potential.

For asymmetric system in non-equilibrium condition however, a net probability current can be possible. For instance, an oscillating driving force applied on Brownian particles in asymmetric periodic potentials can cause directed transport, i.e. imbalanced current [46, 47, 48, 49, 50]. The keen scientific interest in the transport property of Brownian ratchets is attributed to their role in biological systems, e.g.
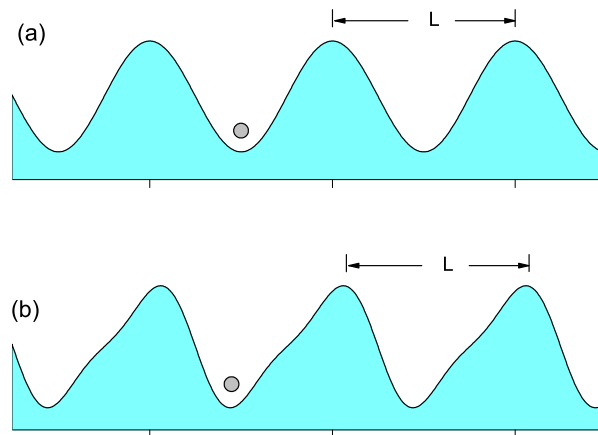
Figure 4.1: Schematic diagram of L-periodic potential profiles for (a) a symmetric (sinusoidal) periodic potential: $V(x) = \sin(2\pi x/L)$; and (b) asymmetric periodic potential (ratchets): $V(x) = \sin(2\pi x/L) + 0.25\sin(4\pi x/L)$.

the astonishing energy-motion conversion of ATP hydrolysis [51]. and the potential of using ion pumps to power the uphill transport of ions [52, 53, 54]. Here we introduce several type of Brownian ratchets:

The flashing ratchets

"On-Off" ratchets, the simplest form of flashing ratchets, switches between the "On" state potential and "Off" state potential. As shown in Fig. (4.2), when the potential is off, a particle moves to the left and right with appropriate probabilities. After some time, the potential is turned on and the particle is trapped at the bottom of a well - more likely the well to the right than the well to the left of where the particle started. Hence, this leads to a directed probability current towards to the right.

Bier and Astumian further investigated a 3-state fluctuating potential
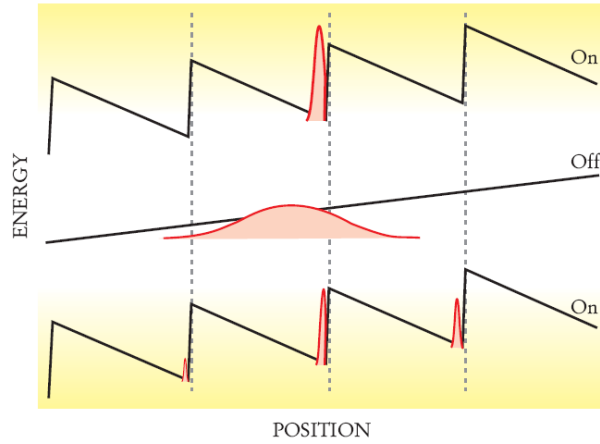
Figure 4.2: Schematic diagram of an On-Off ratchet. A right direction favored in transport is possible even when a small force is applied to the left in this case. Figure drawn from Ref. [48]

and found that current reversal is possible by varying the system configurations [55]. This suggests a possible application for construction of a device for the separation of small particles [56, 57].

Ratchets driven by external force

An oscillating driving force applied on Brownian particles in asymmetric periodic potentials can cause directed transport. The driving force can be, for example a sinuous force, a periodical two state force, a Markovian dichotomous noise (telegraph noise) or a Markovian colored noise such as the Ornstein-Uhlenbeck process [12]. Many research works have been focused on this type of ratchets, due to their potential to build a controllable device for biological applications. For example, as shown by Kula *et al.* asymmetry in the potential profile and dichotomous fluctuations can result in current reversal [58].

Temperature ratchets

In temperature ratchets, the thermal noise intensity is set to be oscillating. This is similar to the On-Off ratchets but physically it is proposed to model the variation of some thermodynamical variables such as pressure and volume [46].

4.1.2 Description of the Problem

One of the key questions in the study of Brownian ratchets is obtaining the expression for the current. This will be useful in, e.g. identifying the conditions for current reversal. Thus, an analytical solution of the problem would be of much interest and importance. In general, the stochastic transport in the ratchets is modeled by Langevin equations of the form:

$$\gamma \dot{x} = -U'(x, z(t)) + \xi(t), \tag{4.1}$$

where $\xi(t)$ is a mean zero Gaussian white noise term, i.e. $\langle \xi(t)\xi(s) \rangle = 2\gamma k_B T \cdot \delta(t - s)$, and $z(t)$ is a Markov dichotomous process with correlation time τ_c. $\xi(t)$ represents the effects of thermal fluctuations, while $z(t)$ models stochastic processes such as impurities or defects jumping between metastable states [58]. The current is calculated by solving the corresponding Fokker-Planck equation under periodic boundary conditions. However, the explicit current expression can only be obtained for a few simple cases [58, 59, 60], due to the complexity of dichotomous processes induced dynamics. For non-trivial cases, the ratchet current can be calculated by simulating the Langevin equation [61] or from numerical solutions of the Fokker-Planck equations [55].

Numerical calculations are computationally intensive and do not yield as much physical insights as analytical solutions. Our objective is thus to derive the analytical expression of the current for an arbitrary ratchet potential.

4.2   Methods and Models

Unlike previous methods, we based derivation of the current in ratchets on the Monte Carlo scheme, specifically the Gambler's Ruin model.

In the *Gambler's Ruin* problem, a player plays a series of games against an adversary, winning (or losing) one dollar for every success (or failure), until one of them is "ruined". Given the probability of winning each game, the Gambler's Ruin problem considers the probability of ultimate ruin of one of the players, as well as the number of games required [34]. In this Chapter, we show an intimate relationship between this classic random walk problem and the thermally activated dynamics in arbitrary potentials. The linkage between these two disparate topics is made possible by recent advances in the time quantification of Monte Carlo [20, 35, 62, 63]. In particular, the evolutionary techniques for the Gambler's Ruin problem can be utilized to analyze the transition probabilities and the mean first passage time (MFPT) of the complex stochastic transport in Brownian ratchets.

Our analysis is presented in three main stages: i) First, we justify the theoretical basis of using the Monte Carlo approach. This is done by establishing the time-quantification factor between a Monte Carlo step (MCS) and real time in seconds; ii) Second, we formulate the Brownian ratchet problem in the Monte Carlo framework. Each periodic unit of the ratchet is first discretized into a finite site chain with absorbing boundaries. The stochastic transport in the ratchets thus reduces into random walks within the site chain. This is essentially the classic Gambler's Ruin problem, with some modifications to account for the dichotomous process; and iii) Finally, by applying the evolutionary techniques in the Gambler's Ruin model, we analytically derive the expression of ratchets current for the thermal equilibrium case, and the more complex case of dichotomous noise. By applying the aforementioned time-quantification factor the current expression is verified by means of numerical Langevin simulations.

4.2.1 Random Walk Method with Discrete Step

To utilize the evolutionary techniques, i.e. difference equations, in the Gambler's Ruin model, We choose the heat-bath random walk Monte Carlo method with *discrete step* as the base of our analysis. This leads to a slight difference between the present model and the 1-D random walk model ($\mathcal{MC}1$) we introduced in Sec. 3.1. Hence the time quantification of the MCS for the present model has to be first justified.

Following Sec. 3.3, time quantification of the MCS is most easily introduced by considering an overdamped Brownian particle in a steady potential $U(x, z(t)) = V(x)$. The random walk on x takes a fixed length trial move: $\Delta x = -R, R$ ($R \rightarrow 0$) with equal trial probability in both directions but subject to the heat-bath acceptance rate of $A(\Delta V) = 1/(1 + \exp(\beta \Delta V))$. Here ΔV is the energy difference in the proposed transition and $\beta \equiv 1/k_B T$. Expanding the heat-bath acceptance rate, i.e.,

$$
\begin{aligned}
A(\Delta V) &= 1/[1 + \exp(\beta \Delta V)] \approx \frac{1}{2}\left[1 - \frac{1}{2}\beta\left(\frac{dV}{dx}\Delta x\right)\right] \\
&= \frac{1}{2}\left[1 + \frac{1}{2}\beta f(x)\Delta x\right]
\end{aligned}
$$

we obtain the mean μ and variance σ of Δx in *one* MCS:

$$
\begin{aligned}
\mu &= \sum_{\Delta x = \pm R} \frac{1}{2}\Delta x \cdot A(\Delta V) = \frac{1}{4}\beta f(x)R^2 \\
\sigma^2 &= \sum_{\Delta x = \pm R} \frac{1}{2}\Delta x^2 \cdot A(\Delta V) = \frac{1}{2}R^2 + O(R^4)
\end{aligned}
\tag{4.2}
$$

where $f(x) = -V'(x)$ is the external force. Since $R \ll 1$, the change of $f(x)$ within a few MCS is negligible. According to the Central Limit Theorem, after a large number n MCS the spread of displacement from x_0 approximates the normal distribution:

$$
P(\Delta x_{\text{MC}}) = N(n\mu, n\sigma^2) = f(x_0) \cdot n\frac{1}{4}\beta R^2 + \eta\sqrt{2n\frac{1}{4}R^2},
\tag{4.3}
$$

where $\eta \sim N(0,1)$ follows the standard Gaussian distribution. We note that the integration form (Ito's interpretation) of the overdamped Langevin equation of Eq. (4.1) also results in a normal distribution of the displacement Δx after a time interval Δt:

$$P(\Delta x_{\mathrm{LD}}) \;\; = \;\; \frac{1}{\gamma} f(x_0)\Delta t + \eta\sqrt{2(k_B T/\gamma)\Delta t}. \qquad (4.4)$$

Comparing Eq. (4.3) and Eq. (4.4), we obtain a term-by-term equivalence between Δx_{MC} and Δx_{LD} if

$$1 \text{ MCS} = \Delta t/n = \gamma\beta R^2/4. \qquad (4.5)$$

Since the dichotomous process $z(t)$ simply produces transitions between the two potential profiles, the equivalence established in Eq. (4.5) is still valid in the presence of $z(t)$, subject to the condition that $1 \text{ MCS} \ll \tau_c$. Such requirement can always be fulfilled by choosing an infinitesimal $R \to 0$. This equivalence justifies the use of MC methods to analyze the ratchet current instead of the Langevin equation.

4.2.2   Definition of Ratchets Current

Macroscopically, the transport in L-periodic ratchets can be characterized as a series of successive "$\mathcal{L}$-transitions". An $\mathcal{L}$-transition is said to occur when a stochastic particle which is initially at x reaches an equivalent site a period away in either direction i.e. $x + L$ or $x - L$, as shown in Fig. (4.3). Individually, an $\mathcal{L}$-transition can be analyzed as a classic random walk problem with absorbing boundaries. We define the forward transition probability as the probability of being absorbed to the right boundary $g \equiv p(x \to x + L)$, during the $\mathcal{L}$-transition. Conversely, the backward transition probability is defined as $h \equiv p(x \to x - L)$. Since the particle will ultimately reach either of the absorbing boundaries after a sufficiently long time, we have $g + h = 1$. The difference between g and h results in a non-zero
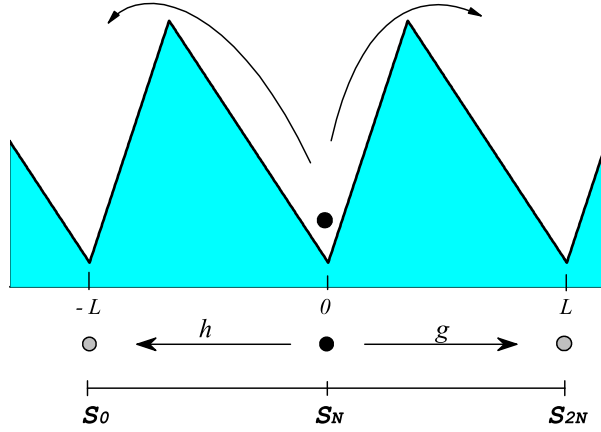
Figure 4.3: Schematic diagram of a L-periodic ratchet potential.

current, and we thus have the steady current:

$$\langle \dot{x} \rangle := \lim_{t \to \infty} \frac{x(t) - x(0)}{t} = \frac{(g-h)L}{\tau_{\mathrm{MFPT}}}, \tag{4.6}$$

where τ_{MFPT} is the MFPT for the particle starting at position x to hit either boundary at $x + L$ or $x - L$. τ_{MFPT} is a critical factor in describing the transport in the ratchets and has been studied for limited cases [60, 64].

Based on Eq. (4.6), we require the analytical solutions for g, h and τ_{MFPT} in order to obtain the current expression.

4.3 Brownian Ratchets in Thermal Equilibrium

We start our analysis with a simple illustrative case – thermal equilibrium Brownian ratchets without a driven noise, i.e. $U(x, z(t)) = V(x)$. We first discretize the ratchets of length $2L$ into $2N + 1$ micro-sites, i.e. $\{S_0, \ldots, S_{2N}\}$ as illustrated in Fig. (4.3). A particle starts at site S_m, and moves to adjacent micro-sites randomly, e.g. with steady probability μ_m to site S_{m-1} and with probability w_m to site S_{m+1} (see Fig. (4.4)). We define $g(m)$ as the probability that the particle from site S_m
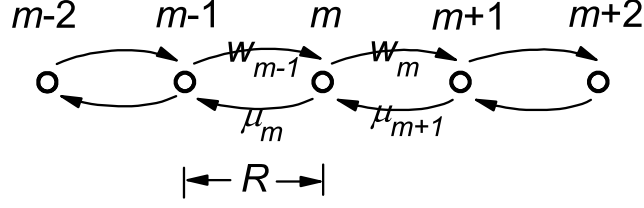
Figure 4.4: Schematic diagram of the random walk algorithm.

reachs the end site S_{2N} before it reaches the site S_0. We further define $\tau(m)$ as the MFPT (in MCS) for the particle to reach either end site S_0 or S_{2N}. At the next MCS, the particle can either move to the left or right, or stay put. According to the Gambler's Ruin problem [34], we obtain the difference relations for $g(m)$ and $\tau(m)$:

$$g(m) = \mu_m \cdot g(m-1) + w_m \cdot g(m+1) + (1 - \mu_m - w_m) \cdot g(m) \qquad (4.7)$$

$$\tau(m) = \mu_m \cdot \tau(m-1) + w_m \cdot \tau(m+1) + (1 - \mu_m - w_m) \cdot \tau(m) + 1, \quad (4.8)$$

which are analogous to those of the Gambler's Ruin problem. The initial conditions $g(0) = 0$, $g(2N) = 1$ and $\tau(0) = \tau(2N) = 0$ apply.

The solution to Eq. (4.7) can be obtained by the recurrence relation:

$$g(m+1) - g(m) = (\mu_m/w_m)(g(m) - g(m-1)).$$

Starting from the middle minima i.e. $m = N$, we can obtain the forward transition probability g between the adjacent supersites:

$$g = g(N) = \frac{\sum_{i=0}^{N-1} k(i)}{\sum_{i=0}^{2N-1} k(i)} = \frac{1}{1 + k(N)}, \qquad (4.9)$$

where $k(0) \equiv 1$, $k(m) \equiv \prod_{i=1}^{m} \mu_i/w_i$ for $m \geq 1$. In the last step we have used the periodic condition: $\mu_j = \mu_{N+j}$ and $w_j = w_{N+j}$, which leads to $k(N+i) = k(N) \cdot k(i)$. The backward transition probability can be obtained immediately from $h = (1-g)$.

Similarly for Eq. (4.8), after some simplification we obtain, for $m = N$:

$$\tau_{\text{MFPT}} = \tau(N) = g \cdot \sum_{i=1}^{N} \left((w_i k(i))^{-1} \sum_{j=i}^{N+i-1} k(j) \right). \tag{4.10}$$

Substituting the heat-bath rate definition $\frac{1}{1+\exp(\beta \Delta V)}$ for w_i and μ_i into $k(i)$, we obtain: $k(i) = (w_0/w_i)e^{\beta V_i} = 2w_0(e^{\beta V_i} + e^{\beta V_{i+1}})$, where V_i is the potential at the ith site and $V_0 \equiv 0$. Particularly, $k(N) = \exp(\beta V_N)$ since $w_0 = w_N$. Thus, by considering Eqs. (4.5) and (4.6), the current expression for ratchets in thermal equilibrium converges to the well-discussed continuous form [12] as $N \to \infty$:

$$\langle \dot{x} \rangle = \frac{(g-h)L}{\tau_{\text{MFPT}}} = \frac{L \cdot (1 - e^{\beta V(L)})}{\gamma \beta \int_0^L dx \, e^{-\beta V(x)} \int_x^{x+L} dy \, e^{\beta V(y)}}. \tag{4.11}$$

We shall also point out that for $N = 2$, our above discussion reduces to the three-state discrete-time minimal Brownian ratchet model [65]. In particular, if we replace the transition rates with $\mu_i' = \tilde{\gamma}\mu_i + \gamma/2$ and $w_i' = \tilde{\gamma}w_i + \gamma/2$ following the definitions in Ref. [65], we achieve the same current expression via Eq. (4.6) directly.

4.4 Brownian Ratchets Driven out of Equilibrium

We now generalize our analysis to a non-equilibrium case, i.e. with an additional dichotomous noise $z(t)$ applied to the ratchets potential. We consider a mean-zero $z(t)$, which takes two discrete values $\{1, -\theta\}(\theta > 0)$ with correlation $\langle z(t)z(s) \rangle = \theta \exp(-|t-s|/\tau_c)$ [66]. For clarity, we denote "+" and "−" as representing the two states $z = 1$ and $z = -\theta$ respectively. Similar to our previous analysis, we define $g(m; \sigma; \sigma')$ as the probability for a particle at initial site S_m with $z(0) = \sigma$ to reach the absorbing site S_{2N} after some time t with $z(t) = \sigma'$ before it reaches the other

absorbing site S_0. We also define $\tau(m; \sigma)$ as the MFPT for the particle starting at S_m under $z(0) = \sigma$ to reach any end sites.

$g(m; \sigma; \sigma')$ can be generalized from Eq. (4.7), i.e.

$$g(m; \sigma; \sigma') = \sum_{\tilde{\sigma}=\pm} v(\tilde{\sigma}|\sigma) \cdot \left[w_m^{\tilde{\sigma}} g(m+1; \tilde{\sigma}; \sigma') + \mu_m^{\tilde{\sigma}} g(m-1; \tilde{\sigma}; \sigma') \right.$$
$$\left. + (1 - w_m^{\tilde{\sigma}} - \mu_m^{\tilde{\sigma}}) g(m; \tilde{\sigma}; \sigma') \right], \qquad (4.12)$$

where $v(\tilde{\sigma}|\sigma)$ is the transition probability for dichotomous state from σ to $\tilde{\sigma}$ in *one* MCS [66]. $w_m^{\tilde{\sigma}}$ and $\mu_m^{\tilde{\sigma}}$ denote the spatial transition rates at dichotomous state $z = \tilde{\sigma}$. Equation (4.12) can be rewritten into a 2×2 matrix difference equation. After some algebra we obtain:

$$G_{m+1} = W_m^{-1} (\lambda \cdot C + W_m + U_m) \cdot G_m - W_m^{-1} U_m \cdot G_{m-1}, \qquad (4.13)$$

where $\lambda \equiv \frac{v(-|+)}{1 - v(-|+) - v(+|-)} \ll 1$, $W_m = \text{Diag}\{w_m^+, w_m^-\}$, $U_m = \text{Diag}\{\mu_m^+, \mu_m^-\}$, and

$$C = \begin{pmatrix} 1 & -1 \\ -\theta & \theta \end{pmatrix}; \quad G_m = \begin{pmatrix} g(m; +; +) & g(m; +; -) \\ g(m; -; +) & g(m; -; -) \end{pmatrix}.$$

The initial conditions are $G_0 = \mathbf{0}$; $G_{2N} = \text{Diag}\{1, 1\} \equiv I$. Again, setting the starting position $m = N$, we obtain the *forward transition probability matrix*: $G = G_N$.

By giving the details of derivation in Appendix A, we give directly the explicit solution to G, at $N \to \infty$:

$$G = Q(L) \cdot [Q(2L)]^{-1}. \qquad (4.14)$$

Here $Q(y) = \{q(y; \sigma; \sigma')\}$ is a 2×2 matrix with $q(y; \sigma; \sigma')$ having the definition:

$$\frac{\sigma\sigma'}{|\sigma\sigma'|} q(y; \sigma; \sigma') = \delta_{\sigma\sigma'} \int_0^y dx \cdot e^{\beta U(x,\sigma)}$$

$$+ \sum_{n=2}^{\infty} \left(\frac{\gamma\beta}{(1+\theta)\tau_c}\right)^{n-1} \left[\sum_{\substack{\sigma_1 = \sigma'; \sigma_n = \sigma; \\ \text{other } \sigma_i = \pm}} \int_{x_0=0}^{x_n=y} \int_{x_0}^{x_{n-1}} \cdots \int_{x_0}^{x_2} dx_{n-1} \dots dx_1 \right.$$

$$\left. \cdot \left(\prod_{j=2}^{n} |\sigma_j| \int_{x_{j-1}}^{x_j} dx \cdot e^{\beta[U(x,\sigma_j) - U(x_j,\sigma_j)]} \right) \cdot \int_{x_0}^{x_1} dx \cdot e^{\beta U(x,\sigma_1)} \right]. \quad (4.15)$$

The *backward transition probability matrix* H can be calculated in a similar manner.

Similarly, the calculation of $\tau(m; \sigma)$ is based on the difference equation that generalized from Eq. (4.8):

$$\tau(m; \sigma) = \sum_{\tilde{\sigma}=\pm} v(\tilde{\sigma}|\sigma) \cdot \left[w_m^{\tilde{\sigma}} \tau(m+1; \tilde{\sigma}) + \mu_m^{\tilde{\sigma}} \tau(m-1; \tilde{\sigma}) \right.$$

$$\left. + (1 - w_m^{\tilde{\sigma}} - \mu_m^{\tilde{\sigma}}) \tau(m; \tilde{\sigma}) \right] + 1, \quad (4.16)$$

which leads to the matrix difference equation:

$$W_m \cdot T_{m+1} = (\lambda \cdot C + W_m + U_m) \cdot T_m - U_m \cdot T_{m-1} - E, \quad (4.17)$$

where $T_m = (\tau(m; +), \tau(m; -))^T$, $E = (1,1)^T$ and $T_0 = T_{2N} = 0$. The explicit solution to the *MFPT matrix* $T = T_N$, has the form:

$$T = G \cdot R(2L) - R(L) \quad (4.18)$$

as $N \to \infty$, where the matrix $R(y) = (r(y; +), r(y; -))^T$, with $r(y; \sigma)$ given by:

$$\frac{r(y; \sigma)}{\gamma\beta} = \sum_{n=2}^{\infty} \left(\frac{\gamma\beta}{(1+\theta)\tau_c}\right)^{n-2} \left[\sum_{\substack{\sigma_{n-1} = \sigma; \\ \text{other } \sigma_i = \pm}} \int_{x_0=0}^{x_n=y} \int_{x_0}^{x_{n-1}} \cdots \int_{x_0}^{x_2} dx_{n-1} \dots dx_1 \right.$$

$$\left. \frac{|\sigma|}{\sigma\sigma_1} \cdot \prod_{j=1}^{n-1} |\sigma_j| \int_{x_j}^{x_{j+1}} dx \cdot e^{\beta[U(x,\sigma_j) - U(x_j,\sigma_j)]} \right]. (4.19)$$

With the transition probabilities G, H and the MFPT T, the expression for the steady state current can be derived. We note $Z = G + H$ is the actual *transition*

matrix for the probability distribution of dichotomous state over one $\mathcal{L}$-transition. Hence, the steady state (after $n \to \infty$ transitions) yields the following probabilities of the dichotomous states at the start of the $(n+1)^{\text{th}}$ $\mathcal{L}$-transition: $\text{Prob}(z = 1) = Z_{21}/(Z_{12} + Z_{21})$ and $\text{Prob}(z = -\theta) = Z_{12}/(Z_{12} + Z_{21})$. The effective forward transition probability is then given by the weighted sum: $g_{\text{eff}} = \sum_{\sigma,\sigma'} \text{Prob}(z = \sigma)g(N;\sigma;\sigma')$, and similarly for h_{eff}. Based on Eq. (4.6), this then leads to our main result, i.e. the analytical expression of the ratchets current:

$$\langle \dot{x} \rangle = \frac{G_{11} + G_{22} - H_{11} - H_{22} - 2(|G| - |H|)}{(G_{21} + H_{21})T_1 + (G_{12} + H_{12})T_2} L. \tag{4.20}$$

For verification, we performed a numerical simulation based on the Langevin equation of Eq. (4.1), and assuming a ratchet potential profile of:

$$U(x, z(t)) = \begin{cases} -\frac{1}{\hat{k}}L\hat{x} - z(t) \cdot Fx; & \hat{x} \leq \hat{k} \\ \frac{1}{1-\hat{k}}L\hat{x} - z(t) \cdot Fx; & \hat{x} > \hat{k} \end{cases}, \tag{4.21}$$

where $\hat{x} = x - [x/L]$, and $\hat{k} = 2/3$ reflects the asymmetry of the potential [58].

In Table (4.1), the simulated and analytical results for the forward transition probability G are in agreement with each other within simulation errors. In Fig. (4.5), we plotted the particle current from the Langevin simulation and found extremely close agreement with the predictions of Eq. (4.20). We remark that recurring Eqs. (4.13) and (4.17) is a very efficient approach to calculate the G, H and T to arbitrary precision as $N \to \infty$.

Asymmetry in potential profile and dichotomous fluctuations can result in current reversal [58]. The MC method enables us to obtain precisely the vanishing current condition (see the inset of Fig. 4.5) which is of importance in rectifying particles with only small differences in γ. Interestingly, since $\lambda \cong \frac{\Delta t}{(1+\theta)\tau_c} = \frac{\gamma}{\tau_c} \frac{\beta R^2}{4(1+\theta)}$, from Eq. (4.15) we found (γ/τ_c) determines the current direction. In Figs. (4.5) and (4.6), we observed two facts: 1) there is a *threshold temperature* β_c, below which no current reversal can occur regardless of γ and τ_c, and 2) the zero-current condition

Table 4.1: A comparison between simulated forward transition probabilities matrix G and our exact results. Simulation parameters are: $L = 1.0$, $F = 0.6$, $\theta = 0.42$, $\hat{k} = 0.333$, $\beta = 2$ and $\gamma/\tau_c = 2$. The difference between the simulation results and the exact analytical values from Eq. (4.14) was found to be within 1% and within the simulation errors.

G	Langevin simulation		Exact values	
	+	−	+	−
+	0.346(3)	0.234(2)	0.346387	0.233022
−	0.165(2)	0.300(3)	0.164366	0.300344

H	Langevin simulation		Exact values	
	+	−	+	−
+	0.118(1)	0.303(3)	0.117946	0.302644
−	0.0724(7)	0.462(5)	0.072188	0.463101
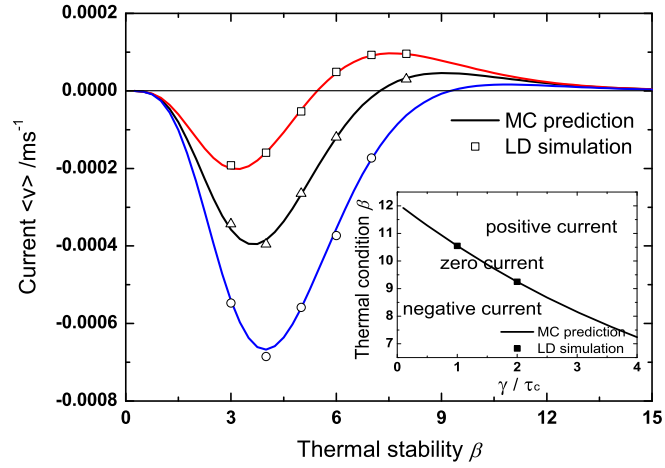
Figure 4.5: Temperature-driven reversal of ratchets current. Close agreement between analytical MC prediction and Langevin dynamical (LD) simulation. The simulation parameters are: $R = 0.005$, $L = 1.0$, $F = 0.6$, $\theta = 0.42$, $\gamma = 1$ and $\tau_c = 0.15, 0.25, 0.5$ from top to bottom. Error bars are smaller than the symbol size. Inset: extracted zero-current curve with respect to γ/τ_c.
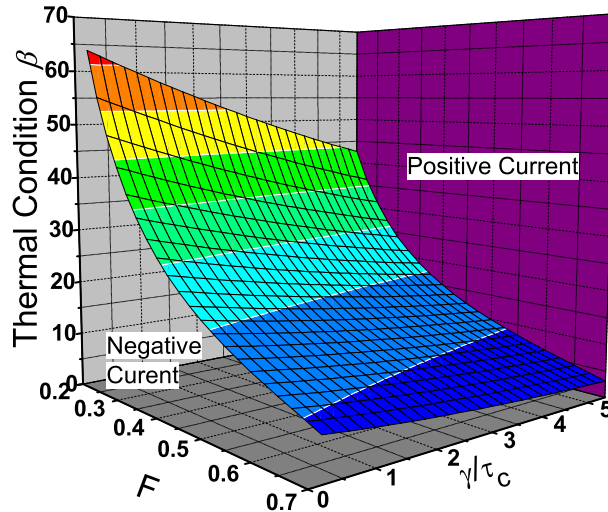
Figure 4.6: The zero-current surface with respect to parameters β, γ/τ_c and F.

curve is *monotonic* in character, i.e. a decrease in the required γ/τ_c with increasing β. A qualitative explanation may be obtained by considering the energy barrier between the adjacent energy minima, ΔV^+, ΔV^-, when the ratchet is tilted by the dichotomous noise $z = 1$ and $z = -\theta$ respectively. In the present application, $\Delta V^+ < \Delta V^-$, and hence a positive current occurs in the limit of high β. While at *low β* and *large τ_c* limit that $\tau_{\mathrm{MFPT}} \ll \tau_c$, a negative current will be formed if $[\exp(-\beta\Delta V^+)/\theta] < \exp(-\beta\Delta V^-)$. Therefore, the bottom-left (top-right) corner of the phase diagram of Fig. (4.6) corresponds to a negative (positive) current region, thus implying a monotonic trend of the zero-current surface dividing the two regions.

4.5 Generalizations and Conclusion

Note that the analytical ratchet current in Eq. (4.20) is derived without the assumption of low temperature as in [60]. For the specific case of $N = 2$, our discussion on ratchets transport in the presence of dichotomous process reduces to the minimal Astumian game [67]. Additionally, the above Monte Carlo analysis can reasonably be extended to ratchets driven by an n-state process or even an Ornstein-Uhlenbeck (O-U) process [12] (an O-U process is equivalent to an infinite n-state process from the Monte Carlo point of view). With some modifications, the Monte Carlo analysis can also be applied to model the temperature (generalized Smoluchowski-Feynman) ratchets [46].

To summarize, we presented a time-quantified MC method, based on and extended from the Gambler's Ruin problem, to analyze the directed transport in overdamped Brownian ratchets. By considering the transition probabilities and the MFPT between the adjacent minima of the periodic ratchet, we derived the analytical expression for the current in the presence of dichotomous noise, as well

as the vanishing current condition. Generally, the Monte Carlo formalism offers an alternative way to solve intractable stochastic dynamics and the corresponding Fokker-Planck equations. Extensions to the classic Gambler's Ruin or other MC problems, e.g. inclusion of correlations [68] or multiple currencies [69], may yield further insights into other areas of stochastic dynamics, e.g. turbulence or high-dimensional thermally activated dynamics.

Thermally Activated Dynamics of Several Dimensions: A Micromagnetic Study

In this chapter we discuss methods for solving thermally activated dynamics in higher dimensions. In particular, we focus our research in the area of micromagnetics, which constitutes an important theoretical/computational method to complement the rapid development of ultra-high density data storage devices.

It will be helpful for us to begin with an overview of the basics of the standard micromagnetism. Subsequently, we will discuss a micromagnetic model which incorporates thermal activation, before introducing our time quantified Monte Carlo method. With the Monte Carlo method, we analyze the damping effect on the thermally induced magnetization reversal behavior.

5.1 Background

5.1.1 Overview

Micromagnetism is the *continuum* theory of magnetic moments, which determines the magnetization configuration of magnetic microstructures of a size range from a few nanometers to a few micrometers. The length scale under consideration is generally considered as intermediate level. On the one hand the size of the microstructure is large enough such that the magnetostatic interaction induced magnetic domains becomes indispensable. Thus, the effects of magnetic domain formation and its structure have to be included in the physical model. On the other hand effects which arise from the atomic structure of solids have to be considered as well. This includes magnetocrystalline anisotropy which originates from the specific orientation in which orbitals of neighboring atoms overlap in the crystal lattice. In addition, another energy term under consideration is the quantum exchange interaction between the spin momentum of electrons.

Nevertheless, the size of the microstructures is too large to be modeled by purely quantum mechanical models with present computing power. Therefore, the acceptable way is to classify quantum mechanics, i.e. ignore the atomic nature of matter, and use classical physics in a continuous medium, i.e. assuming the magnetization to be a continuous function of position.

5.1.2 Development of Micromagnetic Modeling

Micromagnetic modeling is concerned with obtaining the detailed magnetization configurations usually at equilibrium, and to model the dynamics of magnetization reversal in magnetic materials.

The basic principle of micromagnetism is the *energy minimization*, as proposed by

Landau and Lifshitz in 1935 to explain the formation of magnetic domains [70]. They analyzed the competing effect between the exchange energy and the magnetostatic energy, and pointed out the domains are formed to minimize the total energy, avoiding poles and forming flux-closure type structure. In 1948, Stoner and Wohlfarth postulated the reversal mechanism of a single domain particle based on the static method of energy minimization, which beautifully explains the magnetic hysteresis phenomena. With these pioneering works, Brown in 1963 established the rigorous theoretical base for the micromagnetic framework [15]. He derived the conditions for the system at energy minimum by using perturbation techniques, which is known as the Brown's static equation for micromagnetics.

However, the dynamical process for the system to relax into equilibrium static state remained unclear since a purely Larmor precessional motion of the magnetic moment would not automatically lead to energy minimization. It was not until 1955 that Gilbert [71] proposed a phenomenological damping effect that applies to the magnetic moment. The resulting Landau-Lifshitz-Gilbert (LLG) equation is the most commonly recognized dynamical model for magnetic moments, and is actually equivalent to an older form of Landau and Lifshitz equation.

There has been increasing interest in the field of micromagnetism among researchers in recent years. One reason is the advent of new experimental imaging techniques with resolutions at the order of tens of nanometers or less, and hence can provide experimental confirmation of the micromagnetic theories. For example, electron holography, a form of imaging, produces an optical hologram with resolution of about 1 nanometer. Others like scanning electron microscopy with polarization analysis, magnetic near-field microscopy, and the magnetic force microscopy can also have resolutions on the order of tens of nanometers.

Another practical reason is the utilization of micromagnetic theory to model the

magnetization process and domain structures. With the rapid advance of computing resources, micromagnetic modeling are being implemented for understanding the magnetization process of magnetic nanostructures [72]. For example, stochastic micromagnetic modeling has important practical implications, e.g. in predicting the storage lifetime of hard-disk magnetic media [15, 73]. Numerical simulation of magnetic nanostructures has become an indispensable tool that can complement experimental efforts in understanding the collective behaviors of magnetic domains as well as developing new devices. Hence, theoretical modeling and simulation techniques need to keep pace with advances in experiments and practical applications to remain effective.

5.1.3 Objective and Scope

A large number of scientific papers are focused on the following areas (i) to incorporate thermally activated magnetization reversal in the micromagnetic framework and (ii) to simulate the influence of environmental conditions and complex microstructures on the magnetization reversal and to expand the theory to new techniques for the simulation of large-scale systems, such as magnetic storage devices and sensors. Research activities also concentrate on (iii) the development of efficient hybrid micromagnetic models.

The main objectives of our research are (i) to investigate the theory underlying the stochastic behavior of magnetic nanoparticles under the influence of thermal fluctuations, by utilizing both Monte Carlo and Langevin methods, and (ii) to apply these methods for the specific application of coupled magnetic grains, which form the basic units of magnetic storage media. For objective (i), we first consider the simpler case of noninteracting grains, and derive the analytical time quantification of the Monte Carlo method, by comparison with the Langevin method via the Fokker-Planck equation. In this way, we can utilize the Monte Carlo method to

model both the short- and long-term magnetization dynamics of the magnetic grains. For objective (ii), we apply the Monte Carlo method to analyze the storage lifetime of magnetic grains, and spin wave properties in interacting spin arrays.

5.2   The Stochastic Landau-Lifshitz-Gilbert Equation Revisited

Micromagnetic simulation based on the Landau-Lifshitz-Gilbert dynamical equation is now widely used to study the magnetic recording performance,[74, 75, 76, 77, 78] i.e. signal-to-noise [79], and bit transition parameter [80]. Magnetic media constructed in the simulation usually consists of structured nanomagnets with grain size of only a few nanometers. In present magnetic media, in order to maximize the storage density, the grain size has been reduced to almost the superparamagnetic limit, where thermal fluctuations become strong enough to destabilize the grain magnetization and hence, the information stored. In addition, these fluctuations may also adversely affect the accuracy of the writing process.

The problem of thermally induced magnetization behavior is very important from both fundamental and application points of view. Langevin dynamics constitute a general method to model a dynamical system subject to stochastic thermal fluctuations. Specifically, for the case of magnetization dynamics, the Langevin equation takes the form of the stochastic Landau-Lifshitz-Gilbert equation, which consists of the usual LLG dynamical equation of motion, with an additional thermal field representing the thermal fluctuations, following Brown [15].

Previous research works have been done to investigate the properties of the stochastic LLG equation. Being the one who first proposed that the thermal fluctuations be described by a white noise term, Brown [15] derived approximate eigenvalues

of the Fokker-Planck equation of thermally induced magnetic reversal for the simplest case of isolated (i.e. noninteracting) uniaxial magnetic single domain particles [15]. Aharoni [81, 82] and Scully [83] investigated the asymptotic relaxation time of isolated uniaxial ferromagnetic particles with an applied field. Coffey and coworkers [84] extended the theoretical study by deriving formulas for the nonaxially symmetric case. They also investigated the different regimes, corresponding to different values of the damping parameter α in the stochastic LLG equations. This work represents an important basis for understanding the magnetization dynamics in single-domain particles.

Unfortunately, the extension of this work to the important case of strongly coupled spin systems such as those used in granular information storage media is nontrivial. Furthermore, for a large array of grains, the number of degrees of freedom increases exponentially with the number of grains, and realistic calculations would appear to be impossible except by purely numerical or computational approaches.

5.2.1   The Dynamical Equation

In the micromagnetic theory, the motion of the spin vector (magnetic moment) is driven by the torque of the effective magnetic fields $\mathbf{H}_{\text{eff}}$, which is defined as:

$$\mathbf{H}_{\text{eff}} = -\frac{1}{\mu_0}\left(\frac{\partial \mathcal{H}}{\partial \mathbf{M}}\right) \tag{5.1}$$

where $\mathcal{H}$ is the Hamiltonian of the system, $\mathbf{M} = M_s\hat{\mathbf{s}}$ is the magnetization of the particle. Here μ_0 is the magnetic permeability, M_s is the saturation magnetization, and $\hat{\mathbf{s}}$ represents the unit spin vector.

There are four important contributions to the Hamiltonian of a ferromagnetic body: the exchange energy, the magnetocrystalline anisotropy energy, the magnetostatic energy, and the Zeeman energy in an external field.

The Exchange Energy

The Heisenberg Hamiltonian of the exchange interaction is usually written in the form:

$$\mathcal{H}_{\text{exch}} = -\sum_{i,j=1} J_{ij} \hat{\mathbf{s}}_i \cdot \hat{\mathbf{s}}_j \tag{5.2}$$

where J_{ij} is the exchange integral, which is calculated from first principles quantum calculations. It decreases rapidly with increasing distance between the atoms, and so the sum has to be taken only for nearest neighbors and we can write J for J_{ij}.

Magnetocrystalline anisotropy energy

Real magnetic materials are not isotropic, otherwise permanent magnets in microphones and loudspeakers would lose their magnetization after production. The most common type of anisotropy is the magnetocrystalline anisotropy, which is caused by the spin-orbit interaction of the electrons.

The magnetocrystalline energy is usually small compared to the exchange energy. But the direction of the magnetization is determined only by the anisotropy, because the exchange interaction just tries to align the magnetic moments parallel, regardless of which direction.

In the simplest case, the anisotropy is uniaxial with a special axis known as the easy direction. We assume $\hat{\mathbf{k}}$ as the unit vector of the easy direction of anisotropy. The Hamiltonian component can be written as:

$$\mathcal{H}_{\text{ani}} = K_u V (\hat{\mathbf{s}} \cdot \hat{\mathbf{k}})^2, \tag{5.3}$$

where K_u is the anisotropy constant and V is the total volume of the magnetic particle.

Magnetostatic energy

The Magnetostatic energy accounts for the magnetostatic interaction between the magnetic dipoles. For an interacting spin array, the total magnetostatic interaction energy is given by

$$\mathcal{H}_{\text{static}} = \sum_i \sum_j \frac{\mu_0}{4\pi r^3} \left\{ \mathbf{M}_i \cdot \mathbf{M}_j - 3(\mathbf{M}_i \cdot \hat{\mathbf{r}})(\mathbf{M}_j \cdot \hat{\mathbf{r}}) \right\} \qquad (5.4)$$

where $\hat{\mathbf{r}}$ is the unit vector pointing from the i-th dipole to the j-th dipole. r is the distance between $\mathbf{M}_i$ and $\mathbf{M}_j$. Unlike exchange coupling, the magnetostatic interaction is a long-range behavior. Therefore, the calculation of the magnetostatic energy should be carried out over the whole volume of the system.

Zeeman energy

For the energy of a magnetic body in an external field we obtain

$$\mathcal{H}_{\text{ext}} = -\mu_0 V \mathbf{M} \cdot \mathbf{H}_{\text{ext}}. \qquad (5.5)$$

Due to the linearity of Maxwell's equations, the superposition principle allows a simple addition of this energy term.

Since we are interested in the dynamic properties and time evolution of the magnetization, we have to consider the precession of the magnetization in a magnetic field. The precessional motion for the magnetization can be simply written in the form:

$$\frac{d\mathbf{M}}{dt} = -\gamma_0 \mathbf{M} \times \mathbf{H}. \qquad (5.6)$$

This equation describes the undamped precession of the magnetization vector about the field direction. It is the well known Larmor precession with the Larmor frequency $\omega = \gamma_0 \mathbf{H}$. From experiments it is known that changes in the magnetization decay in finite time. As this damping cannot be derived rigorously from basic principles, it is just added as a *phenomenological* term. In reality, it is caused by

a complex interaction of the electron's magnetic moment with the crystal lattice. Gilbert [71] proposed a damping term of the form:

$$\frac{\alpha}{M_s}\mathbf{M} \times \frac{d\mathbf{M}}{dt} \tag{5.7}$$

with the dimensionless damping parameter α.

Mathematically, the Gilbert equation:

$$\frac{d\mathbf{M}}{dt} = -\gamma_0 \mathbf{M} \times \mathbf{H} + \frac{\alpha}{M_s}\mathbf{M} \times \frac{d\mathbf{M}}{dt} \tag{5.8}$$

is equivalent to the well known Landau-Lifshitz-Gilbert (LLG) equation in the following form:

$$\frac{d\mathbf{M}}{dt} = -\frac{\gamma_0}{1+\alpha^2}\mathbf{M} \times \mathbf{H} - \frac{\alpha\gamma_0}{(1+\alpha^2)M_s}\mathbf{M} \times \mathbf{M} \times \mathbf{H}. \tag{5.9}$$

5.2.2   Thermal Activation

Thermal activation is introduced in the Landau-Lifshitz-Gilbert equation by a stochastic thermal field, which is added to the effective field $\mathbf{H}$. It accounts for the effects of the interaction of the magnetization with the microscopic degrees of freedom (eg. phonons, conducting electrons, nuclear spins, etc.), which cause fluctuations of the magnetization distribution. This interaction is also responsible for the damping effect, since fluctuations and dissipation are related manifestations of one and the same interaction of the magnetization with its environment.

Since a large number of microscopic degrees of freedom contribute to this mechanism, the thermal field $\mathbf{H}_{\text{th}}(t)$ is assumed to be a Gaussian random process with the following statistical properties:

$$\begin{aligned} \langle H_{\text{th},i}(t) \rangle &= 0, \\ \langle H_{\text{th},i}(t)H_{\text{th},j}(t') \rangle &= 2D\delta_{ij}\delta(t-t'). \end{aligned} \tag{5.10}$$

The average of the thermal field taken over different realizations vanishes in each direction $i \in \{x, y, z\}$ of space. The correlation term relates the strength of the thermal fluctuations (the thermal field) to the dissipation due to the damping of our system. The value of D is first calculated by W. F. Brown [15] to be:

$$D = \frac{\alpha k_B T}{\mu_0 V \gamma_0 M_s} \tag{5.11}$$

5.2.3   Variable Renormalization

To implement the stochastic Landau-Lifshitz-Gilbert equation for finite differential simulation, we shall first simplify the equation with variable renormalization. The reduced Landau-Lifshitz-Gilbert equation has the form:

$$\frac{d\mathbf{m}}{dt} = -\frac{\gamma_0 H_k}{1 + \alpha^2} \mathbf{m} \times (\mathbf{h}_{\text{eff}} + \alpha \cdot \mathbf{m} \times \mathbf{h}_{\text{eff}}) \tag{5.12}$$

The physical meaning of all variables and its renormalization unit is given in Table (5.1).

Table 5.1: Table for reduced variables in Eq. (5.12).

Energy Components	Mathematical Formulae	Remarks
Exchange Energy	$\mathcal{H}_{\text{exch}} = -\sum_{i,j} J_{ij}\hat{\mathbf{s}}_i \cdot \hat{\mathbf{s}}_j$	$\hat{\mathbf{s}}_i = \mathbf{M}_i/M_s$
Anisotropy Energy	$\mathcal{H}_{\text{ani}} = -K_u V(\hat{\mathbf{s}}_i \cdot \hat{\mathbf{k}})^2$	$\hat{\mathbf{s}}_i = \mathbf{M}_i/M_s$
Magnetostatic Energy	$\mathcal{H}_{\text{dip}} = -\mu_0 V \sum_{i,j}\left[\frac{3(\mathbf{M}_i\cdot\mathbf{r})(\mathbf{M}_j\cdot\mathbf{r})}{r^5} - \frac{\mathbf{M}_i\cdot\mathbf{M}_j}{r^3}\right]$	
Zeeman Energy	$\mathcal{H}_{\text{ext}} = -\mu_0 V \mathbf{M} \cdot \mathbf{H}_{\text{ext}}$	

Variables	Original Form	Normalized by	Reduced Form
Magnetic Moment	$\mathbf{M}_i$	M_s	$\hat{\mathbf{s}}_i$
Exchange Field	$\mathbf{H}_{\text{exch},i} = \frac{1}{\mu_0 V M_s}\sum_{j\neq i} J_{i,j}\hat{\mathbf{s}}_j$	$H_k = \frac{2K_u}{\mu_0 M_s}$	$\mathbf{h}_{\text{exch},i} = \frac{1}{2K_u V}\sum_{j\neq i} J_{i,j}\hat{\mathbf{s}}_j$
Anisotropy Field	$\mathbf{H}_{\text{ani},i} = \frac{2K_u}{\mu_0 M_s}(\hat{\mathbf{s}}_i\cdot\hat{\mathbf{k}})\hat{\mathbf{s}}_i$	$H_k = \frac{2K_u}{\mu_0 M_s}$	$\mathbf{h}_{\text{ani},i} = (\hat{\mathbf{s}}_i\cdot\hat{\mathbf{k}})\hat{\mathbf{s}}_i$
Magnetostatic Field	$\mathbf{H}_{\text{dip},i} = M_s\sum_{i,j}\left[\frac{3(\hat{\mathbf{s}}_j\cdot\mathbf{r})\mathbf{r}}{r^5} - \frac{\hat{\mathbf{s}}_j}{r^3}\right]$	$H_k = \frac{2K_u}{\mu_0 M_s}$	$\mathbf{h}_{\text{dip},i} = \frac{\mu_0 M_s^2}{2K_u}\sum_{i,j}\left[\frac{3(\hat{\mathbf{s}}_j\cdot\mathbf{r})\mathbf{r}}{r^5} - \frac{\hat{\mathbf{s}}_j}{r^3}\right]$
Zeeman Field	$\mathbf{H}_{\text{ext},i} = \mathbf{H}_{\text{ext}}$	$H_k = \frac{2K_u}{\mu_0 M_s}$	$\mathbf{h}_{\text{ext},i} = \mathbf{H}_{\text{ext}}/H_k$
Thermal Field	$H_{\text{th}} = \eta\sqrt{\frac{2\alpha k_B T}{\mu_0\gamma_0 V M_s\Delta t}}$	$H_k = \frac{2K_u}{\mu_0 M_s}$	$\eta\sqrt{\alpha\frac{k_B T}{K_u V}\frac{1}{\gamma_0 H_k\Delta t}}$
Total Field	$\mathbf{H}_i = \mathbf{H}_{\text{exch},i} + \mathbf{H}_{\text{ani},i} + \mathbf{H}_{\text{dip},i} + \mathbf{H}_{\text{ext},i} + \mathbf{H}_{\text{th},i}$		

5.2.4 The Fokker-Planck Equation

There are many forms of the Fokker-Planck equation corresponding to the stochastic Landau-Lifshitz-Gilbert equation (Eq. (5.12)). Let $P(\mathbf{m}, t)$ be the probability distribution function of the stochastic Landau-Lifshitz-Gilbert equation. The Fokker-Planck equation has the form of:

$$\frac{\partial P}{\partial t} = -\frac{\partial}{\partial \mathbf{m}} \cdot \left\{ \left[-\frac{\gamma_0 H_k}{1 + \alpha^2} \mathbf{m} \times \mathbf{h} - \frac{\alpha \gamma_0 H_k}{(+\alpha^2} \mathbf{m} \times \mathbf{m} \times \mathbf{h} \right.\right.$$
$$\left.\left. + \frac{\alpha \gamma_0 k_B T}{(1 + \alpha^2) \mu_0 V M_s} \mathbf{m} \times \left(\frac{\partial}{\partial \mathbf{m}} \right) \right] P \right\} \tag{5.13}$$

The formula of the Fokker-Planck equation will be different, if the probability distribution function is defined by using the spherical coordinators $\{\theta, \phi\}$, i.e. $P(\theta, \phi, t)$. We will introduce this form of the Fokker-Planck equation in the latter sections [see Eq. (5.14)].

5.3 The Time-quantified Monte Carlo Algorithm

Brown in 1963 proposed a micromagnetic model in the presence of thermal fluctuations. In this model, the thermal activated dynamics are modeled in the Langevin scheme, using the stochastic Landau-Lifshitz-Gilbert equation [15]. Langevin-based micromagnetics has proved to be a highly useful computational method, because of its ease of use and close correspondence to actual experimental data in previous literatures [84]. However, it has certain limitations. For example, it is practically infeasible to model the long-time dynamics of large scale arrays of magnetic grains by using the stochastic LLG equation.

In contrast, the Monte Carlo schemes have distinct advantages in reducing the simulation efforts for large scale systems in many other scientific fields. The flexibility of the Monte Carlo scheme is due to its abstract formalism which can be realized in

an almost infinite number of ways. Hence it is natural to look for an implementation of the Monte Carlo scheme in studying the thermally induced magnetization reversal.

Increasingly, Monte Carlo methods are being implemented in the stochastic micromagnetic modeling of magnetic nanostructures [72], e.g. in predicting the storage lifetime of hard-disk magnetic media [73, 85]. However, Monte Carlo schemes have the drawback of having its time calibrated in MC steps, instead of physical time units. Thus, both the Monte Carlo and the Langevin approach are useful computational methods in micromagnetics, with complementary strengths and drawbacks. Hence, it is very important to devise a general way of mapping one method to the other, and vice versa.

Early efforts to link Monte Carlo to LLG were done by Nowak *et al.* [20]. They focused on deriving a time quantification factor to relate one Monte Carlo step (MCS) to the real physical time unit used in the LLG equation. Recently, we also proposed another time-quantifiable Monte Carlo method which involves the determination of a macroscopic density of states, and the use of the Master equation for time evolution. This method is applicable in simulating extremely long time magnetization reversal process [38]. The effect of precession on Nowak's time-quantification was investigated by Chubykalo *et al.* [16]. They concluded that Nowak's time quantification of Monte Carlo breaks down in the low damping case, in the presence of an oblique external field, due to the influence of (athermal) precessional motion.

In the rest of this chapter, we will first introduce our Monte Carlo method, which is modified to include the precessional motion. We prove its validity in a simple isolated single particle scheme, and in a more complex interacting spin array. We shall discuss the application of our Monte Carlo method, e.g. investigation of the effects of damping constant α in magnetization reversal and spin wave dynamics.

5.3.1 Isolated Single Particle

We consider an isolated single domain magnetic particle whose moment can be represented by a Heisenberg spin with an easy axis anisotropy [15]. To describe the dynamics of a Heisenberg spin, it is convenient to use the spherical coordinate system. The Fokker-Planck equation in spherical coordinates θ and φ can be written in the form of:

$$
\begin{aligned}
\frac{\partial P}{\partial t} &= -\frac{\partial}{\partial \theta}\left(A_\theta \cdot P\right) - \frac{\partial}{\partial \varphi}\left(A_\varphi \cdot P\right) + \frac{1}{2}\frac{\partial^2}{\partial\theta\partial\varphi}\left(B_{\theta\varphi} \cdot P\right) \\
&\quad + \frac{1}{2}\frac{\partial^2}{\partial\theta^2}\left(B_{\theta\theta} \cdot P\right) + \frac{1}{2}\frac{\partial^2}{\partial\varphi^2}\left(B_{\varphi\varphi} \cdot P\right).
\end{aligned}
\tag{5.14}
$$

$P = P(\theta, \varphi, t)$ is the probability density of the moment orientation. A and B are the so-called drift and diffusion coefficients respectively, defined as the ensemble mean of an infinitesimal change of θ and φ with respect to time [12].

The reduced stochastic LLG dynamical equation can be written as:

$$
\frac{d\mathbf{m}}{dt} = -\frac{\gamma_0 H_k}{1+\alpha^2}\mathbf{m} \times \left[(\mathbf{h} + \mathbf{h}_t) + \alpha \cdot \mathbf{m} \times (\mathbf{h} + \mathbf{h}_t)\right]
\tag{5.15}
$$

where $\mathbf{m}$ is the magnetic moment unit vector, α and γ_0 are the damping and gyromagnetic constant respectively, $\mathbf{h}$ is the effective field normalized by the anisotropy field $H_k = 2K_u/\mu_0 M_s$, where K_u is the anisotropy constant, μ_0 is the magnetic permeability and M_s is the saturation magnetization. The thermal field $\mathbf{h}_t$ is introduced as a white noise term. The Fokker-Planck equation corresponding to the LLG equation has been derived by Brown [15], and its factors are as follows:

$$
\begin{aligned}
A_\theta^{LLG} &= -h'\frac{\partial E}{\partial \theta} - g'\frac{1}{\sin\theta}\frac{\partial E}{\partial \varphi} + k'\cot\theta \\
A_\varphi^{LLG} &= g'\frac{1}{\sin\theta}\frac{\partial E}{\partial \theta} - h'\frac{1}{\sin^2\theta}\frac{\partial E}{\partial \varphi} \\
B_{\theta\theta}^{LLG} &= 2k' \\
B_{\varphi\varphi}^{LLG} &= \frac{1}{\sin^2\theta}2k' \\
B_{\theta\varphi}^{LLG} &= 0
\end{aligned}
\tag{5.16}
$$
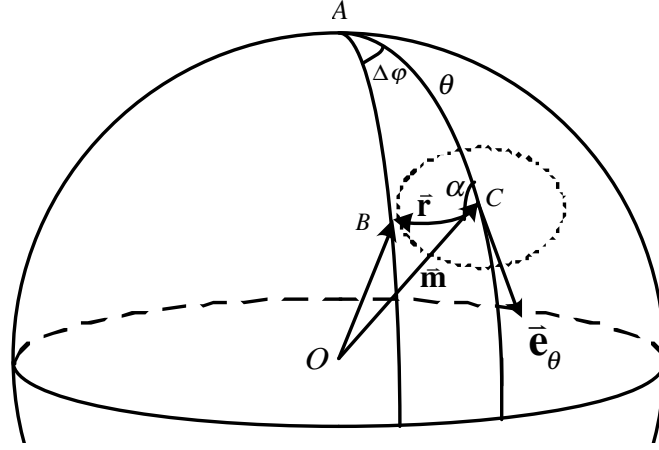
Figure 5.1: Diagram of random walk step of length r and angle α to $\vec{e}_\theta$ which define a spherical triangle ABC.

where in above equations, $h' = \frac{\alpha\gamma_0}{\mu_0 V M_s (1+\alpha^2)}$, $g' = h'/\alpha$, $k' = h'/\beta$, E is the total energy [15, 20], V is the volume of the particle and $\beta = (k_B T)^{-1}$, k_B is the Boltzmann constant and T is the temperature in Kelvin.

We will now derive the Fokker-Planck equation corresponding to our Monte Carlo method. For the MC method, we choose with probability q, to displace the magnetic moment within a small cone centered at the original magnetization direction, and with probability $(1-q)$ to perform a rejection-free precession about an effective field. For the displacement about a cone, we pick a random vector lying within a sphere of radius R to the original magnetic moment and then normalize the resulting vector. The precessional step vector, i.e. the displacement of the magnetic moment due to precession, is $\Delta\mathbf{m} = -\Phi \cdot \mathbf{m} \times \mathbf{h}$, where $\Phi \ll 1$ is a precessional step size to be determined. The probability q is chosen to be $1/2$, which yields a near-optimal balance of efficiency and accuracy of our simulation.

To calculate the Fokker-Planck coefficient A_θ^{MC} for the MC method, we obtain the ensemble mean of a small change of θ in *one Monte Carlo step*. Contributions from the random walk and the precessional step are $A_\theta^{MC} = \langle\Delta\theta\rangle_{\text{rand}} /2 + \Delta\theta_{\text{prec}}/2$,

where the angle brackets denote the ensemble average.

We first calculate the $\langle \Delta\theta \rangle_{\text{rand}}$, where the angular displacement is defined by two random variables r and angle α, as shown in Fig. 5.1. After some geometrical analysis, we obtain:

$$\Delta\theta_{\text{rand}} = -\cos\alpha \cdot r + \frac{1}{2}\cot\theta \sin^2\alpha \cdot r^2 + O\left(r^3\right) \tag{5.17}$$

$$\Delta\varphi_{\text{rand}} = \frac{1}{\sin\theta}\sin\alpha \cdot r + \frac{1}{2}\frac{\cot\theta}{\sin\theta}\sin 2\alpha \cdot r^2 + O\left(r^3\right). \tag{5.18}$$

Next, we require the probability for the displacement vector to be of size r ($r < R$) and angle α with respect to $\vec{e}_\theta$. This probability is given by Nowak *et al.* [20] as $p(r) = 3\sqrt{R^2 - r^2}/2\pi R^3$. Based on the heat-bath Metropolis MC scheme, the acceptance rate is

$$A\left(\Delta E\right) = 1/\left(1 + \exp\left(\beta\Delta E\right)\right)$$
$$\approx \frac{1}{2}\left(1 - \frac{1}{2}\beta\left(\frac{\partial E}{\partial \theta}\Delta\theta + \frac{\partial E}{\partial \varphi}\Delta\varphi\right)\right) \tag{5.19}$$

where ΔE is the energy change in the random walk step. Thus, integrating over the projected surface of Fig. 5.1, one obtains $\langle \Delta\theta \rangle_{\text{rand}}$:

$$\langle \Delta\theta \rangle_{\text{rand}} = \int_0^{2\pi} d\alpha \int_0^R (rdr)\Delta\theta \cdot p(r) \cdot A(\Delta E)$$
$$= \frac{R^2}{20}\left(\cot\theta - \beta\frac{\partial E}{\partial \theta}\right) + O(R^3). \tag{5.20}$$

Next we calculate the other contribution from the precessional step $\Delta\theta_{\text{prec}}$:

$$\Delta\theta_{\text{prec}} \cong \mathbf{e}_\theta \cdot (-\Phi \cdot \mathbf{m} \times \mathbf{h}) = \Phi \cdot (\mathbf{e}_\varphi \cdot \mathbf{h})$$
$$= -\frac{1}{\sin\theta}\frac{\Phi}{2K_uV}\frac{\partial E}{\partial \varphi}. \tag{5.21}$$

In the above derivation, we have used the vector identity $\mathbf{a} \cdot (\mathbf{b} \times \mathbf{c}) = (\mathbf{a} \times \mathbf{b}) \cdot \mathbf{c}$ and $\mathbf{h} = -(\nabla_{\mathbf{m}}E)/2K_uV$. Using Eqs. (5.20) and (5.21), A_θ^{MC} becomes,

$$A_\theta^{MC} = \frac{R^2}{40}\left(\cot\theta - \beta\frac{\partial E}{\partial \theta}\right) - \frac{1}{\sin\theta}\frac{\Phi}{4K_uV}\frac{\partial E}{\partial \varphi} + O(R^3). \tag{5.22}$$

The other FPE factors can be obtained with the same procedure.

$$
\begin{aligned}
A_\varphi^{MC} &= -\frac{1}{\sin^2\theta}\frac{R^2}{40}\beta\frac{\partial E}{\partial\varphi} + \frac{1}{\sin\theta}\frac{\Phi}{4K_uV}\frac{\partial E}{\partial\theta} + O(R^3) \\
B_{\theta\theta}^{MC} &= \frac{R^2}{20} + \frac{1}{2}\left(\frac{1}{\sin\theta}\frac{\Phi}{2K_uV}\frac{\partial E}{\partial\varphi}\right)^2 + O(R^4) \\
B_{\varphi\varphi}^{MC} &= \frac{1}{\sin^2\theta}\frac{R^2}{20} + \frac{1}{2}\left(\frac{1}{\sin\theta}\frac{\Phi}{2K_uV}\frac{\partial E}{\partial\theta}\right)^2 + O(R^4) \\
B_{\theta\varphi}^{MC} &= -\left(\frac{1}{\sin\theta}\frac{\Phi}{2K_uV}\right)^2\frac{\partial E}{\partial\theta}\frac{\partial E}{\partial\varphi} + O(R^3).
\end{aligned} \tag{5.23}
$$

We can now compare the Fokker-Planck equation factors corresponding to the Langevin (LLG) equation in Eq. (5.16), with those of the Metropolis MC method in Eqs. (5.22) and (5.23). Performing a term-wise comparison and omitting $O(R^3)$ and higher order terms, we found that there is a one-to-one mapping between all Fokker-Planck terms of MC and LLG if:

$$
R^2\Delta\tau_{\mathrm{MC}} = \frac{40\alpha}{1+\alpha^2}\frac{\gamma_0}{\beta\mu_0 V M_s}\Delta t_{\mathrm{LLG}} \tag{5.24}
$$

$$
\Phi = \frac{\beta K_u V}{10\cdot\alpha}R^2. \tag{5.25}
$$

Note that Φ is on the order of R^2, thus we are justified in neglecting $O(\Phi^2)$ terms in the above comparison between Eq. (5.16), and Eqs. (5.22) and (5.23). From Eq. (5.24), we obtain the time quantification factor of our hybrid Metropolis Monte Carlo method, while Eq. (5.25) determines the precessional step size Φ. After taking into consideration the probability factor q, Eqs. (5.24) and (5.25) can be reduced to Nowak's results [20] in the high damping case.

To test the validity of Eqs. (5.24) and (5.25), we perform numerical calculations of the switching process for a magnetic particle in which the easy axis is oriented at $\pi/4$ to the applied field direction. All results are averaged from a few thousand simulations. We consider the time evolution behavior of the mean magnetization component along the easy axis, and found a close convergence between our time-quantified MC method and the LLG equation (Fig. 5.2). In these calculations, we
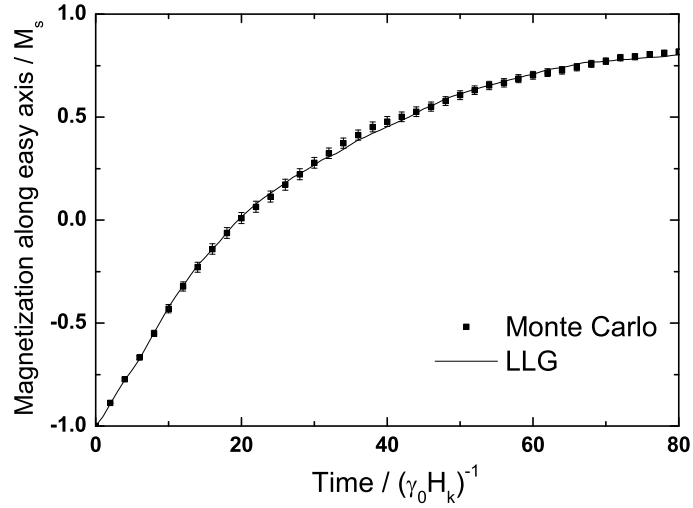
Figure 5.2:   Time dependence of magnetization along easy axis, for an isolated particle. $K_u V / k_B T = 15$, applied field $h = 0.42$ tilted at $\pi/4$ relative to easy axis. Damping constant $\alpha = 0.5$.

use $R = 0.03$ for MC, and $\Delta t = 0.001$ for the LLG integration.

Note that our derivation of the FPE factors is applicable in a very general case. For instance, we do not require the assumption of the system being in the vicinity of an energy minimum [20]. The derivation also provides additional information, e.g., it explains mathematically why the Metropolis MC random walk method of Ref. [20] fails to include the energy conservative precessional motion. The FPE expression for the pure Metropolis MC does not contain terms corresponding to the g'-factor related terms of the LLG method [Eq. (5.16)], which are precisely the terms which reflect the precessional part of the magnetization dynamics [1]. Thus, as shown in Fig. 5.3, we have successfully implemented the representation of precessional motion in our MC method. We investigate the influence of the damping constant on the switching time, where the switching time is defined as the time required for the magnetic moment to reach zero from the initial state. The precessional step size Φ guarantees a precise description of the switching process even in the
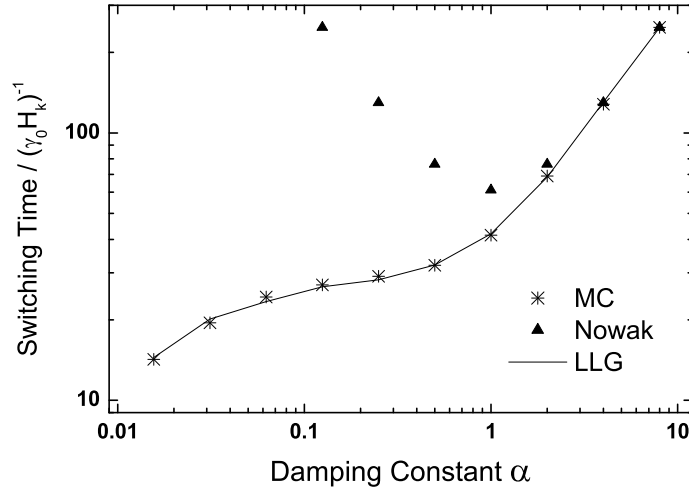
Figure 5.3: Switching time versus damping constant α. $K_uV/k_BT = 15$, applied field $h = 0.42$ at a tilted angle of $\pi/4$ relative to easy axis. Error bars are smaller than the size of the symbols. Note that Nowak's method diverges from the LLG equation at $\alpha < 2$.

case of very low damping constant α, in which precessional motion dominates the reversal process [79]. By contrast, the results obtained from the pure Metropolis MC method of Nowak *et al.* diverges significantly from that of the LLG equation at low α.

5.3.2 Interacting Spin Array

The validity of using the Time-quantified Monte Carlo method to simulate an isolated single domain particle is first demonstrated by Nowak *et al.* [20] and later rigorously proved in previous chapters by using the Fokker-Planck equation as a bridge between the Monte Carlo and Langevin methods. In the case of interacting spin arrays, the validity of the TQMC has not been analytically proved although it has been numerically shown [62, 86]. It thus becomes a necessity to establish

the proof for the case of interacting spin systems, since in practical applications the discrete spins or moments (in the form of magnetic nanoparticles) are usually closely packed together, and hence are strongly coupled to one another. It is also important to show explicitly whether the analytical equivalence between the Time-quantified Monte Carlo method and the stochastic LLG equation and the time quantification factor, are dependent in any way on the nature (e.g. magnetostatic or exchange) or strength of the coupling interactions.

In the following, we provide a rigorous proof for this case, based on the technique presented earlier. The physical model under consideration is a spin array (which represents an array of magnetic nanoparticles), whose spin configuration is represented as $\{\mathbf{s}\} = \{\cdots, \hat{\mathbf{s}}_i, \cdots\}$, where $\mathbf{s} = \mathbf{M}/M_s$ is a normalized unit vector representing the magnetic moment of the spin and i refers to the ith spin in the vector list of length N. For a spin array, the corresponding the Landau-Lifshitz-Gilbert (LLG) equation is:

$$\frac{d}{dt}\{\mathbf{s}\} = -\frac{\gamma_0 H_k}{1+\alpha^2}\{\mathbf{s}\} \times (\{\mathbf{h}\} + \alpha \cdot \{\mathbf{s}\} \times \{\mathbf{h}\},) \qquad (5.26)$$

where α and γ_0 are the damping constant and the gyromagnetic constant respectively, $\{\mathbf{h}\} = \frac{1}{2K_uV}\nabla_{\{\mathbf{s}\}}E$ is the effective field which is normalized with respect to the anisotropy field $H_k = 2K_u/\mu_0 M_s$, where K_u is the anisotropy constant and μ_0 is the magnetic permeability. $E = E(\{\mathbf{s}\})$ is the total energy of the system which consists of the typical contributions in a micromagnetic system, e.g., Zeeman term, anisotropy term, magnetostatic term and exchange coupling term. The operator $\{\mathbf{s}\} \times \{\mathbf{h}\} = \{\cdots, \mathbf{s}_i \times \mathbf{h}_i, \cdots\}$ is understood. As before, to represent the thermal fluctuation, white noise-like stochastic thermal fields are added to the effective field according to Brown [15].

Alternatively, a random walk Monte Carlo algorithm can also be used in simulating the magnetization reversal dynamics [20]. At each Monte Carlo step, one of the N spin sites is randomly selected to undergo a trial move, in which a random

displacement lying within a sphere of radius R ($R \ll 1$) is added into the original magnetic moment and the resulting vector is then renormalized. The magnetic moment changes according to a heat bath acceptance rate as $A(\Delta E) = 1/(1 + \exp(\beta\Delta E))$. Here ΔE is the energy change within the random walk step and $\beta = (k_B T)^{-1}$, k_B is the Boltzmann constant and T is the temperature in Kelvin.

Fokker-Planck Equations

To link the MC scheme with the stochastic LLG equation, we shall derive the respective Fokker-Planck coefficients corresponding to the LLG equation and the random walk MC [62]. The general Fokker-Planck equation for a spin array in spherical coordinates is given as

$$
\begin{aligned}
\frac{d}{dt}P(\{\theta\},\{\varphi\},t) = & -\sum_i \frac{\partial}{\partial\theta_i}\left(A_{\theta_i}\cdot P\right) - \sum_i \frac{\partial}{\partial\varphi_i}\left(A_{\varphi_i}\cdot P\right) + \frac{1}{2}\sum_{i,j}\frac{\partial^2}{\partial\theta_i\partial\theta_j}\left(B_{\theta_i\theta_j}\cdot P\right) \\
& + \frac{1}{2}\sum_{i,j}\frac{\partial^2}{\partial\varphi_i\partial\varphi_j}\left(B_{\varphi_i\varphi_j}\cdot P\right) + \frac{1}{2}\sum_{i,j}\frac{\partial^2}{\partial\theta_i\partial\varphi_j}\left((B_{\theta_i\varphi_j} + B_{\varphi_j\theta_i})\cdot P\right)
\end{aligned}
$$

$$(5.27)$$

where drift terms A_x and diffusion terms B_{xy} ($x = \{\theta_i, \varphi_i\}$, $y = \{\theta_j, \varphi_j\}$) are defined as the ensemble mean of an infinitesimal change of x and y with respect to time [12]. By giving the detailed derivation in the appendix, we obtained the Fokker-Planck coefficients for LLG:

$$
\begin{aligned}
A_{\theta_i}^{LLG} &= -h'\frac{\partial E}{\partial\theta_i} - g'\frac{1}{\sin\theta_i}\frac{\partial E}{\partial\varphi_i} + k'\cot\theta_i \\
A_{\varphi_i}^{LLG} &= g'\frac{1}{\sin\theta_i}\frac{\partial E}{\partial\theta_i} - h'\frac{1}{\sin^2\theta_i}\frac{\partial E}{\partial\varphi_i} \\
B_{\theta_i\theta_j}^{LLG} &= 2k'\cdot\delta_{ij} \\
B_{\varphi_i\varphi_j}^{LLG} &= \frac{1}{\sin^2\theta_i}2k'\cdot\delta_{ij} \\
B_{\theta_i\varphi_j}^{LLG} &= B_{\varphi_j\theta_i}^{LLG} = 0
\end{aligned}
$$

$$(5.28)$$

as well as for the TQMC method:

$$
\begin{aligned}
A_{\theta_i}^{MC} &= N^{-1}\frac{R^2}{20}\left(\cot\theta_i - \beta\frac{\partial E}{\partial\theta_i}\right) \\
A_{\varphi_i}^{MC} &= -N^{-1}\frac{1}{\sin^2\theta_i}\frac{R^2}{20}\beta\frac{\partial E}{\partial\varphi_i} \\
B_{\theta_i\theta_j}^{MC} &= N^{-1}\frac{R^2}{10}\cdot\delta_{ij} \\
B_{\varphi_i\varphi_j}^{MC} &= N^{-1}\frac{1}{\sin^2\theta_i}\frac{R^2}{10}\cdot\delta_{ij} \\
B_{\theta_i\varphi_j}^{MC} &= B_{\varphi_j\theta_i}^{MC} = 0
\end{aligned}
\tag{5.29}
$$

where in Eq. (5.28), $h' = \frac{\alpha\gamma_0}{\mu_0 V M_s(1+\alpha^2)}$, $g' = h'/\alpha$, $k' = h'/\beta$.

Mapping MC to LLG

In the high damping limit where the damping constant α is large, so that $g' = h'/\alpha \to 0$, a term-wise equivalence can be established between the FPE coefficients in Eqs. (5.28) and (5.29), corresponding to the LLG and MC methods, if:

$$
R^2\Delta\tau_{\mathrm{MC}} = \frac{20\alpha}{1+\alpha^2}\frac{\gamma_0}{\beta\mu_0 V M_s}\Delta t_{\mathrm{LLG}}.
\tag{5.30}
$$

Eq. (5.30), in which $\Delta\tau_{\mathrm{MC}}$ is calibrated in MCS/site (one Monte Carlo step for each site on the average), is the time quantification factor for the TQMC method in interacting spin arrays. The time quantification factor is found to be the same as the one in Ref. [20] for an isolated single particle case, and is thus consistent with the previous numerical convergence observed in Refs. [62, 86].

For the low damping limit where precessional motion becomes significant, one may wish to use the precessional (hybrid) Metropolis Monte Carlo algorithm [62]. We confirm that, by using the same derivation techniques, one is able to prove the validity of including the precessional move in the MC algorithm in simulating the micromagnetic properties of an interacting spin array.
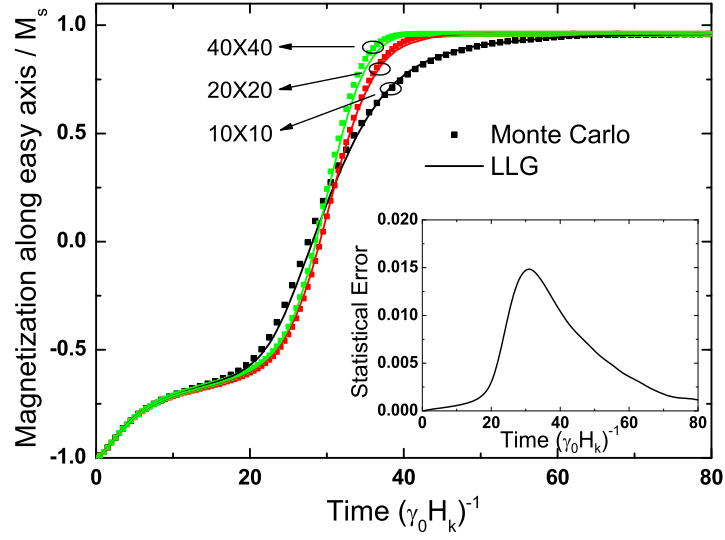
Figure 5.4: Time dependence of magnetization along the easy axis for an interacting spin array. Periodic boundary conditions were used and $K_uV/k_BT = 25$, applied field $h = 0.5$ at a tilted angle of $\pi/4$ relative to the easy axis. Damping constant $\alpha = 1$, exchange coupling strength $J/K_u = 2$ (Hamiltonian of an interacting system with exchange coupling strength J can be found, i.e. in Ref. [86]). $R = 0.025$ is used in the Monte Carlo simulation. Statistical error for the 10×10 lattice Monte Carlo simulation is shown in the inset.

Numerical Verifications

The equivalence between the MC method and LLG, which is expressed by Eq. (5.30), provides the theoretical justification for the use of the Monte Carlo method as an alternative to the LLG equation in micromagnetic studies. The equivalence which has been established is very general because no explicit form of the Hamiltonian is used in the derivation. This implies that the validity of the equivalence is independent of many physical and simulation parameters. For illustration, we apply our analytic results to 10×10, 20×20 and 40×40 interacting spin array systems and found that the convergence between MC and LLG are very good (Fig. 5.4). We also test the validity of the TQMC method for a simple 10×10 spin array which is subject to a varying exchange coupling strength J. As shown in Fig. (5.5), the time evolution behavior of the (asymmetric) magnetization reversal is simulated for different values of J. We find good convergence between the simulated results from both LLG and MC schemes, even when the switching mechanism of the spin array changes from independent reversal (small J) to the nucleation-driven reversal (large J). We also confirm that the mapping between the Monte Carlo and LLG time steps as expressed in Eq. (5.30), is also independent of other simulation and physical parameters, e.g. the chosen boundary condition (periodic / free), the lattice size, and the nature of the coupling (magnetostatic / exchange).

Next, we show that the equivalence between the MC method and LLG enables the MC method to be utilized in most of the situations where LLG applies, and beyond the above time-evolution simulation. As an example, we consider the dispersion relation for the primary spin wave mode of a one-dimensional spin chain. This example is chosen because it tests the capability of the precessional TQMC method to simulate both spatial and time correlation of the spin-wave dynamics. By comparison, conventional MC methods are more suited for equilibrium or steady-state studies rather than time correlation dynamics.
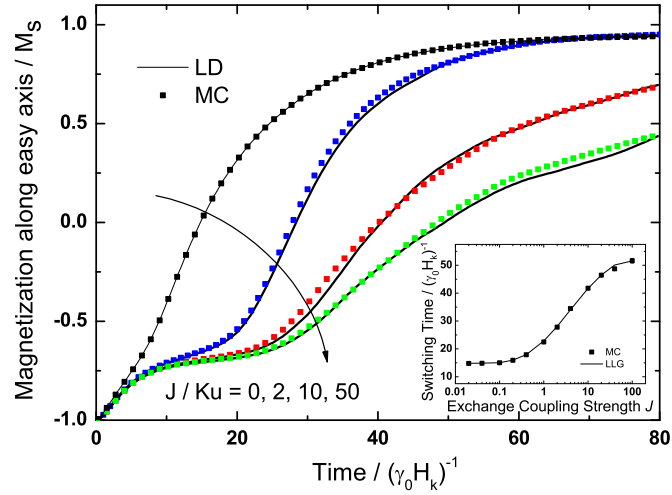
Figure 5.5: The time evolution behavior of the magnetization reversal in a spin array system. The following simulation parameters are assumed: lattice size of 10×10, periodical boundary condition, thermal condition $K_u V / k_B T = 25$, damping constant $\alpha = 1.0$ and external field $h = 0.5$ applied at an angle $\theta = \pi/4$ with respect to the easy axes. The exchange coupling strength J is the adjustable variable. To guarantee the simulation accuracy, the time interval Δt for the LLG integration changes with J as $\Delta t = 0.01/(1 + h + J/K_u V)$ [87], while the trial move step size R in the MC simulation is chosen to reflect the Δt in one MCS. Error bars are smaller than the symbol size.

The Hamiltonian of the spin chain system is set to be

$$\mathcal{H} = \sum_i \left(-J \sum_{j<i}^{\{i\}} \hat{\mathbf{s}}_i \cdot \hat{\mathbf{s}}_j - K_u V (\hat{\mathbf{s}}_i \cdot \hat{\mathbf{k}}_n)^2 - \mu_0 M_s V \cdot \hat{\mathbf{s}}_i \cdot \mathbf{H}_{\text{ext}} \right) \qquad (5.31)$$

where $\{i\}$ represents the neighboring spins of the ith spin, J is the coupling strength, $\mathbf{H}_{\text{ext}}$ is the applied field and $\hat{\mathbf{k}}_n$ refers to the unit vector along the easy axis. Magnetostatic coupling was not included in this test. The dispersion relation for the one-dimensional spin wave mode has been theoretically studied [88] and is given by:

$$\omega(k) = \frac{\gamma_0 H_k}{1 + \alpha^2}[1 + h_{\text{ext}} + 4(J/2K_u V) \sin^2(ka/2)] \qquad (5.32)$$

where $h_{\text{ext}} = H_{\text{ext}}/H_k$ and a is the lattice constant. The calculations were done using the computational techniques of Refs. [89, 90]. Spins were initially aligned along the z direction, in parallel with both the easy axes and applied fields. Stochastic simulation was performed on this initial configuration for 100 $(\gamma_0 H_k)^{-1}$, in order to achieve the quasi-equilibrium state. Space and time Fourier transforms were then performed on the off-axis components. From the resulting spin wave spectra, the peak frequency ω was determined for a range of wavevector k. The resulting dispersion relation in Fig. (5.6) shows a very good convergence between the simulated results (calculated from both LLG and MC) and the theoretical prediction of Eq. (5.32), as seen in Fig. 5.6.

5.4   Application – Analyzing the role of damping

The precessional motion delivers nontrivial effects to the thermally activated magnetization reversal behavior, especially in modeling the switching process of tilted perpendicular recording media. The tilted perpendicular recording media [91, 92] has recently been proposed as an alternative to perpendicular media, due to its
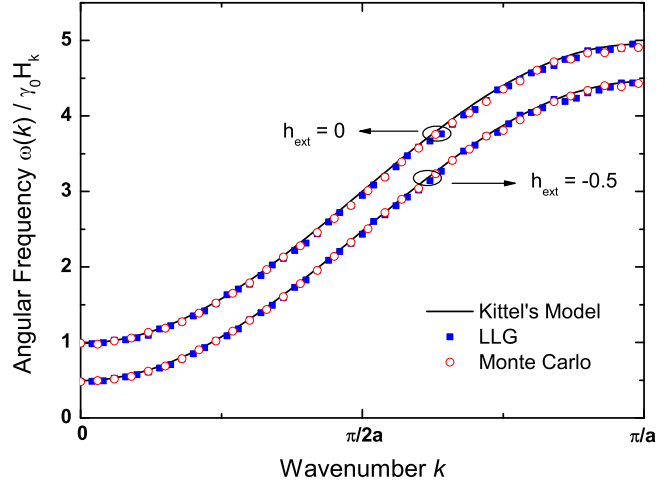
Figure 5.6: Dispersion relation for the simulated spin wave mode. Simulation parameters are: chain length $N = 200$, free boundary condition, thermal condition $K_u V / k_B T = 50$, exchange coupling strength $J/2K_u V = 1$ and damping constant $\alpha = 0.1$. Kittel's model refers to the theoretical dispersion relation of Eq. (5.32).

higher thermal stability. In such a media, precessional dynamics plays a major role because the applied external field is in the oblique orientation compared to the easy axis of the magnetic grains.

Thus, it is essential to have a means of investigating the precessional contribution to stochastic magnetization reversal. This precessional motion is closely intertwined with the damping motion and thermal fluctuations. For instance, a change of the damping parameter α not only affects the relative ratio between the precessional and damping contributions, but also modifies the amplitude of the thermal fluctuations in the magnetization [see Eqs. (5.11) and (5.12)]. In contrast, the TQMC method models the precessional effect in only one parameters the precessional step size $\Phi(\alpha)$. From this point of view, the TQMC method provides a convenient avenue to analyze the damping effect.

5.4.1 Damping Effects in Single Particle

In the following, we apply the TQMC method with precessional motion on a specific case of a non-interacting single domain particle with its easy axis' direction lying along the z axis. An oblique applied field $\mathbf{h}$, normalized by H_k is added in the x-z plane at an angle of ϕ with respect to the z axis. Thus, we can write down the total energy of the system as:

$$\frac{E(\theta)}{2K_u V} = -\frac{1}{2}\cos^2\theta - h\cos(\phi - \theta) \qquad (5.33)$$

where θ is the angle between the magnetic moment and the z-axis. To understand the role of precession in inducing a magnetization reversal, we need to consider the energy profile E versus θ based on Eq. (5.33), as shown in Fig. 5.7. Initially, the moment of the particle is fluctuating stochastically about the minima A. The random walk due to thermal fluctuations has a finite probability of increasing the particle's energy. By contrast, the precessional motion is an energy conserving motion, which does not lead to any change in the energy of the particle. Thus, the precessional motion will have a minimal contribution to the switching process when the energy level is lower than the peak point B. After some time, the random walk of the magnetic moment will cause the energy of the system to reach E_B, the energy level of B. The average time interval (which we term as τ_R, the random walk delay time) for this to occur is a function of temperature, which determines the size of the thermal fluctuations, and the energy barrier height. It is independent of the precessional motion.

Note that the system does not necessarily undergo magnetization reversal, once it has attained the energy E_B. This is because in general the solution $E(\theta, \phi) = E_B$ traces out a closed curve in the (θ, ϕ) space [say $\theta = f(\phi)$, which is also the trajectory of the precessional motion], where θ and ϕ are the axial and azimuthal orientations of the moment. Switching only occurs when $E = E_B$ and $\theta = \theta_B$.
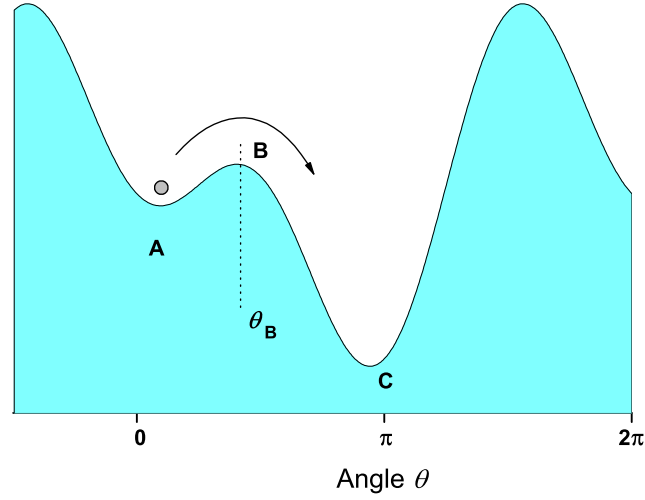
Figure 5.7: Energy versus magnetization orientation θ. The parameters used are easy axis orientation $\phi = \pi/4$, and applied field $h = -0.32$.

We investigate the two extreme cases of: a) very low damping, and b) very high damping. For the low damping condition, the magnetic moment precesses around rapidly. Thus, all points along the path $f(\phi)$ are quickly accessed, including the point B. Once point B is reached, the system is in an unstable equilibrium, and rapidly transits or switches to the other minima C. Thus, in the low damping limit, the switching time τ_L is predominantly due to the random walk delay time τ_R required to raise the energy from the local minima E_A to E_B. In the high damping limit, however, the precessional motion along $f(\phi)$ is so slow that before the system has managed to reach point B, the random walk fluctuations have caused the system to change to another (usually a relaxation to a lower) energy level. Thus in this case, we require the random walk not just to bring the system to energy E_B but to reach the specific point B as well. This requires a longer time interval, which we term as τ_H. In general, for an intermediate damping constant between the two limits, the switching time τ will be $\tau_L < \tau < \tau_H$.

We now numerically confirm the role of precession in switching, which has been

qualitatively described above. First we define the switching time as the time for the magnetic moment to reach zero along the easy axis. Fig. 5.8 shows switching time in units of $(\gamma_0 H_k)^{-1}$ versus damping constant. For the simulation parameters, $K_u V/k_B T = 15$ and $R = 0.03$. There is an optimum switching time at $\alpha = 0.3$ and the switching time increases at both small and large damping constant. From our qualitative discussion, the switching mechanism at small damping constant is predominately due to precession, and at large damping constant switching is mainly due to thermal fluctuations. To see the relative effects of precession and thermal fluctuations more clearly, we plot the switching time in units of Monte Carlo steps (Fig. 5.9). Note that Monte Carlo steps are not in units of real time and their conversion into real time depends on α. Figure 5.9 shows saturation in the switching times for small and large damping constant. This observation is consistent with our qualitative argument. At small damping constant, switching is due to the random walk delay time τ_R (measured in MC steps), which is independent of the damping constant. At large damping values, there is little precession and switching is due to the random walk delay τ_H which is also independent of damping.

We also find that the damping constant only affects the switching time threshold, but not the reversal behavior, since all switching curves show almost the same gradient in Fig. 5.9 during reversal. This may be understood by the fact that the reversal process is an energy relaxation to the minima C of Fig. 5.9 and is independent of any precessional motion. Another feature of Fig. 5.9 is the presence of distinct magnetization oscillations, especially for curves corresponding to low damping factors. These oscillations occur prior to the actual magnetization reversal. This may be explained by the fact that the moment precesses about the minima during the random walk delay required to excite it to the required energy level E_B. The magnetization oscillation thus can be observed if the simulation time
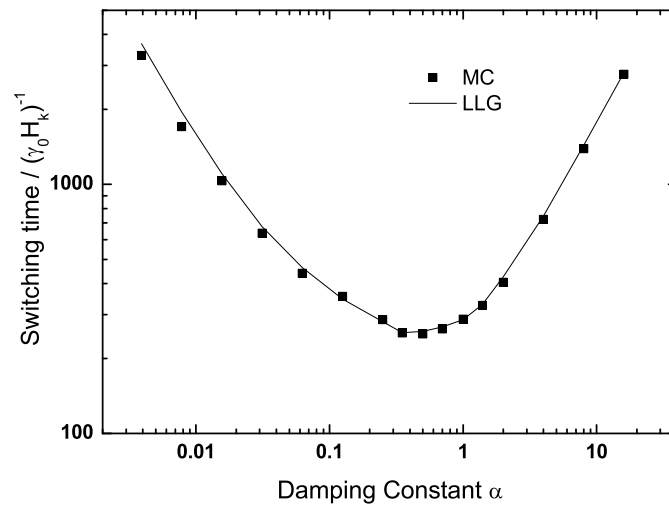
Figure 5.8: Switching time (in real time units) as a function of damping constant.
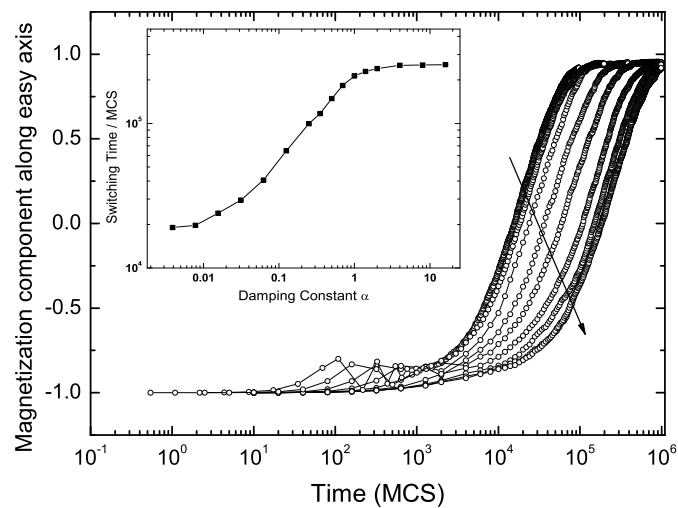
Figure 5.9: Magnetization component along the z axis as a function of time (in units of MCS). The damping constant α is varied from 1/64 to 4 (top to down), with a multiplication factor 2 between adjacent curves. Inset figure: Switching time (in units of MCS) as a function of damping constant α.

is of the order of the precession period. A quick check of the time τ_p corresponding to the first peak shows that it varies linearly with the damping constant. This is in accordance to the fact that τ_p is inversely proportional to the precessional frequency, while the latter itself is inversely proportional to the damping constant.

In summary, our calculations reveal an upper and lower limit to the reversal time corresponding to high and low damping constants. We also observe distinct magnetization oscillations prior to the actual switching event, for the case of low damping constants. These numerical findings are explained qualitatively, based on the energy profile of the system.

5.4.2 Damping Effects in Coupled Spin Array

The effect of the damping constant on the magnetization reversal in a coupled spin array is more complex. It has been shown that the damping constant affects both the rate of magnetization reversal [79, 93] and the reversal modes [78]. Nevertheless, the underlying reasons for the influence of damping on magnetization dynamics, e.g. the spin wave propagation, has not been elucidated completely.

In this section, we apply the TQMC method to study the effect of the damping constant on the magnetization dynamics and magnetization reversal. We focus on an interacting Heisenberg spin chain. A study on such a one-dimensional spin system is a useful starting point in understanding the basic physics of magnetization dynamics. It would also form a basis for further investigation into the magnetization reversal processes in the more practically relevant two and three dimensional systems [23, 94, 95]. We first study the spin wave spectra for the spin chain, and the resulting dispersion relation as a function of the damping constant α. Next, we study the reversal mechanism in the spin chain, and observe three distinct reversal modes at different α values. The existence of these modes is explained with reference to the spatial correlation between spins, as shown by the k-distribution

of the spin wave spectra.

Model and Method

We consider a one-dimensional chain of interacting magnetic moments (spins) of length L. The Hamiltonian of the spin chain is defined as:

$$\mathcal{H} = -\sum_i \left(J \cdot \hat{\mathbf{s}}_i \cdot \hat{\mathbf{s}}_{i+1} + K_u V (\hat{\mathbf{s}}_i \cdot \hat{\mathbf{k}}_n)^2 + \mu_0 M_s V \hat{\mathbf{s}}_i \cdot \mathbf{H} \right) \qquad (5.34)$$

where $\hat{\mathbf{s}}_i$ is the normalized vector representing the magnetic moment, $\mathbf{H}$ is the applied field, and J, K_u and μ_0 are the coupling strength, anisotropy constant and permeability of the vacuum, respectively. We assume that all the magnetic particles have the same volume V and easy axis orientation $\hat{\mathbf{k}}_n$.

Spin Wave Dispersion

The magnetization reversal in an interacting spin system is a complex process due to coupling between individual spins. It is thus useful to study the correlated dynamics of a linear spin array, represented by its spin wave spectra. The microscopic equivalence between precessional TQMC and stochastic LLG dynamics [62] allows the former to be used in modeling the spin wave behavior instead of the stochastic LLG integration, as was done conventionally [89, 90]. The spin wave spectra are obtained by using the Discrete Fourier Transform methods, described in Refs. [89, 90].

The parameters used in the simulations are as follows: chain length $L = 200$ unless otherwise stated, periodic boundary conditions, inverse temperature $K_u V/k_B T = 50$, and exchange coupling strength $J/2K_u V = 1$. We verified that the spin wave dispersion relation calculated using the TQMC method [37] matches the dispersion relation calculated using the linear spin wave model [88] in the previous section. Here, we analyze the spin wave behavior at different damping conditions,
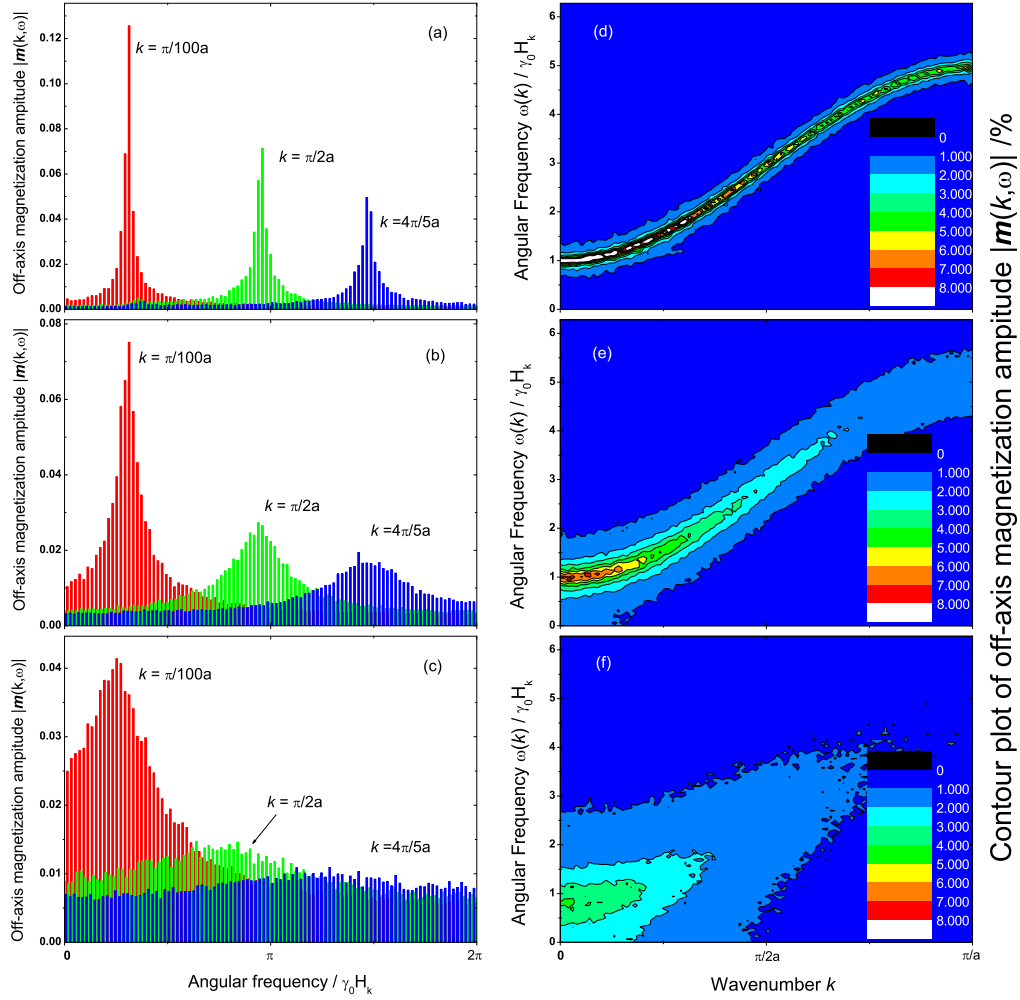
Figure 5.10: Figures in the left column: spin wave frequency spectra of three different wavevectors k, corresponding to the damping case of (a) $\alpha = 0.01$; (b) $\alpha = 0.1$; (c) $\alpha = 0.5$. Figures in the right column: Contour plot of the Fourier transformed off-axes component $|\Delta\mathbf{m}(k,\omega)|$ with respect to wavenumber k and angular frequency ω. Damping constant (d) $\alpha = 0.01$; (e) $\alpha = 0.1$; (f) $\alpha = 0.5$.

corresponding to $\alpha = 0.01$, 0.1 and 0.5, as shown in Figs. (5.10a), (5.10b) and (5.10c), respectively. For each spin wave spectrum, we consider three representative wavevector k values, i.e. $k = \pi/100a, \pi/2a, 4\pi/5a$, where a is the lattice spacing.

An important trend which can be observed by comparing Figs. (5.10a), (5.10b) and (5.10c) is the increasing degradation of the spectra peaks at higher wavevector k, with increasing damping constant α. For instance, at the high k value of $4\pi/5a$ the distinct spectral peak obtained at a low α value, as shown in Figs. (5.10a) and (5.10b), has almost disappeared at the high damping case of $\alpha = 0.5$. By contrast, the spectral peaks at low k values are less susceptible to noise with increasing α. This trend is further confirmed via the comparison between the contour plots of Figs (5.10d), (5.10e) and (5.10f) for low and high damping case. In the low damping case, we observed a clear dispersion relation of the spin wave, which agrees closely with the analytical curve predicted by the linear spin wave model. In the high damping case, however, the spin wave spectrum is completely overwhelmed by noise in the high k region.

This phenomenon may be quite readily understood from the viewpoint of the TQMC, as compared to the Langevin scheme (LLG equation). We note that there is an inverse relation between the precessional step size $\Phi(\alpha)$ and the damping constant α [see Eq. (5.25)]. Thus, increasing α has the effect of reducing the contribution of the precessional step size relative to the random walk motion. Since the ideal spin wave spectrum arises from the precessional motion, it thus becomes increasingly overwhelmed by the noise generated by the stochastic random walk at high α. This effect of noise is particularly significant when we are considering short wavelengths, corresponding to high k approaching $k_{\max} = \pi/a$. As a result, the damping effect increases the relative contribution of spin waves with long wavelengths, as shown in Fig. (5.10c).

α-dependence of Magnetization Reversal

Based on the information extracted from the above spin wave spectra, we proceed to investigate the effect of damping on the magnetization reversal mechanism of the spin array. For an interacting spin chain, there are two extreme reversal mechanisms i.e. coherent rotation and nucleation [94, 96, 97, 98]. The former is favored in short arrays in which the moments are strongly coupled together (i.e. small L and large J). In coherent rotation, there is a collective and uniform rotation of all the magnetic moments in the array, in order to minimize the exchange energy. As the array length L increases, nucleation-driven reversal becomes energetically favorable, since the reduction of the anisotropy energy outweighs the exchange energy cost. It also becomes entropically favored for long arrays to undergo nucleation, since the number of possible nucleation sites increases as $\sim L$.

Hinzke *et al.* had identified three distinct reversal modes of a spin chain as a function of the chain length L [86]. For small chain lengths, coherent rotation dominates the reversal process and the characteristic reversal time increases exponentially with L. As L increases, the system adopts the solition-antisolition nucleation process. In this mechanism, the reversal nucleates from a single site within the array, before propagating across the entire array. This mode is characterized by a $1/L$ dependence in the reversal time. As the system size L increases further, the spin array is able to accommodate more than a single soliton-antisoliton pair, allowing multiple nucleation sites to arise. In this multidroplet nucleation mechanism, the number of nucleation sites is proportional to L, so that the characteristic reversal time is independent of the chain length.

Our earlier analysis on spin waves has shown that the damping factor α plays a major role in the precessional motion, which is driven by the torque $(\mathbf{s} \times \mathbf{h})$. This suggests that α may also have a strong effect on the magnetization reversal process. We thus investigate the reversal mechanism adopted by a spin chain as a function of
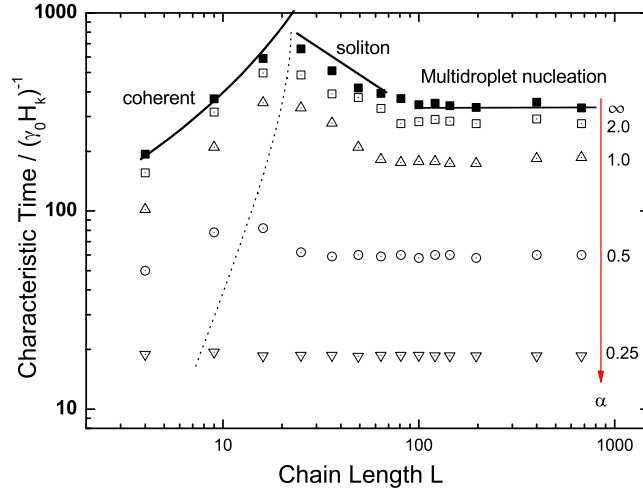
Figure 5.11: Characteristic reversal time versus the spin chain length L. The simulation parameters are: periodic boundary conditions, thermal condition $K_u V/k_B T = 8$, applied field $h = 0.48$ at an angle of $\pi/6$ to the easy axis, and exchange coupling strength $J/2K_u V = 5$. The damping constant takes the values of $\alpha = \infty, 2.0, 1.0, 0.5, 0.25$, corresponding to the curves from top to bottom. The dotted line in the figure marks the critical chain length L_{cr} for different α, at which the reversal mechanism changes from coherent rotation to nucleation.

both the array length L and damping parameter α. The characteristic reversal time τ obtained via the TQMC method is plotted in Figure (5.11) for different L and α values. We found that the L-dependence of τ shows three regions, corresponding to the three reversal mechanisms as described by Hinzke [86]. However, the damping strength α has a significant influence on the relative dominance of different reversal regimes, and thus the boundaries between them.

To account for the above trend, we review the frequency spectra of Figs. (5.10a) to (5.10f). At low α, the high-k contribution is greater and less susceptible to thermal fluctuations. This suggests a greater probability of "fanning"-like reversal, leading to a multidroplet nucleation where the magnetization rotation is correlated among

only a few spins per nucleation site. For the high damping case, however, there is a greater contribution from the low-k spectra, since the high-k spectra have been virtually destroyed by noise. This suggests that long-range spatially correlated dynamics, such as coherent-like rotation involving many spins is preferred. This agrees with the observed shift in the critical chain length L_{cr} which marks the boundary between soliton-antisoliton and coherent nucleation in Fig. (5.11). We find that with decreasing α, there is a shift of L_{cr} to smaller chain length. In particular, for a fixed $L = 16$, we find a change in the reversal mode from multidroplet to single nucleation, and finally to coherent rotation, as the damping factor is increased from 0.25 to 2. Lastly, the results in Fig (5.11) corresponding to the high damping conditions ($\alpha \geq 2$) agree qualitatively with those previously reported by Hinzke [86], which apply at the asymptotic high damping limit.

5.5 Conclusion

It is crucial to have a fundamental understanding of thermally induced magnetization reversal, especially in practical data storage applications, where the shrinking magnetic grain size is approaching the superparamagnetic limit.

In this chapter, we proposed a modified time quantified Monte Carlo method which exhibits much higher simulation efficiency than the traditional Langevin dynamical integration. This Monte Carlo is based on and extended from the random-walk-in-a-cone algorithm introduced by Nowak, with modification to account for the energy conservative precessional motion. We examined its validity in the case of an isolated single particle, as well as the interacting spin array.

We applied our time quantified Monte Carlo method to study the effects of the damping constant in thermally induced magnetization reversal. We investigated

the switching time for isolated single particle in a tilted external field. Our prediction via Monte Carlo analysis about the upper limit and lower limit for the switching time is verified by the comparison between the Monte Carlo and Langevin simulations. The damping effects in the spin wave phenomena for a interacting spin chain system was also discussed. We observed a spreading distribution of the spin wave modes with the increase of the damping constant. We also discussed the reversal mechanism in the spin chain system as influenced by the damping effects.

Chapter 6

Conclusion and Future Work

In this chapter we provide a summary of our work done in the thesis. Our main contributions are presented, followed by some suggestions for future work.

6.1   Summary

In this thesis, we studied the stochastic models of thermally activated dynamics. Thermally activated dynamics, such as Brownian motion, is usually modeled by either the Fokker-Planck equation or the Langevin dynamical equation. These two models have a firm physical basis, but there is a paucity of numerical techniques based on either model, for highly efficient modeling especially of high dimensional systems. We thus proposed a novel time quantifiable random walk Monte Carlo method, as an alternative method for modeling thermally activated dynamics.

We discovered that the Fokker-Planck equation can be used as a bridge to link different stochastic descriptions, from which the exact equivalence can be achieved between the random walk Monte Carlo algorithm and the overdamped Langevin equation. Simulations of a double well system were performed, which numerically verified the equivalence between the two stochastic models. Such equivalence thus

provided the theoretical basis for using the Monte Carlo method to study various stochastic dynamics, where the Langevin model usually applies. We further explained the origin of Gaussian white noise in the Monte Carlo algorithm via the Central Limit Theorem, which may also serve as a link between the Monte Carlo method and Langevin dynamics. To demonstrate the advantages of using Monte Carlo method in analyzing the stochastic dynamics, we investigated several applications of the time quantified Monte Carlo method, such as in Brownian ratchets and micromagnetism.

We studied the non-equilibrium noise-induced current in overdamped Brownian ratchet systems. By utilizing the random walk Monte Carlo method with fixed trial move step size, the difference equations for both transition probabilities and the mean first passage time between adjacent energy minima were derived. We considered the case of Brownian ratchet systems driven by Markov dichotomous noise. By solving the difference equations, the first analytical current expression for transport in Brownian ratchets was obtained. This Monte Carlo approach could be further generalized to analyze ratchets driven by n-th state processes and the continuous Ornstein-Uhlenbeck processes.

In the field of micromagnetics, we developed a hybrid algorithm that combined on-sphere random walk steps with deterministic precessional steps. The proposed algorithm was found to be equivalent, for both cases of isolated and interacting spins, to the stochastic Landau-Lifshitz-Gilbert equation. In the latter case, especially, the hybrid method results in great improvements in simulation efficiency. Comparison between our algorithm and previous (Nowak's) Monte Carlo model justifies our inclusion of the precessional walk to describe the energy-conserving precessional motion. We obtained better convergence of our model in low damping cases, while by contrast, previous Monte Carlo methods, e.g. by Nowak shows

a large divergence. Our algorithm was also found to have advantages in investigating the effects of the damping constant on the magnetization dynamics as compared to the Langevin description, because it clearly separates the damping type of dynamics from all others variables.

6.2 Limitations and Future Work

Our work suggests a new approach in analyzing thermally activated stochastic dynamics. For example, the extensive analytical tools developed for solving difference equations are now available for use in solving fixed-step-size random walk Monte Carlo methods. Nevertheless, the Monte Carlo methods have their limitations. Monte Carlo models are less well-suited for describing energy conservative motions (e.g. precessional motions in the micromagnetism and underdamped Brownian motions). For such motions, *ad hoc* methods have to be devised and combined with the Monte Carlo random walk, resulting in a hybrid method. Furthermore, promising as it is, the Monte Carlo algorithm does not lead to simulation efficiency improvements of different orders, as compared to Langevin dynamics.

We suggest some possible new areas where our Monte Carlo analysis may be able to contribute in future:

- Developing new time quantifiable Monte Carlo methods so as to improve the simulation efficiency. The kinetic Monte Carlo algorithm (also called N-fold way Monte Carlo model) [24, 95, 99, 100] may be considered.

- Probing new research fields, especially problems including quantum effects and quantum transportation [101, 102], where Monte Carlo analysis could apply.

- The Master equation, which is equivalent to the Monte Carlo algorithm [23],

may provide an alternative way to solve a stochastic differential equation by using matrix techniques.

Appendix A

Derivations for Current Expression in Brownian Ratchets

In this appendix we provide detailed derivations of some of the main results presented in Chat. 4.

1. Derivation of Equations (4.9) and (4.10)

From the Chap. 4 we have:

$$g(m) \;=\; \mu_m \cdot g(m-1) + w_m \cdot g(m+1) + (1 - \mu_m - w_m) \cdot g(m) \qquad \text{(A.1)}$$

$$\tau(m) \;=\; \mu_m \cdot \tau(m-1) + w_m \cdot \tau(m+1) + (1 - \mu_m - w_m) \cdot \tau(m) + 1, \text{(A.2)}$$

with initial conditions: $g(0) = 0$, $g(2N) = 1$ and $\tau(0) = \tau(2N) = 0$. To solve Eq. (A.1), we rearrange the formula:

$$
\begin{aligned}
g(m+1) - g(m) &= (\mu_m/w_m)[g(m) - g(m-1)] = \ldots \\
&= \left[\prod_{i=1}^{m} (\mu_m/w_m) \right] \cdot (g(1) - g(0)) \equiv k(m) \cdot (g(1) - g(0)).
\end{aligned}
$$

Hence we have:

$$g(m) - g(0) = \sum_{i=0}^{m-1} k(i) \cdot (g(1) - g(0)). \tag{A.3}$$

Substituting the initial conditions $g(0) = 0$, $g(2N) = 1$ into Eq. (A.3), we obtain:

$$
\begin{aligned}
g(m) &= \left(\sum_{i=1}^{m-1} k(i) \right) \cdot g(1) = \left(\sum_{i=1}^{m-1} k(i) \right) \cdot \left(\sum_{i=1}^{2N-1} k(i) \right)^{-1} \cdot g(2N) \\
&= \frac{\sum_{i=0}^{m-1} k(i)}{\sum_{i=0}^{2N-1} k(i)}.
\end{aligned}
$$

The solution to Eq. (A.2) is similar. We have:

$$\tau(m) - \tau(0) = \sum_{i=0}^{m-1} k(i) \cdot (\tau(1) - \tau(0)) - \sum_{i=1}^{m-1} \left[k(i) \cdot \sum_{j=1}^{i} (w_j k(j))^{-1} \right]. \tag{A.4}$$

Hence we obtain the expression for $\tau(m)$ by considering the initial conditions:

$$
\begin{aligned}
\tau(m) &= \left(\sum_{i=0}^{m-1} k(i) \right) \cdot \tau(1) - \sum_{i=1}^{m-1} \left[k(i) \cdot \sum_{j=1}^{i} (w_j k(j))^{-1} \right] \\
&= g(m) \cdot \sum_{i=1}^{2N-1} \left[k(i) \cdot \sum_{j=1}^{i} (w_j k(j))^{-1} \right] - \sum_{i=1}^{m-1} \left[k(i) \cdot \sum_{j=1}^{i} (w_j k(j))^{-1} \right]
\end{aligned}
$$

Further simplification by noting the periodical conditions: $w_{N+i} = w_N$, $\mu_{N+j} = \mu_N$, will leads to Eq. (4.10) in the manuscript.

2. Derivation of Equations (4.13) and (4.17)

From Equation (11) in the manuscript, we have:

$$g(m; \sigma; \sigma') = \sum_{\tilde{\sigma}} v(\tilde{\sigma}|\sigma) \cdot \left[w_m^{\tilde{\sigma}} g(m+1; \tilde{\sigma}; \sigma') + \mu_m^{\tilde{\sigma}} g(m-1; \tilde{\sigma}; \sigma') + (1 - w_m^{\tilde{\sigma}} - \mu_m^{\tilde{\sigma}}) g(m; \tilde{\sigma}; \sigma') \right], \tag{A.5}$$

which could be rewritten into a 2×2 matrix form:

$$MW_m \cdot X_{m+1} = [I - M(I - W_m - U_m)] \cdot X_m - MU_m \cdot X_{m-1}$$

where $X_m = \{g(m; \sigma; \sigma')\}$, $M = \{v(\sigma'|\sigma)\}$, $W_m = \text{Diag}\{w_m^\sigma\}$ and $U_m = \text{Diag}\{\mu_m^\sigma\}$. M is the transition matrix of the dichotomous processes and is generally non-singular. The above equation can be simplified into Eq. (12) in the manuscript easily:

$$X_{m+1} = W_m^{-1} (\lambda \cdot C + W_m + U_m) \cdot X_m - W_m^{-1} U_m \cdot X_{m-1}, \qquad \text{(A.6)}$$

where $\lambda \equiv \frac{v(-|+)}{1 - v(-|+) - v(+|-)} \ll 1$ and

$$C = \begin{pmatrix} 1 & -1 \\ -\theta & \theta \end{pmatrix}.$$

For Equation (15) in the manuscript, the derivation is similar:

$$Y_{m+1} = W_m^{-1} (\lambda \cdot C + W_m + U_m) \cdot Y_m - W_m^{-1} U_m \cdot Y_{m-1} - W_m^{-1} E. \qquad \text{(A.7)}$$

3. Derivation of G and T

Setting the starting point $m = N$, we obtain the *forward transition probability matrix* $G = X_N$ and the *MFPT matrix* $T = Y_N$. We first solve Eq. (A.6). X_m can be reduced into a linear combination of X_1 and X_0 by recurring Eq. (A.6). Noting the initial condition $X_0 = \mathbf{0}$ and $X_{2N} = I$, we are justified to define a 2×2 matrix Q_m that:

$$X_m = Q_m \cdot X_1 \quad (m \geq 1)$$

with $Q_0 = 0$, and $Q_1 = 1$. From Eq. (A.6):

$$\begin{aligned} Q_{m+1} - Q_m &= W_m^{-1} U_m \cdot (Q_m - Q_{m-1}) + \lambda \cdot W_m^{-1} C \cdot Q_m = \dots \\ &= K_m \cdot (Q_1 - Q_0) + \lambda \cdot K_m \left(\sum_{i=1}^m K_i^{-1} W_i^{-1} C \cdot Q_i \right) \end{aligned}$$

in which $K_i = \text{Diag}\{k_i^+, k_i^-\}$ where $k_i^\sigma \equiv \prod_{j=1}^i \mu_j^\sigma / w_j^\sigma$. Hence by considering the

initial conditions: $X_0 = 0$ and $X_{2N} = I$, we have

$$Q_m = \sum_{i=0}^{m-1} K_i + \lambda \cdot \sum_{i=1}^{m-1} \left[\left(\sum_{j=i}^{m-1} K_j \right) K_i^{-1} W_i^{-1} C \cdot Q_i \right]. \tag{A.8}$$

Q_m can be expressed as a polynomial function of λ:

$$Q_m(\lambda) = \sum_{l=0}^{m-1} D_l^m \cdot \lambda^l. \tag{A.9}$$

We can therefore obtain the coefficients D_l^m from Eq. (A.8) easily:

$$
\begin{aligned}
D_0^m &= \sum_{i=0}^{m-1} K_i, \\
D_l^m &= \sum_{i=l}^{m-1} \left[\left(\sum_{j=i}^{m-1} K_j \right) (W_i K_i)^{-1} C \cdot D_{l-1}^i \right].
\end{aligned}
\tag{A.10}
$$

We note that since $\lambda \ll 1$, the first few components in the polynomial function actually dominate the value of Q_m. Our experience shows that truncating at $O(\lambda^3)$ could yield very good approximation to the exact Q_m.

We hence obtain the expression of G, by noting the initial condition $X_{2N} = Q_{2N} X_1 = I$:

$$G = X_N = Q_N \cdot X_1 = Q_N \cdot Q_{2N}^{-1}. \tag{A.11}$$

Let $N \to \infty$ one can write down the continuous expression of $Q(y)$ and therefore G from Eqs. (A.11), (A.9) and (A.10). We remark that some characteristics of the correlation matrix C can simplify the derivation: for an diagonal matrix $K = \{\{k_{11}, 0\}, \{0, k_{22}\}\}$, $C \cdot K \cdot C$ will yield a simple result that $C \cdot K \cdot C = (k_{11} + \theta k_{22})C$. We next caclulate Y_m appeared in Eq. (A.7). We define:

$$Y_m = Q_m \cdot Y_1 - R_m \quad (m \geq 1)$$

with initial conditions: $R_0 = 0$ and $R_1 = 0$.

R_m can also be expressed as a polynomial function of λ that similar to Q_m:

$$R_m(\lambda) = \sum_{l=0}^{m-1} J_l^m \cdot \lambda^l$$

where J_l^m is similar to D_l^m:

$$
\begin{aligned}
J_0^m &= \sum_{i=1}^{m-1} \left[(W_i K_i)^{-1} \sum_{j=i}^{m-1} K_j \right] \cdot E \\
J_l^m &= \sum_{i=l}^{m-1} \left[\left(\sum_{j=i}^{m-1} K_j \right) (W_i K_i)^{-1} C \cdot J_{l-1}^i \right].
\end{aligned}
\tag{A.12}
$$

Hence we obtain the MFPT matrix T by noting the initial conditions $Y_0 = Y_{2N} = 0$:

$$
T = Y_N = Q_N Y_1 - R_N = Q_N Q_{2N}^{-1} R_{2N} - R_N = G \cdot R_{2N} - R_N.
$$

Again let $N \rightarrow \infty$ one can write down the continuous expression of $R(y)$ and therefore T.

Derivations of Fokker-Planck Coefficients for Interacting Spin Array

FP coefficients for the LLG equation

Previous study of the thermal fluctuation on interacting spin array system proves that the inter-particle coupling does not introduce correlations into thermal fluctuations [103]. To the best of our knowledge, a detailed derivation of the Fokker-Planck coefficients for an interacting particle system has not been presented. Hence we include, as an appendix, a derivation of the FP coefficients for an interacting particle system. We extend Brown's derivation [15] for the Fokker-Planck coefficients of isolated single domain particles to obtain the Fokker-Planck coefficients for the case of interacting particles.

The thermal field $\mathbf{h}(t)$ representing the thermal fluctuations, according to Brown [15], has the properties of a white noise, i.e.

$$\langle h_i^p(t) \rangle = 0, \quad \langle h_i^p(0) h_j^q(t) \rangle = 2D \cdot \delta_{pq} \delta_{ij} \delta(t) \tag{B.1}$$

where $i, j = \{1, 2, 3\}$ denote the Cartesian coordinate components $\{x, y, z\}$ and

$p, q = \{1, \ldots, N\}$ refer to the pth and q^{th} spin in the list. Hence, if:

$$K_i^p \equiv \int_t^{t+\Delta t} h_i^p(t')dt', \tag{B.2}$$

then

$$\langle K_i^p \rangle = 0, \quad \langle K_i^p K_j^q \rangle = 2D \cdot \delta_{pq}\delta_{ij}\Delta t. \tag{B.3}$$

Rewriting Eq. (5.26) in spherical coordinates, we obtain

$$
\begin{aligned}
\text{Left side} \quad &= \quad \frac{d\mathbf{s}_i}{dt} = \frac{\partial \mathbf{s}_i}{\partial \theta_i}\frac{d\theta_i}{dt} + \frac{\partial \mathbf{s}_i}{\partial \varphi_i}\frac{d\varphi_i}{dt} = \vec{\mathbf{e}}_\theta \cdot \dot{\theta}_i + \vec{\mathbf{e}}_\varphi \cdot \sin\theta_i\dot{\varphi}_i \tag{B.4}\\
\text{Right side} \quad &= \quad \frac{\gamma_0}{\mu_0 M_s V(1+\alpha^2)}\left(\mathbf{s}_i \times \frac{\partial E}{\partial \mathbf{s}_i} + \alpha \cdot \mathbf{s}_i \times \left(\mathbf{s}_i \times \frac{\partial E}{\partial \mathbf{s}_i}\right)\right)\\
&= \quad \left(-h'\frac{\partial E}{\partial \theta_i} - g'\frac{1}{\sin\theta_i}\frac{\partial E}{\partial \varphi_i}\right)\vec{\mathbf{e}}_\theta + \left(g'\frac{\partial E}{\partial \theta_i} - h'\frac{1}{\sin\theta_i}\frac{\partial E}{\partial \varphi_i}\right)\vec{\mathbf{e}}_\varphi \tag{B.5}
\end{aligned}
$$

in which the partial differential relationships such as $\frac{\partial E}{\partial \mathbf{s}} = \frac{\partial E}{\partial \theta}\frac{\partial \theta}{\partial \mathbf{s}} + \frac{\partial E}{\partial \varphi}\frac{\partial \varphi}{\partial \mathbf{s}} = \frac{\partial E}{\partial \theta}\vec{\mathbf{e}}_\theta + \frac{\partial E}{\partial \varphi}\frac{1}{\sin\theta}\vec{\mathbf{e}}_\varphi$ have been used. With the inclusion of the thermal fluctuations, additional terms will be added into the right side as $-\frac{\gamma_0 H_k}{1+\alpha^2}\left(\mathbf{s}_i \times \mathbf{h}(t) + \alpha \cdot \mathbf{s}_i \times (\mathbf{s}_i \times \mathbf{h}(t))\right)$. By considering the relation between Cartesian and spherical base vectors:

$$
\begin{aligned}
\vec{i} \quad &= \quad \sin\theta\cos\varphi \cdot \vec{\mathbf{e}}_r + \cos\theta\cos\varphi \cdot \vec{\mathbf{e}}_\theta - \sin\varphi \cdot \vec{\mathbf{e}}_\varphi\\
\vec{j} \quad &= \quad \sin\theta\sin\varphi \cdot \vec{\mathbf{e}}_r + \cos\theta\sin\varphi \cdot \vec{\mathbf{e}}_\theta + \cos\varphi \cdot \vec{\mathbf{e}}_\varphi\\
\vec{k} \quad &= \quad \cos\theta \cdot \vec{\mathbf{e}}_r - \sin\theta \cdot \vec{\mathbf{e}}_\theta \tag{B.6}
\end{aligned}
$$

and equating Eqs. (B.4) and (B.5), we thus obtain $2N$ simultaneous equations as:

$$
\begin{aligned}
\frac{d\theta_i}{dt} \quad &= \quad h'H'_{\theta_i} + g'\frac{1}{\sin\theta_i}H'_{\varphi_i}\\
\frac{d\varphi_i}{dt} \quad &= \quad -g'\frac{1}{\sin\theta_i}H'_{\theta_i} + h'\frac{1}{\sin^2\theta_i}H'_{\varphi_i} \tag{B.7}
\end{aligned}
$$

where

$$H'_{\theta_i} = -\frac{\partial E}{\partial \theta_i} + H_{\theta_i}, \quad H'_{\varphi_i} = -\frac{\partial E}{\partial \varphi_i} + H_{\varphi_i} \tag{B.8}$$

H_{θ_i} and H_{φ_i} are the contributions of $\mathbf{h}(t)$ to the generalized forces corresponding to θ_i and φ_i :

$$
\begin{aligned}
(2K_uV)^{-1}H_{\theta_i} &= h_1^i(t)\cos\theta_i\cos\varphi_i + h_2^i(t)\cos\theta_i\sin\varphi_i - h_3^i(t)\sin\theta_i \\
(2K_uV)^{-1}H_{\varphi_i} &= -h_1^i(t)\sin\theta_i\sin\varphi_i + h_2^i(t)\sin\theta_i\cos\varphi_i
\end{aligned}
\tag{B.9}
$$

Eq. (B.7) can be expressed directly in a general form as:

$$
\dot{x}_i^p = F_i^p(x) + \sum_{k=1}^{3} G_{ik}^p(x)h_k^p(t)
\tag{B.10}
$$

where x represents the set of $2N$ variable $\{x_i^p\}$ (here $i = \{1,2\}$ denotes angular coordinates $\{\theta, \varphi\}$ and $p = \{1, 2, \ldots, N\}$ refers to the pth spin in the list). To evaluate the FP coefficients A_{x_i} and $B_{x_ix_j}$, we need Δx_i only to terms of the order Δt for A_{x_i} and only to terms of order $(\Delta t)^{1/2}$ for $B_{x_ix_j}$. Taking note of Eq. (B.2), Δx_i itself is of order $(\Delta t)^{1/2}$. Expanding $F_i^p(x)$ and $G_{ik}^p(x)$ in Taylor's series at initial state x_0:

$$
\begin{aligned}
F_i^p(x) &= F_i^p(x_0) + \sum_{q,j} F_{i,j}^{p,q} \cdot \Delta x_j^q + \frac{1}{2}\sum_{q,r,j,l} F_{i,jl}^{p,qr} \cdot \Delta x_j^q\Delta x_l^r + \cdots \\
G_{ik}^p(x) &= G_{ik}^p(x_0) + \sum_{q,j} G_{ik,j}^{p,q} \cdot \Delta x_j^q + \frac{1}{2}\sum_{q,r,j,l} G_{ik,jl}^{p,qr} \cdot \Delta x_j^q\Delta x_l^r + \cdots
\end{aligned}
\tag{B.11}
$$

where, for example, $F_{i,j}^{p,q} = \partial F_i^p/\partial x_j^q$ and $G_{ik,j}^{p,q} = \partial G_{ik}^p/\partial x_j^q$. Hence by integration of Eq. (B.10) with respect to Δt, and truncate the terms that has order higher than Δt, we have:

$$
\Delta x_i^p = F_i^p\Delta t + \sum_k G_{ik}^p \int_0^{\Delta t} h_k^p(t_1)dt_1 + \sum_{q,j,k} G_{ik,j}^{p,q} \int_0^{\Delta t} \Delta x_j^q h_k^p(t_1)dt_1
\tag{B.12}
$$

and in the last integral we may express Δx_j^q to the order of $\Delta t^{1/2}$, namely, as $\sum_j G_{jl}^q \int_0^{\Delta t_1} h_l^q(t_2)dt_2$. Thus,

$$
\Delta x_i^p = F_i^p\Delta t + \sum_k G_{ik}^p \int_0^{\Delta t} h_k^p(t_1)dt_1 + \sum_{q,j,k,l} G_{ik,j}^{p,q} G_{jl}^q \int_0^{\Delta t} dt_1 \int_0^{t_1} h_k^p(t_1)h_l^q(t_2)dt_2
$$

$$
\tag{B.13}
$$

the second term is of order $\Delta t^{1/2}$, the others of order Δt; therefore, to the first order in Δt:

$$\Delta x_i^p \Delta x_j^q = \sum_{k,l} G_{ik}^p G_{jl}^q \int_0^{\Delta t} dt_1 \int_0^{\Delta t} h_k^p(t_1) h_l^q(t_2) dt_2. \qquad (\text{B.14})$$

It is easily seen that the double integral in Eq. (B.13) is half that in Eq. (B.14). We now evaluate the statistical average by considering Eq. (B.3) and dividing by Δt:

$$
\begin{aligned}
A_{x_i^p} &= \lim_{\Delta t \to 0} \frac{\langle \Delta x_i^p \rangle}{\Delta t} = F_i^p + D \cdot \sum_k G_{ik,j}^{p,p} G_{jk}^p \\
B_{x_i^p x_j^q} &= \lim_{\Delta t \to 0} \frac{\langle \Delta x_i^p \Delta x_j^q \rangle}{\Delta t} = 2D \cdot \sum_k G_{ik}^p G_{jk}^p \cdot \delta_{pq} \delta_{ij}.
\end{aligned}
\qquad (\text{B.15})
$$

In the present application,

$$
\begin{aligned}
F_1^p &= -h' \frac{\partial E}{\partial \theta_p} - g' \frac{1}{\sin \theta_p} \frac{\partial E}{\partial \varphi_p} \\
F_2^p &= g' \frac{1}{\sin \theta_p} \frac{\partial E}{\partial \theta_p} - h' \frac{1}{\sin^2 \theta_p} \frac{\partial E}{\partial \varphi_p}
\end{aligned}
\qquad (\text{B.16})
$$

and

$$
\begin{aligned}
(2K_u V)^{-1} G_{11}^p &= h' \cos \theta_p \cos \varphi_p - g' \sin \varphi_p \\
(2K_u V)^{-1} G_{12}^p &= h' \cos \theta_p \sin \varphi_p + g' \cos \varphi_p \\
(2K_u V)^{-1} G_{13}^p &= -h' \sin \theta_p \\
(2K_u V)^{-1} G_{21}^p &= -g' \cot \theta_p \cos \varphi_p - h' \csc \theta_p \sin \varphi_p \\
(2K_u V)^{-1} G_{22}^p &= -g' \cot \theta_p \sin \varphi_p + h' \csc \theta_p \cos \varphi_p \\
(2K_u V)^{-1} G_{23}^p &= g'.
\end{aligned}
\qquad (\text{B.17})
$$

Partial differentiation of Eqs. (B.17) with respect to θ_p and φ_p gives the formulas for the twelve quantities $G_{ik,j}^{p,p}$ ($i, j = 1, 2; k = 1, 2, 3$). Substitution of the values of F_i^p, G_{ik}^p and $G_{ik,j}^{p,p}$ into Eqs. (B.15) gives the value of the FP coefficients for the

LLG dynamical equation as follows:

$$
\begin{aligned}
A_{\theta_i}^{LLG} &= -h'\frac{\partial E}{\partial \theta_i} - g'\frac{1}{\sin\theta_i}\frac{\partial E}{\partial \varphi_i} + k'\cot\theta_i \\
A_{\varphi_i}^{LLG} &= g'\frac{1}{\sin\theta_i}\frac{\partial E}{\partial \theta_i} - h'\frac{1}{\sin^2\theta_i}\frac{\partial E}{\partial \varphi_i} \\
B_{\theta_i\theta_j}^{LLG} &= 2k'\cdot\delta_{ij} \\
B_{\varphi_i\varphi_j}^{LLG} &= \frac{1}{\sin^2\theta_i}2k'\cdot\delta_{ij} \\
B_{\theta_i\varphi_j}^{LLG} &= B_{\varphi_j\theta_i}^{LLG} = 0
\end{aligned}
\tag{B.18}
$$

where $k' = D(h'^2 + g'^2)(2K_uV)^2$ is to be determined since the value of D is still unknown. Substituting Eqs. (B.18) into Eq. (5.27) and taking note that $P(\{\theta\},\{\varphi\},t)$ should reduce to the Boltzmann distribution at statistical equilibrium ($\partial P/\partial t = 0$), one thus obtains the value of k': $k' = h'/\beta$.

FP coefficients for TQMC

We next derive the FP Coefficients for the TQMC. The Monte Carlo algorithm starts with a random selection of the spin site. We consider the ith spin in the list. For a trial move with the displacement vector to be of size r_i ($r_i < R$) and angle α_i with respect to $\vec{\mathbf{e}}_\theta$, we have the corresponding change with respect to θ_i and φ_i as [62]

$$
\begin{aligned}
\Delta\theta_i &= -r_i\cos\alpha_i + \frac{r_i^2}{2}\cot\theta_i\sin^2\alpha_i + O\left(r_i^3\right) \\
\Delta\varphi_i &= r_i\frac{1}{\sin\theta_i}\sin\alpha_i + r_i^2\frac{\cot\theta_i}{\sin\theta_i}\cos\alpha_i\sin\alpha_i + O\left(r_i^3\right).
\end{aligned}
\tag{B.19}
$$

The displacement probability of the size to be r_i is given by Nowak *et al.* [20] as

$$
p(r_i) = 3\sqrt{R^2 - r_i^2}/2\pi R^3
\tag{B.20}
$$

and the acceptance probability for this trial move is given by the heat bath rate as

$$
\begin{aligned}
A\left(\Delta E\right) &= \frac{1}{1 + \exp\left(\beta\Delta E\right)} \\
&\approx \frac{1}{2}\left(1 - \frac{1}{2}\beta\left(\frac{\partial E}{\partial \theta_i}\Delta\theta_i + \frac{\partial E}{\partial \varphi_i}\Delta\varphi_i\right)\right) \quad\quad \text{(B.21)}
\end{aligned}
$$

where ΔE is the energy change in the random walk step and $\beta = (k_B T)^{-1}$. Integrating over the projected surfaces [see Fig. 5.1 for a clear diagram], we obtain a series of the required means

$$
\begin{aligned}
\langle\Delta\theta_i\rangle &= \int_0^{2\pi} d\alpha_i \int_0^R (r_i dr_i)\Delta\theta_i \cdot p(r_i)\cdot A(\Delta E) = \frac{R^2}{20}(\cot\theta_i - \beta\frac{\partial E}{\partial\theta_i}) + O(R^3) \\
\langle\Delta\varphi_i\rangle &= -\frac{1}{\sin^2\theta_i}\frac{R^2}{20}\beta\frac{\partial E}{\partial\varphi_i} + O(R^3) \\
\langle\Delta\theta_i^2\rangle &= \frac{R^2}{20} + O(R^4) \quad\quad\quad\quad\quad\quad\quad\quad\quad\quad\quad\quad\quad\quad \text{(B.22)} \\
\langle\Delta\varphi_i^2\rangle &= \frac{1}{\sin^2\theta_i}\frac{R^2}{20} + O(R^4) \\
\langle\Delta\theta_i\Delta\varphi_i\rangle &= O(R^3).
\end{aligned}
$$

Let subscript i (j) refers to the ith (j^{th}) spin in the list and X, Y denote either θ or φ. One easily finds that when $i \neq j$: $\langle\Delta X_i\Delta Y_j\rangle\,|_{i\neq j} = 0$. This is because in the Monte Carlo algorithm, only 1 spin site is chosen at each Monte Carlo step. Truncating the higher order terms in the above equations and including the probability factor of $(1/N)$ in choosing the ith spin from all N spins, we then obtain the FP coefficients for the TQMC method as in Eqs. (5.29).

Bibliography

[1] W. T. Coffey, Yu. P. Kalmykov, and J. T. Waldron. *The Langevin equation with Applications in Physics, Chemistry and Electrical Engineering.* World Scientific, 1996.

[2] F. Jensen. *Introduction to Computational Chemistry.* John Wiley & Sons, 1999.

[3] P. Jaeckel. *Monte Carlo Methods in Finance.* John Wiley & Sons, 2002.

[4] Wolfgang Paul and Joȑg Baschnagel. *Stochastic Processes: From Physics to Finance.* Springer, 2000.

[5] E. Nelson. *Dynamical Theories of Brownian Motion.* Princeton University Press, 1967.

[6] Peter Hänggi, Peter Talkner, and Michal Borkovec. Reaction-rate theory: fifty years after Kramers. *Rev. Mod. Phys.*, 62:251–341, 1990.

[7] H. A. Kramers. Brownian motion in a field of force and the diffusion model of chemical reactions. *Physica*, 7:284, 1940.

[8] M. B. A. Jalil. Thermal dependence of magnetotransport in nanogranular magnetic media. *J. Appl. Phys.*, 93:8050, 2003.

[9] A. Einstein. *Investigations on the Theory of Brownian Movement.* New York: Dover, 1956.

[10] F. Reif. *Fundamentals of Statistical and Thermal Physics.* McGraw-Hill, New York, 1967.

[11] W. T. Coffey. Development and application of the theory of Brownian motion. *Adv. Chem. Phys.*, 63:69, 1956.

[12] H. Risken. *The Fokker-Planck Equation.* Springer-Verlag, Berlin, 2 edition, 1967.

[13] David P. Landau and Kurt Binder. *A Guide to Monte Carlo Simulations in Statistical Physics.* Cambridge, 2000.

[14] Anja Riegert, Nilüfer Baba, Katrin Gelfert, Wolfram Just, and Holger Kantz. Hamiltonian chaos acts like a finite energy reservoir: Accuracy of the Fokker-Planck approximation. *Physical Review Letters*, 94:054103, 2005.

[15] W. F. Brown. Thermal fluctuations of a single-domain particle. *Phys. Rev.*, 130:1677, 1963.

[16] O. Chubykalo, U. Nowak, R. Smirnov-Rueda, M. A. Wongsam, R. W. Chantrell, and J. M. Gonzalez. Monte Carlo technique with a quantified time step: Application to the motion of magnetic moments. *Phys. Rev. B*, 67:064422, 2003.

[17] R. Y. Rubinstein. *Simulation and the Monte Carlo Method.* Wiley, 1981.

[18] Y. Limoge and J. L. Bocquet. Temperature behavior of tracer diffusion in amorphous materials: A random-walk approach. *Phys. Rev. Lett.*, 65:60–63, 1990.

[19] K. Kikuchi, M. Yoshida, T. Maekawa, and H. Watanabe. Metropolis Monte Carlo method for Brownian dynamics simulation generalized to include hydrodynamic interactions. *Chemical Physics Letters*, 196:57–61, 1992.

[20] U. Nowak, R. W. Chantrell, and E. C. Kennedy. *Phys. Rev. Lett.*, 84:163, 2000.

[21] P.A. Martin. On the stochastic dynamics of Ising models. *Journal of Statistical Physics*, 16:149, 1977.

[22] K. Park, MA Novotny, and PA Rikvold. Scaling analysis of a divergent prefactor in the metastable lifetime of a square-lattice Ising ferromagnet at low temperatures. *Physical Review E*, 66:56101, 2002.

[23] Hwee Kuan Lee, Yutaka Okabe, X. Cheng, and M. B. A. Jalil. Solving the master equation for extremely long time scale calculations. *Comp. Phys. Comms.*, 168:159, 2005.

[24] O. Chubykalo-Fresenko and R. W. Chantrell. Modeling of long-time thermal magnetization decay in interacting granular magnetic materials. *IEEE Trans. Magn.*, 41:3103, 2005.

[25] B. D. Josephson. The discovery of tunnelling supercurrents. *Rev. Mod. Phys.*, 46:251–254, 1974.

[26] Fischer Black and Myron Scholes. The pricing of options and corporate liabilities. *Journal of Political Economy*, 81:637–654, 1973.

[27] Robert C. Merton. Theory of rational option pricing. *Bell Journal of Economics and Management Sciencey*, 4:141–183, 1973.

[28] R. F. Pawula. Approximation of the linear Boltzmann equation by the Fokker-Planck equation. *Phys. Rev.*, 162:186–188, 1967.

[29] G. E. Uhlenbeck and L. S. Ornstein. On the theory of the Brownian motion. *Phys. Rev.*, 36:823–841, 1930.

[30] N. Metropolis, A.W. Rosenbluth, M.N. Rosenbluth, A.H. Teller, and E. Teller. Equations of state calculations by fast computing machines. *Journal of Chemical Physics*, 21:1087–1092, 1953.

[31] Amikam Aharoni. *An Introduction to the theory of ferromagnetism*. Clarendon Press, Oxford, 1996.

[32] Radford M. Neal. Slice sampling. *The Annals of Statistics*, 31:705–767, 2003.

[33] Bernt K. Øksendal. *Stochastic Differential Equations: An Introduction with Applications*. Springer (Berlin), 2003.

[34] William Feller. *An introduction to probability theory and its applications*, volume 1. Wiley, 3 edition, 1968.

[35] K. Kikuchi, M. Yoshida, T. Maekawa, and H. Watanabe. Metropolis Monte Carlo method as a numerical technique to solve the Fokker-Planck equation. 1991.

[36] Hyunbum Jang, Malcolm J. Grimson, and Thomas B. Woolf. Stochastic dynamics and the dynamic phase transition in thin ferromagnetic films. *Phys. Rev. E*, 70:047101, 2004.

[37] X. Z. Cheng, M. B. A. Jalil, and H. K. Lee. Time-quantified Monte Carlo algorithm for interacting spin array micromagnetic dynamics. *Phys. Rev. B*, 73:224438, 2006.

[38] X. Z. Cheng, M. B. A. Jalil, H. K. Lee, and Y. Okabe. Time-quantifiable Monte Carlo method for simulating a magnetization-reversal process. *Phys. Rev. B*, 72:094420, 2005.

[39] N. G. van Kampen. *Stochastic Processes in Physics and Chemistry*. North-Holland Publishing, 1981.

[40] B. D. Josephson. Possible new effects in superconductive tunnelling. *Phys. Lett.*, 1:251, 1962.

[41] L. Solymar. *Superconductive Tunneling and Applications*. Chapman and Hall, London, 1972.

[42] P. Fulde, L. Pietronero, W. R. Schneider, and S. Strässler. Problem of Brownian motion in a periodic potential. *Phys. Rev. Lett.*, 35:1776–1779, 1975.

[43] W. Dieterich, P. Fulde, and I. Peschel. Theoretical models for superionic conductors. *Advance in Physics*, 29:627, 1980.

[44] J. McConnel. *Rotational Brownian Motion and Dielectric Theory*. Academic, London, 1980.

[45] G. Wyllie. *Phys. Reps.*, 61:329, 1980.

[46] Peter Reimann. Brownian motors:noisy transport far from equilibrium. *Phys. Rep.*, 361:57, 2002.

[47] P. Reimann and P. Hänggi. Introduction to the physics of Brownian motors. *Appl. Phys. A*, 75:169, 2002.

[48] R. Dean Astumian and Peter Hänggi. Brownian motors. *Phys. Today*, 55:33, 2002.

[49] R. Dean Astumian and Martin Bier. Fluctuation driven ratchets: Molecular motors. *Phys. Rev. Lett.*, 72:1766–1769, 1994.

[50] Charles R. Doering, Werner Horsthemke, and Jason Riordan. Nonequilibrium fluctuation-induced transport. *Phys. Rev. Lett.*, 72:2984–2987, 1994.

[51] K. Svoboda, C. F. Schmidt, B. J. Schnapp, and S. M. Block. Direct observation of kinesin stepping by optical trapping interferometry. *Nature*, 365:721, 1993.

[52] R. Dean Astumian. Thermodynamics and kinetics of a Brownian motor. *Science*, 276:917, 1997.

[53] Martin Bier. Processive motor protein as an overdamped Brownian stepper. *Physical Review Letters*, 91:148104, 2003.

[54] Tian Yow Tsong and Cheng-Hung Chang. Ion pump as Brownian motor: theory of electroconformational coupling and proof of ratchet mechanism for Na,K-ATPase action. *Physica A*, 321:124, 2003.

[55] Martin Bier and R. Dean Astumian. Biasing Brownian motion in different directions in a 3-state fluctuating potential and an application for the separation of small particles. *Phys. Rev. Lett.*, 76:4277–4280, 1996.

[56] Sergey Savel'ev, Fabio Marchesoni, and Franco Nori. Interacting particles on a rocked ratchet: Rectification by condensation. *Phys. Rev. E*, 71:011107, 2005.

[57] Baoquan Ai, Liqiu Wang, and Lianggang Liu. Transport reversal in a thermal ratchet. *Phys. Rev. E*, 72:031101, 2005.

[58] J. Kula, T. Czernik, and J. Łuczka. Brownian ratchets: Transport controlled by thermal noise. *Phys. Rev. Lett.*, 80:1377–1380, 1998.

[59] C. Van den Broeck, R. Kawai, and P. Meurs. Microscopic analysis of a thermal Brownian motor. *Phys. Rev. Lett.*, 93:090601, 2004.

[60] P. Reimann and T. C. Elston. Kramers rate for thermal plus dichotomous noise applied to ratchets. *Phys. Rev. Lett.*, 77:5328–5331, 1996.

[61] B. Lindner, L. Schimansky-Geier, P. Reimann, P. Hänggi, and M. Nagaoka. Inertia ratchets: A numerical study versus theory. *Phys. Rev. E*, 59:1417–1424, 1999.

[62] X. Z. Cheng, M. B. A. Jalil, H. K. Lee, and Y. Okabe. Mapping the Monte Carlo scheme to Langevin dynamics: A Fokker-Planck approach. *Phys. Rev. Lett.*, 96:067208, 2006.

[63] X. Z. Cheng, M. B. A. Jalil, and Hwee Kuan Lee. Analytical solution to transport in Brownian ratchets via the Gambler's Ruin model. *Physical Review Letters*, 99:070601, 2007.

[64] Jan Iwaniszewski. Mean escape time over a fluctuating barrier. *Phys. Rev. E*, 68:027105, 2003.

[65] Youngki Lee, Andrew Allison, Derek Abbott, and H. Eugene Stanley. Minimal Brownian ratchet: An exactly solvable model. *Phys. Rev. Lett.*, 91:220601, 2003.

[66] Debashis Barik, Pulak Kumar Ghosh, and Deb Shankar Ray. Langevin dynamics with dichotomous noise; direct simulation and applications. *J. Stat. Mech.*, page P03010, 2006.

[67] R. Dean Astumian. Paradoxical games and a minimal model for a Brownian motor. *Am. J. Phys.*, 73:178, 2005.

[68] W. Bohm. The correlated random walk with boundaries: A combinatiorial solution. *J. Appl. Prob.*, 37:470, 2000.

[69] Craig R. Orr and Doron Zeilberger. A computer algebra approach to the discrete Dirichlet problem. *J. Symbolic Comput.*, 18:87, 1994.

[70] L. D. Landau and E. Lifshitz. On the theory of the dispersion of magnetic permeability in ferromagnetic bodies. *Phys. Z. Sowjetunion*, 8:101, 1935.

[71] T. L. Gilbert. A Lagrangian formulation of the gyromagnetic equation of the magnetization field. *Phys. Rev.*, 10:1243, 1955.

[72] J. Fidler and T. Schrefl. Micromagnetic modelling - the current state of the art. *J. Phys. D*, 33:R135, 2000.

[73] L. Néel. Theorie du trainage magnetique des ferromagnetiques en grains fins avec applications aux terres cuites. *Ann Géophys*, 5:99, 1949.

[74] J. P. Wang, C. H. Hee, and T. C. Chong. Thermal stability study on highly oriented longitudinal thin film media. *IEEE Trans. Magn.*, 36:3199, 2000.

[75] S. N. Piramanayagam, C. H. Hee, and J. P. Wang. Role of thermal energy on the magnetic properties of laminated antiferromagnetically coupled recording media. *J. Appl. Phys.*, 90:3442, 2001.

[76] J. G. Zhu. Micromagnetic modelling: theory and application in magnetic thin films. *MRS BULL*, 20:49, 1995.

[77] Qingzhi Peng and H. Neal Bertram. Micromagnetic studies of switching speed in longitudinal and perpendicular polycrystalline thin film recording media. *J. Appl. Phys.*, 81:4384, 1997.

[78] Dieter Suess, Thomas Schrefl, and Josef Fidler. Reversal modes, thermal stability and exchange length in perpendicular recording media. *IEEE Trans. Magn.*, 37:1664, 2001.

[79] X. Z. Cheng, M. B. A. Jalil, H. K. Lee, and Y. Okabe. Precessional and thermal relaxation dynamics of magnetic nanopaticles - a time-quantified monte carlo approach. *J. Appl. Phys.*, 99:08B901, 2006.

[80] Xiaobin Wang and H. Neal Bertram. Simple transition parameter expression including grain size and intergranular exchange. *Journal of Applied Physics*, 93:7005–7007, 2003.

[81] Amikam Aharoni. Effect of a magnetic field on the superparamagnetic relaxation time. *Phys. Rev.*, 177:793–796, 1969.

[82] C.P. Robert and G. Casella. *Monte Carlo Statistical Methods*. New York: Springer-Verlag, 2004.

[83] C. N. Scully, P. J. Cregg, and D. S. F. Crothers. Asymptotic dependence of the relaxation time of the magnetization of a ferromagnetic particle on the anisotropy of the particle. *Phys. Rev. B*, 45:474–476, 1992.

[84] W. T. Coffey, D. S. F. Crothers, J. L. Dormann, Yu. P. Kalmykov, E. C. Kennedy, and W. Wernsdorfer. Thermally activated relaxation time of a single domain ferromagnetic particle subjected to a uniform field at an oblique angle to the easy axis: Comparison with experimental observations. *Phys. Rev. Lett.*, 80:5655, 1998.

[85] W. F. Brown. Relaxational behavior of fine magnetic particles. *J. Appl. Phys.*, 30:130S, 1959.

[86] D. Hinzke and U. Nowak. Magnetic relaxation in a classical spin chain. *Phys. Rev. B*, 61:6734, 2000.

[87] D. A. Dimitrov and G. M. Wysin. Effects of surface anisotropy on hysteresis in fine magnetic particles. *Phys. Rev. B*, 50:3077, 1994.

[88] Charles Kittel. *Introduction to Solid State Physics*. John Wiley & Sons, 1996.

[89] R. W. Chantrell, J. D. Hannay, and M. A. Wongsam. Computational approaches to thermally activated fast relaxation. *IEEE Trans. Mag.*, 34:1839, 1998.

[90] O. Chubykalo, J. D. Hannay, M. Wongsam, R. W. Chantrell, and J. M. Gonzalez. Langevin dynamic simulation of spin waves in a micromagnetic model. *Phys. Rev. B*, 65:184428, 2002.

[91] X. Z. Cheng and M. B. A. Jalil. The effect of thermal fluctuation on tilted perpendicular media. *J. Appl. Phys.*, 97:10E314, 2005.

[92] C. H. Hee, Y. Y. Zou, and J. P. Wang. Tilted media by micromagnetic simulation: A possibility for the extension of longitudinal magnetic recording? *J. Appl. Phys.*, 91:8004, 2002.

[93] G. Bertotti, I. Mayergoyz, C. Serpico, and M. Dimian. Comparison of analytical solutions of Landau-Lifshitz equation for "damping" and "precessional" switchings. *J. Appl. Phys.*, 93:6811, 2003.

[94] Per Arne Rikvold, H. Tomita, S. Miyashita, and Scott W. Sides. Metastable lifetimes in a kinetic Ising model: Dependence on field and system size. *Phys. Rev. E*, 49:5080, 1994.

[95] M. A. Novotny. Monte Carlo algorithms with absorbing Markov chains: Fast local algorithms for slow dynamics. *Phys. Rev. Lett.*, 74:1, 1995.

[96] J. S. Langer. Theory of nucleation rates. *Phys. Rev. Lett.*, 21:973–976, 1968.

[97] J. S. Langer. Statistical theory of the decay of metastable states. *Ann. Phys.*, 54:258, 1969.

[98] H. Tomita and S. Miyashita. Statistical properties of the relaxation processes of metastable states in the kinetic Ising model. *Phys. Rev. B*, 46:8886–8893, 1992.

[99] A. B. Bortz, M. H. Kalos, and J. L. Lebowitz. A new algorithm for Monte Carlo simulation of Ising spin systems. *Journal of Computational Physics*, 17:10–18, 1975.

[100] Kristen A. Fichthorn and W. H. Weinberg. Theoretical foundations of dynamical Monte Carlo simulations. *Journal of Chemical Physics*, 95:1090–1096, 1991.

[101] Peter Reimann, Milena Grifoni, and Peter Hänggi. Quantum ratchets. *Phys. Rev. Lett.*, 79:10–13, 1997.

[102] Jian-sheng Wang. Quantum thermal transport from classical molecular dynamics. *Phys. Rev. Lett.*, 99:160601, 2007.

[103] O. Chubykalo, R. Smirnov-Rueda, J. M. Gonzalez, M. A. Wongsam, R. W. Chantrell, and U. Nowak. Brownian dynamics approach to interacting magnetic moments. *J. Magn. Magn. Mater.*, 266:28, 2003.

List of Publications

1. X. Z. Cheng, M. B. A. Jalil and Hwee Kuan Lee "Analytical Solution to Transport in Brownian Ratchets via Gambler's Ruin Model", *Phys. Rev. Lett.* **99**, 070601 (2007).

2. X. Z. Cheng, M. B. A. Jalil and Hwee Kuan Lee "Micromagnetic study on thermally induced magnetization reversal of a coupled spin chain system", *IEEE Transactions on Magnetics* **43**, 2899 (2007).

3. M. B. A. Jalil, S. G. Tan and X. Z. Cheng "Advanced Modeling Techniques for Micromagnetic Systems", *J. Nanosci. Nanotech.* **7**, 46 (2007).

4. M. G. Sreenivasan, K.L. Teo, X. Z. Cheng, M. B. A. Jalil, T. Liew, T.C. Chong, A. Y. Du, T. K. Chan and T. Osipowicz "Structural, magnetic and transport investigations of CrTe clustering effect in (Zn,Cr)Te system", *J. Appl. Phys.* **102**, 053702 (2007).

5. X. Z. Cheng, M. B. A. Jalil, Hwee Kuan Lee and Y. Okabe "Mapping the Monte Carlo scheme to Langevin dynamics: A Fokker-Planck approach", *Phys. Rev. Lett.* **96**, 067208 (2006).

6. X. Z. Cheng, M. B. A. Jalil and Hwee Kuan Lee "Time-quantified Monte Carlo algorithm for interacting spin array micromagnetic dynamics", *Phys. Rev. B* **73**, 224438 (2006).

7. X. Z. Cheng, M. B. A. Jalil, Hwee Kuan Lee and Y. Okabe "Time-quantifiable Monte Carlo method in simulating magnetization-reversal process", *Phys. Rev. B* **72**, 094420 (2005).

8. X. Z. Cheng, M. B. A. Jalil, Hwee Kuan Lee and Y. Okabe "Precessional and Thermal Relaxation Dynamics of Magnetic Nanoparticles - A Time-Quantified Monte Carlo Approach", *J. Appl. Phys.* **99**, 08B901 (2006).

9. Hwee Kuan Lee, Y. Okabe, X. Z. Cheng and M. B. A. Jalil "Solving the master equation for extremely long time scale calculations", *Comp. Phys. Comm.* **168**, 159 (2005).

10. X. Z. Cheng and M. B. A. Jalil "Micromagnetic study of Intergranular Exchange Coupling in Tilted Perpendicular Media", *IEEE Transactions on Magnetics* **41**, 3115 (2005).

11. X. Z. Cheng and M. B. A. Jalil "The effect of thermal fluctuation on tilted perpendicular media", *J. Appl. Phys.*, **97**, 10E314 (2005).